DEVELOPMENT OF A WEARABLE BLOOD PRESSURE MONITOR USING ADAPTIVE CALIBRATION OF PERIPHERAL PULSE TRANSIT TIME MEASUREMENTS

by

DEVIN BARNETT MCCOMBIE

Bachelor of Science in Bioengineering
University of California, San Diego, 2000

Master of Science in Mechanical Engineering
Massachusetts Institute of Technology, 2004

Master of Science in Electrical Engineering and Computer Science
Massachusetts Institute of Technology, 2004

SUBMITTED TO THE DEPARTMENT OF MECHANICAL ENGINEERING
IN PARTIAL FULFILLMENT OF THE REQUIREMENTS FOR THE DEGREE OF

DOCTOR OF PHILOSOPHY
AT THE
MASSACHUSETTS INSTITUTE OF TECHNOLOGY

JUNE 2008

Signature of Author.....
Department of Mechanical Engineering
May 19, 2008

Certified By.....
H. Harry Asada
Ford Professor of Mechanical Engineering
Thesis Supervisor

Accepted by.....
Lallit Anand
Chairman, Department Committee on Graduate Students

DEVELOPMENT OF A WEARABLE BLOOD PRESSURE MONITOR USING ADAPTIVE CALIBRATION OF PERIPHERAL PULSE TRANSIT TIME MEASUREMENTS

by

DEVIN BARNETT MCCOMBIE

Submitted to the Department of Mechanical Engineering
on May 19, 2008 in partial fulfillment of the requirements
for the Degree of Doctor of Philosophy

ABSTRACT

The ability to continuously monitor a patient's blood pressure long-term (for hours, days, or weeks) using a wearable device as unobtrusive as a wristwatch or piece of jewelry, could revolutionize the study, diagnosis, and treatment of hypertension, heart failure, and other cardiovascular disorders. Today's familiar blood pressure cuffs are used to diagnose and manage the hypertensive disorders which afflict 65 million Americans. But these existing devices only permit single 'snap-shot' measurements, while true arterial blood pressure fluctuates minute-by-minute, from night-to-day, etc. There is ample evidence that more intense blood pressure monitoring offers better clinical information. Moreover, the existing blood pressure devices are a chore: they are obtrusive, finicky, and uncomfortable.

This thesis presents the design and development of a novel non-invasive BP monitor. The device provides beat-by-beat mean arterial blood pressure (MAP) estimates using adaptive calibration of the measured transit time of a propagating arterial pressure wave. The device employs unique wearable sensor architecture to estimate peripheral pulse transit time measurements. This architecture is comprised of two in-line photoplethysmograph sensors one in the form of a wristwatch measuring the volumetric pulsation in the ulnar artery and one in the form of a ring measuring the volumetric pulsation of the digital artery at the base of the little finger. Use of this architecture eliminates problems associated with the traditional method of estimating pulse transit time using the electrocardiogram (EKG). Additionally, by co-locating the two sensors on the same appendage not only are we able to account for the effect of hydrostatic pressure variation in our pulse transit time (PTT) measurements using an imbedded height sensor, but by actively altering the height of the two sensors relative to the heart we can achieve real-time identification of the calibration equation mapping PTT to MAP. Such real-time calibration of PTT measurements obviates the need for obtrusive cuff-based blood pressure monitors and offers the potential to recursively update the calibration equation as the patient's cardiovascular state evolves throughout the duration of the measurement period. Adaptive PTT calibration through natural patient motion has never previously been explored and offers the potential to achieve the longstanding goal of a truly imperceptible, wearable home BP monitor.

This thesis describes the design and development of the sensor hardware used in the wearable device. Based on both theoretical study and experimental observations a device model has been developed to allow estimation of mean arterial blood pressure using the pulse transit

times measured with our sensors. Additionally, this thesis presents the adaptive calibration methodology and the novel system identification algorithms that were used to parameterize our device model using natural human motion. Finally, this thesis demonstrates the potential of these innovative concepts through human subject testing and data analysis.

Thesis Committee:
Chair
H. Harry Asada, Ph.D.
Ford Professor of Mechanical Engineering

Roger G. Mark, M.D. Ph.D.
Distinguished Professor in Health Sciences and Technology, Professor of Electrical Engineering

Andrew Reisner, M.D.
Visiting Scientist in Health Sciences and Technology and Attending Physician at Massachusetts General Hospital in the Department of Emergency Medicine

Warren Seering, Ph.D.
Weber-Shaughness Professor of Mechanical Engineering

ACKNOWLEDGMENTS

I owe a great deal of thanks to a lot of people because without their support and friendship I could never have completed this thesis. In addition to furthering my professional development which culminated with the completion of my doctoral degree, my years at MIT have been a time of significant personal growth and I will always be thankful for all the opportunities that life as a graduate student here afforded me.

I would like to thank Professor H. Harry Asada my thesis advisor, whose guidance and financial support fostered my development as a researcher and engineer.

I would like to thank Dr. Andrew Reisner who initially championed the idea behind my thesis research and whose knowledge of medicine and cardiovascular monitoring provided me with numerous insights and inspiration.

I would like to thank Professor Roger Mark whose initial skepticism, tough questions, and medical insight proved an invaluable asset towards the development of my work.

I would like to thank Professor Warren Seering for his contributions to my thesis work as a member of my thesis committee.

I want to offer a big thank you to Dr. Timothy Davis for all of his advice and insight both of which served as priceless assets in the completion of this thesis.

Thanks to all the students of the d'Arbeloff Lab both past and present who became my good friends, opened my eyes to different perspectives, and made those long hours in the lab a little easier. Thanks to all of you for offering me a friendly ear when I needed it.

A special thanks to all my friends in the Cambridge Surf Crew, you all have become like family to me over the years and proven to me that a person can be both a successful student and still be a dedicated surfing, skiing, and snowboarding hellman. You all helped me to get through MIT "my way".

Also I would like to thank all the MIT sand volleyballers, I will truly miss summer time in graduate school.

Most importantly, I would like to thank my wife Lisa who has been my biggest supporter throughout the years. You have helped me get through both good times and bad, and never stopped believing in me. I am a very lucky man.

I would also like to thank my family for their support and encouragement throughout the years. And for helping me to believe that I could accomplish anything I set my mind to do.

I dedicate this thesis to the memory of my grandmother, Rowena McCombie who was a graduate of the University of California, Berkeley and who had a life long love of books and learning, and who helped fuel my own academic dreams.

TABLE OF CONTENTS

LIST OF FIGURES

CHAPTER 1
INTRODUCTION

1.1 WEARABLE BLOOD PRESSURE MONITORING

Hypertension or chronic high blood pressure is a major health issue in the United States. It is estimated that between 25%-50% of all adult Americans suffer from this condition [1,2].

Just as feedback from a scale helps people attempting weight loss to adhere to their diet and exercise regimen, patients suffering from hypertension are more likely to adhere to their doctor prescribed treatment when they regularly monitor their blood pressure.

Leading home blood pressure monitors work based on the principle of oscillometry and require an inflatable cuff to measure arterial blood pressure (BP). These cuff based devices permit episodic "snap-shot" measurements of arterial blood pressure while the patient is suspended in a stationary position. Although useful, a single snap-shot measurement of the time varying blood pressure, which fluctuates minute-by-minute, and from night-to-day is incapable of encapsulating the dynamic state of the cardiovascular system. Moreover, the existing BP devices are a chore: they are cumbersome, finicky [3,4], and uncomfortable [5].

Wearable blood pressure monitoring technologies may be able to overcome the drawbacks of existing home BP monitors, (burdensome stationary measurement periods and monitors providing limited snap-shot measurements). There are three levels of potential benefits to wearable blood pressure monitoring. First, extend the proven benefits of today's standard BP cuffs by making home BP monitoring less of a burden. Regular monitoring as a source of feedback has been shown to improve patient compliance with prescribed treatments [6,7]. Second, extend the benefits of intensive 24-hour ambulatory BP monitoring protocols to more patients, and more days per year, allowing better stratification of a patient's risk and tailoring of their prescribed treatment [8,9]. Third, exceed the benefits of intensive 24-hour ambulatory BP monitoring by measuring BP more frequently than every 15 minutes.

In order for a wearable BP device to realize these potential benefits it must meet a number of requirements. The monitoring device must operate unobtrusively and it must be compact, lightweight, and low power. Additionally, it must be capable of providing accurate measurements throughout its use and across changing cardiovascular states, thus the device must

have a means of self calibration. Finally, the wearable device must be able to provide continuous measurements while being worn by the patient.

A number of non-invasive blood pressure (NIBP) measurement methods exist, however none of the existing methods meet all the requirements listed above. A major short-coming of many of these non-invasive BP devices is their use of an obtrusive actuated cuff during device calibration and BP measurement. These actuated devices whether pneumatic or mechanical are not only obtrusive, requiring uncomfortable arterial compression for every measurement, but the actuators also significantly increase the power consumption of the devices. Leading NIBP methods in this category include sphygmomanometry, oscillometry, tonometry, and the volume clamp method of Penaz [10].

An alternative NIBP measurement method exists that is capable of estimating blood pressure without any actuators. This method estimates BP using calibrated pulse wave velocity measurements [10]. This passive method not only eliminates the need for an actuated cuff during measurement but also has the capability of providing continuous beat-to-beat BP estimates. As such, calibrated pulse wave velocity has the potential to satisfy the requirements of wearable monitoring and allow doctors and patients to finally realize the potential benefits of a wearable device. However, pulse wave velocity is not without its shortcomings and several key limitations must be addressed in order to utilize it in a wearable monitor.

1.2 History & Limitations of Blood Pressure Estimation using Pulse Wave Velocity

The study of pulse wave velocity (PWV), the speed at which a pressure pulse is transmitted from the heart through the arterial tree has a long history. The relationship describing the propagation of pressure waves in an elastic tube e.g. a blood vessel, was first described separately by Moens and Korteweg in 1871 [11]. Their seminal work was later confirmed and extended by Bramwell and Hill in 1923 [11]. The utility of pulse wave velocity as a surrogate measure to estimate arterial blood pressure has been the subject of research since the 1960's. Since then there has been extensive academic and commercial effort to use this as a monitoring modality. Yet the accuracy of PWV based BP monitors has been suboptimal e.g. [12]. Per

Chen, "No one has succeeded in realizing a reliable blood pressure monitor when only the pulse wave velocity or pulse arrival time is used [13]."

The difficulties associated with using pulse wave velocity to estimate BP can be divided into two general categories, (1) inaccurate measurement of PWV using non-invasive sensors and (2) employing static calibration equations to map the PWV measurements to BP.

Existing blood pressure estimation methods based on pulse wave velocity rely on measurement of pulse transit time (PTT), the time required for the pressure pulse to travel between two different locations along the arterial tree, and either implicit or explicit measurement of pulse transit distance (Δx). Their relationship is given in (*1.1*).

$$pwv = \frac{\Delta x}{ptt} \tag{1.1}$$

The vast majority of existing PWV devices define and measure the pulse transit time, as the time elapsed between the apex of the R wave of the electrocardiogram (ECG) and the arrival of the photoplethysmograph (PPG) waveform signal in the finger tip. However, the ECG has been shown to be a problematic marker when used to indicate the onset of the pressure pulse as it emanates from the left ventricle because of variations in the electromechanical delay in the heart [37]. These undetectable variations in the delay will cause variations in the measured PTT that are unrelated to arterial blood pressure and thus act as sources of BP estimation error.

Other alternative PTT estimation methods have also proved problematic. The difference in pulse arrival times measured between two PPG waveforms placed at distinct locations on the body, e.g. the finger and the toe, or the finger and the ear have been investigated as a potential proxy metric for BP estimation. Although the difference in pulse transit time measured from these two sensor architectures demonstrated some correlation with changes in systolic (peak) BP the difference did not exhibit a correlation with changes in diastolic (minimum) BP [12,14,15] and limit this measure's utility.

Hydrostatic pressure variations caused by postural changes or elevation change in the extremity where PPG measurements are derived have been shown to influence the measured PTT [15]. If not accounted for, the influence of hydrostatic pressure on measured PTT can serve as a source of error in estimating central BP and may make BP estimates using ECG and PPG unreliable in any position except supine [16].

Pulse wave velocity devices also suffer from a difficulty to accurately measure the pulse transit distance between the two sensor locations. Although the transit distance can be lumped into model parameters identified during initial device calibration it is difficult to keep this distance constant [18] and this imprecision creates another source of error in BP estimation using PTT alone.

Although the use of the ECG and the effects of postural variation may serve as sources of BP estimation error, perhaps the most significant limitation to current PWV technologies is caused by the use of a static calibration equation to map PTT measurements to BP given the dynamic properties of the arterial walls.

Leading pulse wave velocity blood pressure monitors require a calibration equation relating PTT to BP to be identified and parameterized for an individual prior to using the device to estimate BP. This calibration equation is generally identified using a set of training data in which blood pressure measurements from an actuated device (e.g. a cuff-based sphygmomanometer or oscillometer) are collected simultaneously with pulse transit time measurements [17]. Once the parameters of this calibration equation have been determined they are assumed to remain constant throughout the estimation period. However, the relationship between PWV and BP is a function of the patient's vascular physiology (e.g. arterial stiffness) which can be altered by changes in vascular smooth muscle tone [18]. Therefore, the equation relating PTT to BP for any individual is dynamic and changes in conjunction with changes to the patient's cardiovascular state. Thus, accurate estimation of BP using PTT requires that a device update parameters in a dynamic calibration equation across changing physiologic states. Currently, there are no PWV devices that allow adaptive, on-line calibration of PTT to BP.

1.3 ADAPTIVE CALIBRATION OF PERIPHERAL PULSE TRANSIT TIME

Intravascular blood pressure is not only a function of the volume of fluid passing within the vessel lumen due to the contracting heart but it is also a function of gravity. The earth's gravitational field creates a pressure difference (ΔP) along the arterial tree by acting on the columns of blood in the vessels [18], thus the arterial pressure in the foot is much higher than the pressure in the aorta when a person is standing upright. The magnitude of this effect is described by equation (*1.2*) where ρ is the blood density, g is the gravitational acceleration constant, and Δh the relative height of the fluid column formed between the heart and measurement site.

$$\Delta P(t) = \rho g \Delta h(t) \qquad (1.2)$$

Gravity's effect on arterial blood pressure can be exploited in order to calibrate a wearable sensor. Placement of a wearable blood pressure sensor at a peripheral location such as on the wrist or finger allows adjustment of the intravascular pressure at the sensor's measurement point by moving the sensor to different heights relative to the height of the heart. The change in intravascular pressure at the measurement site is equal to the pressure change predicted by (*1.2*) and can be directly estimated using measurements of the sensor's height relative to the heart as depicted in Figure *1-1*. A comparison of changes in intravascular hydrostatic pressure to the observed changes in the sensor's output permits calibration of the non-invasive measured parameter, or height based calibration.

Height based calibration was originally utilized by Shaltis and Asada [19] in a modified form of oscillometry. In their method they proved that the external sensor contact pressure acting on the artery at the measurement site could be reduced and maintained below mean arterial pressure and the maximum PPG pulsation amplitude could still be identified using height variation. However, their method still required a cumbersome, lengthy calibration procedure, an actuated pressure sensor stage, and did not allow continuous BP estimation.

The full potential of this novel height based calibration tool can only be realized when this technique is combined with an innovative device based on a passive NIBP principle and with sophisticated signal processing algorithms that provide a means to adaptively calibrate the device using a patient's natural motion. A combination of this set of enabling technologies could truly deliver an unobtrusive, self-calibrating BP monitor [20].

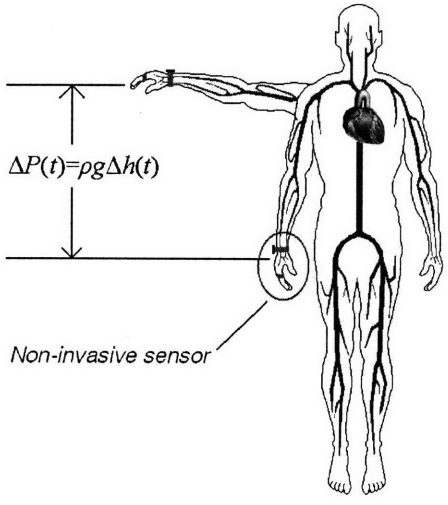

Figure 1-1. Height based calibration of a non-invasive blood pressure sensor

1.4 THESIS SUMMARY & ORGANIZATION

In this thesis I will describe the development of this set of enabling technologies. I will describe a novel method for estimating arterial blood pressure based on pulse wave velocity. This new method will employ a unique sensor architecture that is comprised of two in-line PPG sensors to estimate pulse transit time, one located above the ulnar artery at the wrist and one located along the base of the little finger above the digital artery (Figure *1-2*). Use of this architecture will eliminate problems associated with estimating PTT from the ECG and because of their close proximity will simplify measuring the pulse transit distance. Additionally, by co-locating the two sensors along the same appendage not only will we be able to account for the effect of hydrostatic pressure variation on our measurements, but by actively altering the height of the two sensors relative to the heart, height based calibration can be used along with novel signal processing techniques to adaptively identify the calibration equation mapping PTT to BP. This thesis details the development of an in-line PPG based device model relating PTT to BP, the design of the novel PTT device, potential methods for estimating PTT with the PPG waveforms are evaluated, it presents the system identification algorithms used to identify device model parameters using natural motion, and presents initial human subject test results obtained using the novel device and identification algorithms.

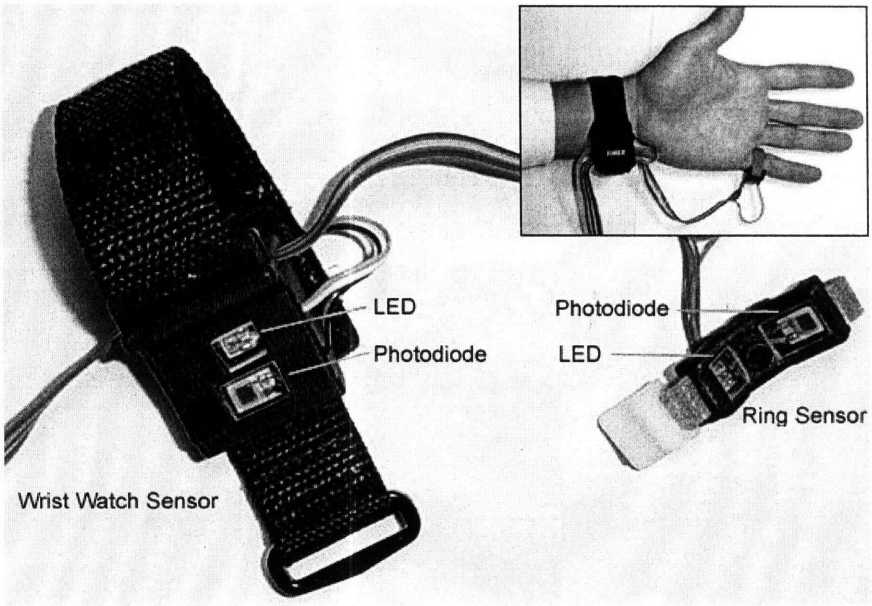

Figure 1-2. Novel peripheral pulse transit time measurement device with dual in-line PPG sensors

CHAPTER 2
DEVELOPMENT OF A PERIPHERAL PULSE TRANSIT TIME DEVICE MODEL

The goal of this chapter of the thesis is to describe the development of a lumped parameter model governing pulse wave velocity in the peripheral arteries monitored by our in-line PPG sensors. The model must characterize the relationship between the measured pulse transit time, the arterial blood pressure, and the pressure change produced by relative height variation.

The development of this model begins by understanding the anatomy of the arteries that form the transit path between the two sensors. Based on a number of assumptions a one-dimensional wave model will be developed to describe the velocity of a pressure pulse in an elastic vessel. The validity of the assumptions used to develop this one-dimensional model will be explored in the context of the peripheral arterial anatomy and the pulse wave velocity model will be augmented to characterize the important features of the arteries that form the transit path. Finally, a lumped parameter model that will be utilized by our device to estimate arterial blood pressure from measured pulse transit time will be presented.

2.1 ANATOMY OF THE PERIPHERAL PULSE TRANSIT PATH

Operation of our novel BP monitor utilizes PTT derived from PPG waveforms recorded from the ulnar artery (PPG 1) at the wrist and from the common palmar digital artery on the outside of the little finger (PPG 2) as shown in Figure *2-1*.

As the left ventricle ejects blood from the heart a pressure pulse wave is transmitted along the arterial tree propagating towards our two PPG measurement sites in the left hand. The path of the pulse wave begins in the ascending aorta, propagating next along the aortic arch, continuing into the left subclavian artery, then along the axillary artery, and into the brachial artery of the upper arm. The brachial artery splits just below the elbow joint into two branches, the ulnar and radial arteries. The pressure pulse wave propagates through both of these arteries into the arteries of the hand.

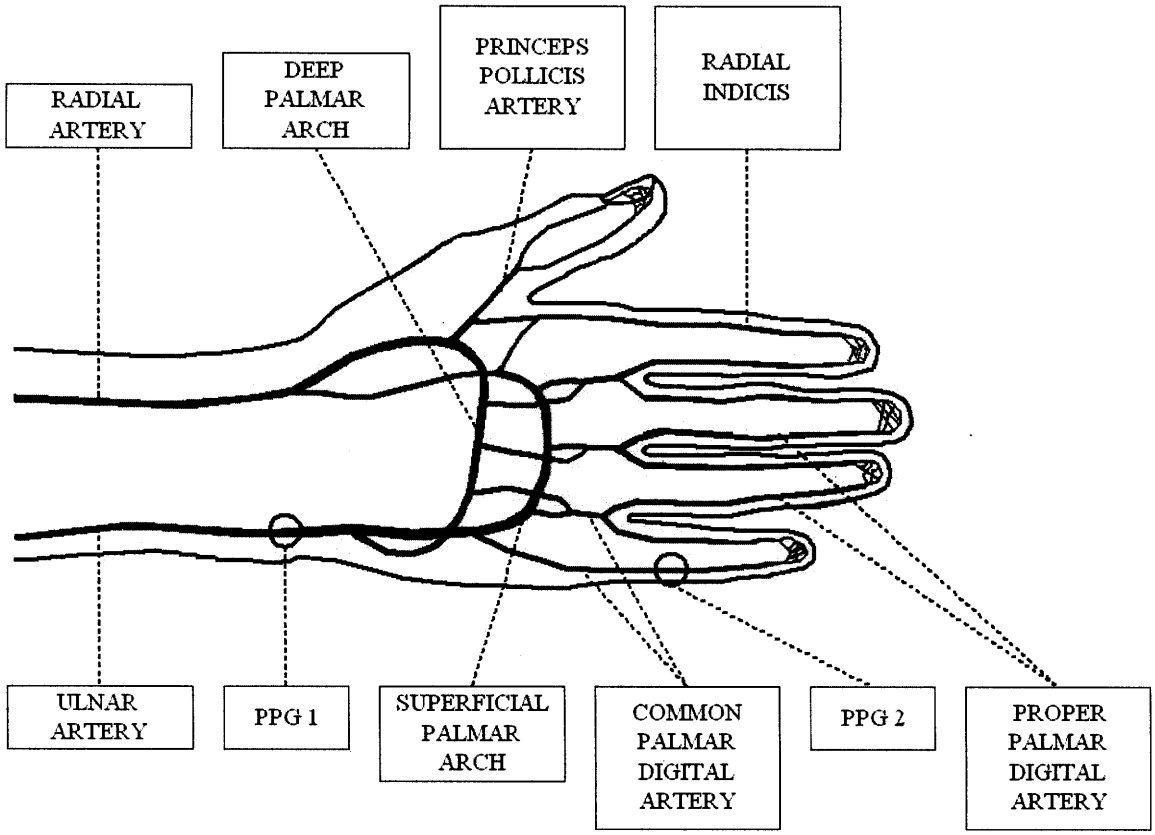

Figure 2-1. Common arterial anatomy of the left hand

The arteries in the hand form a complex network of inter-connected vessels that provide redundant paths along which the pulse wave can propagate and blood can flow. The most common configuration of the arterial network of the hand found in nearly 80% of the population [21] is shown in Figure *2-1*.

The primary paths of blood flow and wave propagation for the various arteries in the hand are displayed in Figure *2-1* using color coding. Arteries displayed in red are primarily supplied by the ulnar artery. The ulnar artery primarily supplies blood to the little finger. In this path blood flows from the ulnar artery into both the common palmar digital artery on the outside of the little finger and into the superficial palmar arch, after passing into the superficial palmar arch blood flows into the common palmar arteries and then into the proper palmar digital arteries in the fingers. Arteries displayed in purple are primarily supplied by the radial artery. The radial artery is the primary blood supply for the thumb, index, middle, and ring fingers. After passing through the radial artery blood flows both into the deep palmar arch and into the princeps pollicis artery supplying the thumb and also into the radial indicis artery supplying the index finger.

Blood supplied to the deep palmar arch flows into the common palmar arteries and then into the proper palmar digital arteries in the fingers.

The primary wave propagation path observed by our device measures the transit time as a pulse wave propagates along the ulnar artery into the common palmar artery on the outside of the little finger. This path consists of one major arterial bifurcation as the ulnar artery branches into the palmar digital artery and also continues into the superficial palmar arch.

Although other anatomical configurations of the arterial network in the hand do exist [21], none of the most common configurations alter the propagation path of our device. However, we should be aware that in a very small minority of the population this propagation path may exhibit some variation.

2.2 ARTERIAL PULSE WAVE PROPAGATION

The framework for understanding the relationship between arterial pulse wave velocity and blood pressure begins with an analysis of wave propagation in a circular, cylindrical, fluid-filled tube given a number of simplifying assumptions [11,22], these assumptions are listed below.

Tube Assumptions:

- Infinitely long
- Straight
- Isolated
- Elastic
- Negligible mass

Fluid Assumptions:

- Homogeneous
- Incompressible
- Nonviscous

The continuity equation for the fluid in an elastic tube with cross-sectional area $A(z, t)$ having an average flow velocity in the axial direction $U(z, t)$ is given in (*2.1*).

$$\frac{\partial A}{\partial t}+\frac{\partial}{\partial z}(UA)=0 \qquad (2.1)$$

The definition of cross-sectional area in a circular tube can be used to transform (*2.1*) into an expression involving tube diameter, $D(z, t)$ as given in (*2.2*).

$$\frac{\partial D^2}{\partial t}+\frac{\partial}{\partial z}(UD^2)=0 \qquad (2.2)$$

Using the product rule the partial derivatives in the expression in (*2.2*) can be expanded into the expression given by *(2.3)*.

$$2D\frac{\partial D}{\partial t}+U2D\frac{\partial D}{\partial z}+D^2\frac{\partial U}{\partial z}=0 \tag{2.3}$$

Assuming the wave amplitude is small and the wavelength is long compared to the diameter of the tube the slope of the tube, $\frac{\partial D}{\partial z}<<1$ and this term in (*2.3*) can be neglected resulting in the expression given by (*2.4*).

$$\left(\frac{2}{D}\right)\frac{\partial D}{\partial t}+\frac{\partial U}{\partial z}=0 \tag{2.4}$$

The equation of motion for the fluid in the tube with density ρ and internal tube pressure P_i is given in (*2.5*).

$$\frac{\partial U}{\partial t}+U\frac{\partial U}{\partial z}+\frac{1}{\rho}\frac{\partial P_i}{\partial z}=0 \tag{2.5}$$

Under the assumption that the fluid velocity U is small the second term in (*2.5*) can be neglected and the expression reduced to the equation given by (*2.6*).

$$\frac{\partial U}{\partial t}+\frac{1}{\rho}\frac{\partial P_i}{\partial z}=0 \tag{2.6}$$

Equations (*2.4*) and (*2.6*) along with a constitutive equation for the tube wall, describing the relationship between transmural pressure, P_{tm} and tube diameter D, form the basic set of equations used to model wave propagation in an elastic tube.

Continuation of the analysis requires an assumption regarding the tube wall's constitutive model. Based on the theory of thin shells [22] the dynamics of the model can be eliminated by neglecting the mass of the tube and ignoring any partial derivatives leaving a simplified algebraic relationship as given by (2.7).

$$D=fcn\left(P_{tm}(z,t)\right) \tag{2.7}$$

Given this algebraic model the chain rule can be used to expand the partial time derivative of diameter in terms of the transmural pressure as given by (*2.8*).

$$\frac{\partial D}{\partial t}=\frac{dD}{dP_{tm}}\frac{\partial P_{tm}}{\partial t} \tag{2.8}$$

The expression in (*2.8*) can be substituted into (*2.4*) leaving a simplified continuity equation as given by (*2.9*).

$$\frac{\partial P_{tm}}{\partial t}+\left(\frac{D}{2}\right)\left(\frac{dP_{tm}}{dD}\right)\frac{\partial U}{\partial z}=0 \tag{2.9}$$

The transmural pressure acting across the tube wall is defined as the difference between the internal pressure P_i, and external pressure P_{ex} as given in (*2.10*).

$$P_{tm}=P_i-P_{ex} \tag{2.10}$$

Substituting the definition of transmural pressure into the partial time derivative term in (*2.9*) and under the assumption that the external pressure is constant simplifies the continuity equation further as given by (*2.11*).

$$\frac{\partial P_i}{\partial t}+\left(\frac{D}{2}\right)\left(\frac{dP_{tm}}{dD}\right)\frac{\partial U}{\partial z}=0 \tag{2.11}$$

Although alternative models describing the relationship presented in equation (*2.7*) will be considered in Section 2.3 the remainder of this analysis assumes that the elastic tube is thin walled and the wall material is a linear elastic solid that obeys Hooke's law. The circumferential strain ε, in a tube wall experiencing small changes in the inner tube diameter D is given by (*2.12*).

$$\varepsilon=\frac{dD}{D} \tag{2.12}$$

The wall strain induces a change in incremental tension dT, across the wall as given by (*2.13*) where E is the Young's modulus of the wall and h is the wall thickness.

$$dT=hE\varepsilon=hE\frac{dD}{D} \tag{2.13}$$

An equilibrium condition requires the tension in the wall be balanced by a change in the transmural pressure acting across the wall this balance is given by (*2.14*).

$$2hE\frac{dD}{D}=DdP_{tm} \tag{2.14}$$

This balance leads to the useful expression given by (*2.15*).

$$\frac{dP_{tm}}{dD}=\frac{2hE}{D^2} \tag{2.15}$$

The expression in (*2.15*) can be substituted into the continuity equation given in (*2.11*) deriving a new expression which is given in (*2.16*).

$$\frac{\partial P_i}{\partial t} + \frac{hE}{D}\frac{\partial U}{\partial z} = 0 \tag{2.16}$$

The final wave equation describing pressure propagation in the tube can be developed by taking the partial derivative of equation (*2.6*) with respect to the axial coordinate *z*, and by taking the partial derivative of equation (*2.16*) with respect to time and then equating the mixed partial derivatives to combine these equations as given by (*2.17*).

$$\frac{\partial^2 P_i}{\partial z^2} - \left(\frac{\rho D}{hE}\right)\frac{\partial^2 P_i}{\partial t^2} = 0 \tag{2.17}$$

The expression in (*2.17*) is an example of the well known wave equation (*2.18*).

$$\frac{\partial^2 P_i}{\partial z^2} - \left(\frac{1}{c^2}\right)\frac{\partial^2 P_i}{\partial t^2} = 0 \tag{2.18}$$

The definition of wave speed *c*, in the elastic tube is given in (*2.19*). This expression is the famous Moens-Korteweg equation.

$$c = \sqrt{\frac{hE}{\rho D}} \tag{2.19}$$

An alternative expression for the velocity of wave propagation (*c*) in an elastic tube can be developed from the Moen-Korteweg equation [11] or based on the analysis of sound wave propagation in air which was first studied by Isaac Newton. Newton's equation is given in (*2.20*) where *B* is the bulk modulus and ρ the density of the fluid.

$$c = \sqrt{\frac{B}{\rho}} \tag{2.20}$$

Substituting the definition of the bulk modulus into (*2.20*) for a tube with cross-sectional area *A*, and unit length provides an alternative equation for wave propagation in an elastic tube as given in (*2.21*).

$$c = \sqrt{\frac{A}{\rho}\frac{dP_{tm}}{dA}} \tag{2.21}$$

2.3 BLOOD PRESSURE & ARTERIAL PULSE WAVE VELOCITY

Although the derivation presented in section 2.2 provides a framework for studying arterial pulse wave propagation it relies on a number of assumptions that are clearly violated by the vessels of the arterial system. In fact, these vessels are finite in length which results in wave

reflection; they demonstrate viscoelastic behavior including hysteresis, stress relaxation, and creep that suggests the need for a dynamic model, and exhibit pressure dependent non-linear elasticity, a characteristic exploited for non-invasive pressure estimation using pulse wave velocity. Additionally, blood is a viscous, non-Newtonian fluid, these fluid properties along with the damping characteristics of the viscoelastic vessel wall may cause attenuation of the pressure pulse as it propagates along the arterial path.

In this section the effects that these non-ideal behaviors have on wave propagation in the ulnar and common digital arteries will be considered and operating conditions given for when these behaviors can be neglected.

Perhaps the most important behavior of the arteries that must be reflected in our model is the non-linear relationship that exists between arterial blood pressure and the elasticity of the arterial wall. The stress-strain relationship of the arterial wall is a complex three-dimensional function. However, this function can be simplified and reduced down to two dimensions by considering only mean stresses in the vessel wall and by neglecting any transverse shear stresses [39]. The following discussion is based on the use of a two dimensional model given these assumptions.

The static elastic modulus (E), of the arterial wall in both human and canine arterial segments has been experimentally studied both *in vivo* and *in vitro* [23,26,27,28]. Based on these studies two leading empirical relationships have been presented to described the pressure dependence of the static elastic modulus.

Langewouters [28] developed a three parameter arctangent model to describe the relationship between arterial cross-sectional area (A) and transmural pressure (P_{tm}) in the abdominal and thoracic aorta of humans as given in (*2.22*) where A_m is the maximal vessel area, P_0 is the pressure at maximum compliance, and P_1 is the pressure when the compliance is equal to half its maximum value.

$$A(P_{tm}) = A_m\left[\frac{1}{2}+\frac{1}{\pi}\arctan\left(\frac{P_{tm}-P_0}{P_1}\right)\right] \tag{2.22}$$

This equation is based on the observation that the incremental Young's modulus increases with pressure according to a second order polynomial function as given in (*2.23*).

$$E=\frac{1}{C}=\frac{dP_{tm}}{dA}=a+bP_{tm}+cP_{tm}^2 \tag{2.23}$$

Experimental results presented by Gizdulich [27] characterizing the pressure-volume relationship in the arteries of the forearm show that the model described by (*2.22*) can be used to represent the relationship between pressure and cross sectional area in these arteries. Experimental results by Langewouters [26] characterizing the pressure-diameter relationship in the arteries of the finger, also qualitatively demonstrated the behavior predicted by these equations.

The relationship in (*2.22*) can be combined with the definition of pulse wave velocity given by equation (*2.21*) to provide an expression for arterial pulse wave velocity as given by (*2.24*).

$$c = \sqrt{\frac{1}{\rho}\left[\frac{1}{2} + \frac{1}{\pi}\arctan\left(\frac{P_{tm} - P_0}{P_1}\right)\right]\frac{dP_{tm}}{dA(P_{tm})}} \tag{2.24}$$

Although, none of the aforementioned authors provided a comparison between actual pulse wave velocity measurements in these arteries and pulse wave velocity values predicted using the model described in (*2.24*), they do provide empirical observations about the static elastic modulus of the arteries monitored by our device and they provide insight regarding the behavior of pulse wave velocity at zero transmural pressure in these arteries.

A popular and more tractable alternative expression for the static elastic modulus (E) of the arterial wall was developed by Hughes et al [23] based on experimental observations of the canine thoracic and abdominal aorta both *in vivo* and *in vitro*. In their experimental procedure the arterial diameter and wall thickness were measured using intravascular ultrasound and pulse wave velocity was measured using two catheter tip pressure sensors spaced a known distance apart. Their observations suggested an empirical relationship for the elastic modulus of the form given by (*2.25*).

$$E = E_0 \exp(aP_{tm}) \tag{2.25}$$

Hughes showed that the elastic modulus values derived from the canine aorta demonstrated a correlation coefficient in excess of 0.95 with values predicted using the model in (*2.25*) when estimated with mean distending pressure measurements.

Hughes derived the expression for elastic modulus of the *in vivo* aorta based on the Moens-Korteweg equation given by (*2.19*). The two equations can be combined to describe a relationship between pulse wave velocity and arterial blood pressure [11] as given by (*2.26*).

$$c = \sqrt{\frac{hE_0}{\rho D}\exp(aP_{tm})} \tag{2.26}$$

This equation suggests that arterial pulse wave velocity increases exponentially with an increase in transmural pressure. However, this exponential relationship is only valid for transmural pressure values equal to or greater than zero and may not provide physiologically meaningful pulse wave velocity predictions for transmural pressures below zero.

Although the Hughes model was not derived from peripheral arteries as was the Langewouters model, the two models predict very similar behavior in regards to the pressure cross-sectional vessel area relationship of the artery and the pressure pulse wave velocity relationship of the arterial wall as shown in Figure *2-2*. Since both models describe similar behavior, the Hughes model which provides a more tractable mathematical expression than the Langewouters model will be used to characterize the static elastic modulus of the peripheral arteries in our lumped parameter model. However, predictions made with the Hughes model may not be valid for extremely negative transmural pressure values.

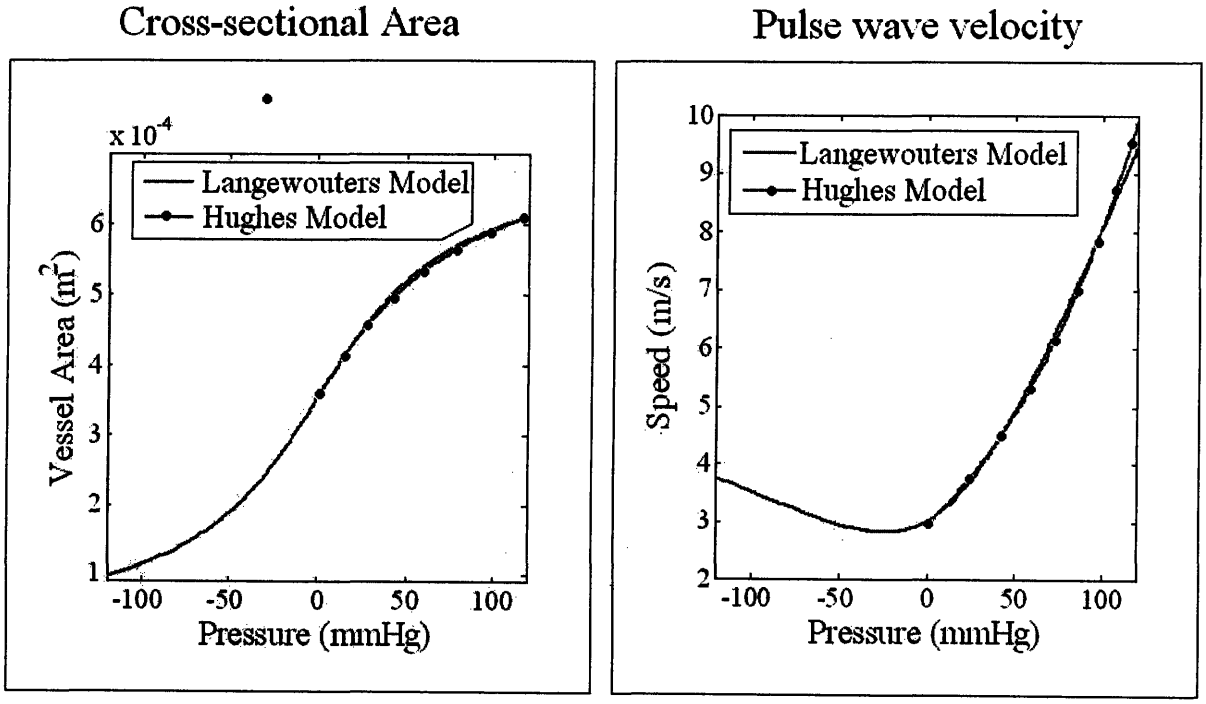

Figure 2-2. A comparison of the vessel area and the pulse wave velocity predicted by the Langewouters Model & the Hughes Model

In addition to the exponential pressure dependence of the elastic modulus, both the wall thickness h, and inner vessel diameter D, are pressure dependent terms. However, their ratio (h/D) can be shown to be relatively constant across a wide physiologic range of transmural pressures. The diameter, D in (*2.26*) refers to the inner diameter of the vessel, which we will now refer to as D_i. The wall thickness can be defined in terms of the inner vessel diameter and the outer vessel diameter D_o as given in (*2.27*).

$$h = D_o - D_i \tag{2.27}$$

Substitution of this expression into the ratio (h/D) yields the equation given in (*2.28*).

$$\frac{h}{D} = \frac{D_o - D_i}{D_i} = \left(\frac{D_o}{D_i}\right) - 1 \tag{2.28}$$

The effect that transmural pressure has on the ratio of outer vessel diameter to inner vessel diameter may be examined given the assumption that the vessel wall volume remains constant as the vessel diameters change throughout the physiologic blood pressure range [39]. The definition of vessel wall volume (V_w) for a unit length of vessel is given in (*2.29*).

$$V_w = \frac{\pi}{4}\left(D_0^2 - D_i^2\right) \tag{2.29}$$

Using equation (*2.29*) a comparison can be made between vessel diameters at time t_1 and vessel diameters at a different time t_2 as given in (*2.30*).

$$\frac{\pi}{4}\left(D_0^2(t_1) - D_i^2(t_1)\right) = \frac{\pi}{4}\left(D_0^2(t_2) - D_i^2(t_2)\right) \tag{2.30}$$

According to published data [11] the internal radial pulsation of the aorta during its transition between diastolic pressure and systolic pressure (~50 mmHg) is between 3-4%. The arterial walls of peripheral arteries such as the ulnar artery and common digital artery are less compliant than the aortic wall [22] therefore we would expect the internal radial pulsation in these arteries to be even smaller. Given the non-linear behavior of the arterial wall a liberal estimate of the total radial pulsation in these arteries as transmural pressure varies across the operating range of our device is approximately 10%. Under this assumption a relationship can be defined between the minimum inner vessel diameter ($D_{i,min}$) and maximum inner vessel diameter ($D_{i,max}$) as given in (*2.31*).

$$D_{i,\max} = 1.1 D_{i,\min} \tag{2.31}$$

Substituting this expression into equation (*2.30*) and equating the vessel wall volume at the maximum and minimum diameters allows derivation of an expression for the maximum outer vessel diameter as given in *(2.32)*.

$$D_{o,\max} = \sqrt{D_{o,\min}^2 - 0.21 D_{i,\min}^2} \tag{2.32}$$

Using a mean value for ulnar artery diameter ($\overline{D}_{i,\min} = 2.5mm$) [21] and assuming an ulnar artery wall diameter-thickness ratio of 12 ($D_i/h = 12$) for the minimum diameter similar to the radial artery [29] using (*2.31*) and (*2.32*) we can calculate the outer to inner diameter ratios as given in (2.33). The percent change between the two ratios is less than one percent.

$$\frac{D_{o,\max}}{D_{i,\max}} = 1.07 \qquad \frac{D_{o,\min}}{D_{i,\min}} = 1.08 \tag{2.33}$$

Therefore this ratio may be assumed constant with respect to transmural pressure with very little loss in accuracy using the model described in (*2.26*).

Along with nonlinear elasticity, the arterial wall demonstrates viscoelastic behaviors including hysteresis, and stress relaxation. This suggests that a dynamic equation is required to characterize the behavior of the arterial wall. Hysteresis is observed in the pressure-volume relationship in the artery. Therefore the arterial pressure and its corresponding arterial volume depend on whether the arterial pressure is increasing or whether it is decreasing. The plot in Figure *2-3* depicts the hysteresis that is observed between the arterial blood pressure, measured with a Finapres BP monitor, and the measured volumetric PPG signal during one cardiac cycle. The sample frequency was 1 kHz.

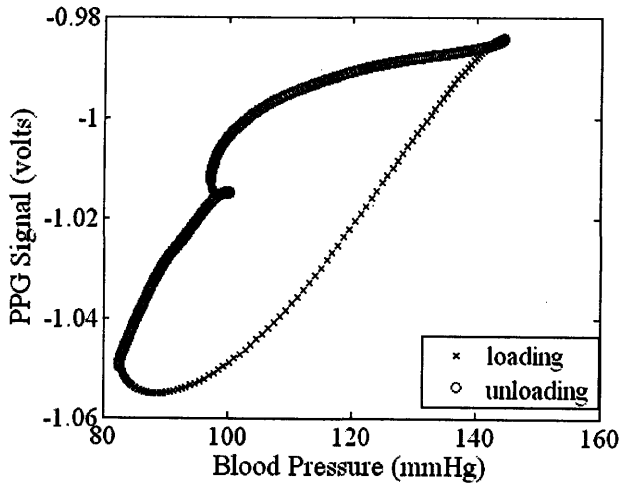

Figure 2-3. Hysteresis observed between blood pressure and volume in one cardiac cycle of a PPG waveform

The pulse wave speed equation given in (*2.21*) shows that PWV is dependent on arterial volume, therefore this equation suggests that the relationship between pulse wave velocity and pressure may exhibit hysteresis and a dynamic equation may be necessary to characterize the magnitude of its effects on our pressure dependent pulse wave velocity as we load and unload the artery using height variation. The effect of this loading and unloading in the pressure-pulse wave velocity relationship was determined experimentally. Pulse wave velocity measurements were taken using our in-line PPG device while diastolic blood pressure was measured simultaneously using the Finapres blood pressure monitor attached to the index finger. During the experiment the height of the sensor measurement points were adjusted by raising and lowering the arm to alter intravascular hydrostatic pressure. A typical result of these experiments is given in Figure *2-4*. Although the figure depicts some variation in PTT due to the inherent transit time measurement error using our in-line PPG sensors, hysteresis was not observed between the measured pulse transit time and diastolic blood pressure as the artery was loaded and unloaded. These experimental results suggests that the dynamic behavior of the arterial wall may be neglected when characterizing the behavior of pulse transit time induced by the loading and unloading of the wall as intravascular arterial pressure is altered by height variation during device calibration.

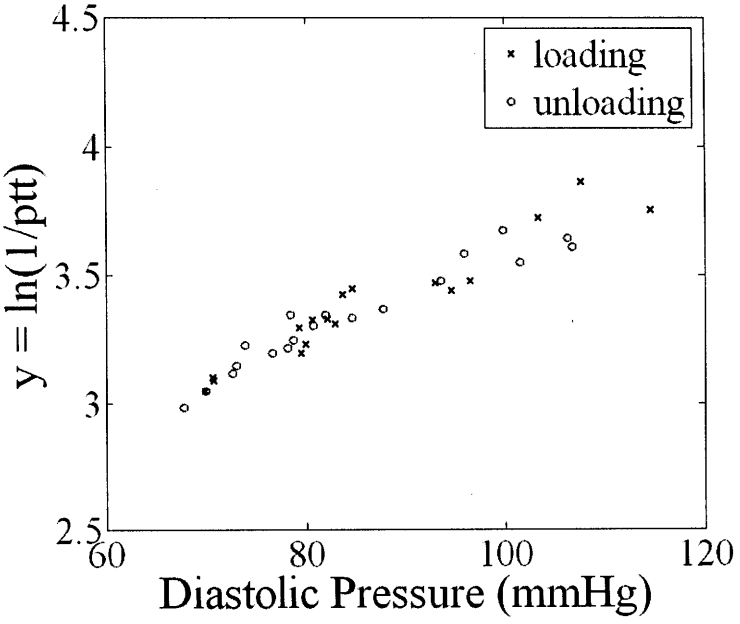

Figure 2-4. Evaluating hysteresis between BP & PTT: experimental observation of intra-vascular pressure loading and unloading on pulse transit time measurements.

In addition to hysteresis, the viscoelastic arterial wall also exhibits the phenomenon of stress relaxation. Therefore any stress imposed in the arterial wall under a constant strain will diminish over time. The result of this behavior is that changes in intravascular volume produced by altering the height of the sensor measurement point may remain constant but the instantaneous arterial pressure may diminish over time if the height is held constant. Since we have shown that the wall thickness – vessel diameter ratio in our model may be considered to be relatively constant over wide pressure ranges stress relaxation should not be a large issue. Despite the assumed insensitivity in our model, the effects of stress relaxation in the arteries underlying our sensors may be considered in the design of a height variation protocol used to identify the parameters of our device model.

To understand the impact of stress relaxation, a stress relaxation model describing the stress T, in the arterial wall in response to a step change in strain [39] is given in (*2.34*) where $T^{(e)}$ is a function of strain or wall stretch ratio λ.

$$T(t,\lambda) = G(t) * T^{(e)}(\lambda) \tag{2.34}$$

The normalized relaxation function $G(t)$ in (*2.34*) is defined as given in (*2.35*). This function with constants $\Re$ and d has been shown to be a useful approximation for times less than 100 seconds.

$$G(t) = \Re \log(t) + d \tag{2.35}$$

Since the stress in the arterial wall is directly proportional to the transmural pressure acting across it the stress variables T and $T^{(e)}$ can be replaced with corresponding transmural pressure terms P_{tm} and $P_{tm}{}^{(e)}$ as given in equation (*2.36*).

$$P_{tm}(t,\lambda) = (\Re \log(t) + d) P_{tm}{}^{(e)}(\lambda) \tag{2.36}$$

Based on experimental observation [39] the decay of the normalized relaxation function requires on the order of 100 seconds. Thus the effect of these slow dynamics may be neglected in our parameter identification by choosing a height variation frequency that is an order of magnitude faster than this time period (T~10-15 seconds).

Based on the previous analysis our device model will assume that the dynamics of the viscoelastic arterial wall are negligible.

In addition to neglecting the viscoelastic properties of the arterial wall, derivation of the Moens-Korteweg equation (*2.19*) assumes that the fluid in the tube is an inviscid liquid however

arterial wave propagation occurs in vessels filled with blood which is a non-Newtonian viscous fluid. The one dimensional wave model and the Moens-Korteweg equation remain valid representations of wave propagation in arteries where the Reynolds number and Womersley number are large. Under these assumptions boundary layer theory can be used to conform to the no-slip condition on the vessel wall imposed by a viscous liquid and still allow the ideal fluid assumption of our previous derivations. The definition of Reynolds number along with approximate values for the ulnar artery and common digital artery are given in (*2.37a*) and (*2.37b*) respectively. Note that flow velocity U is assumed to be the mean velocity during the cardiac cycle and that viscosity of blood is not fixed rather it is dependent on hematocrit (% of blood volume occupied by red blood cells) and shear rate.

$$\mathrm{Re} = \frac{\rho U D}{\mu} = \frac{\left(1060\frac{kg}{m^3}\right)\left(0.20\frac{m}{s}\right)\left(\frac{2.5}{1000}m\right)}{3.4\times10^{-4}\,Pa\cdot s} \approx 1600 \qquad (2.37a)$$

$$\mathrm{Re} = \frac{\rho U D}{\mu} = \frac{\left(1060\frac{kg}{m^3}\right)\left(0.20\frac{m}{s}\right)\left(\frac{1.5}{1000}m\right)}{3.4\times10^{-4}\,Pa\cdot s} \approx 950 \qquad (2.37b)$$

The definition of Womersley number along with approximate values for the ulnar artery and common digital artery are given in (*2.38a*) and (*2.38b*) respectively.

$$\alpha = D\left(\frac{\omega\rho}{\mu}\right)^{1/2} = \left(\frac{2.5}{1000}m\right)\left(\frac{\left(2\pi\frac{rad}{\sec}\right)\left(1060\frac{kg}{m^3}\right)}{3.4\times10^{-4}\,Pa\cdot s}\right)^{1/2} \approx 11.1 \qquad (2.38a)$$

$$\alpha = D\left(\frac{\omega\rho}{\mu}\right)^{1/2} = \left(\frac{1.5}{1000}m\right)\left(\frac{\left(2\pi\frac{rad}{\sec}\right)\left(1060\frac{kg}{m^3}\right)}{3.4\times10^{-4}\,Pa\cdot s}\right)^{1/2} \approx 6.6 \qquad (2.38b)$$

According to Fung [21] as the Reynolds number and/or Womersley number approach 1 or drop below 1 viscosity must be taken into account. Based on the values presented above for these dimensionless parameters it appears that the ideal fluid assumption is valid in these arteries. However, there is not a clear distinction or threshold between when the ideal fluid theory is valid and when viscous effects begin to play a role and some consideration should be

made to understand the potential errors that neglecting their effects could have on our pulse wave propagation model.

In addition to the viscous effects of the fluid, energy dissipation will also occur in the propagating wave due to the viscoelastic arterial wall [21]. The potential results of these two sources of energy dissipation are a reduction in pressure magnitude along the length of the vessel such that intravascular pressure along the length of the artery between the two sensors is not constant $\frac{\partial P_{bp}}{\partial z} \neq 0$ and/or a deceleration of the propagating pulse wave as it travels along the artery such that wave speed is not constant in the arterial segment between the two sensors. Because of the short transit distance between the two pulse waveform sensors in our device and the minimal dissipation predicted by the values in equations (*2.37*) and (*2.38*) these phenomenon will be neglected in our pulse wave speed model.

The final assumption that must be removed from equation (*2.19*) when considering arterial wave propagation is that the vessels are finite in length. This finite length results in pressure pulse wave reflection at locations having an impedance mismatch such as the arterioles. Therefore intravascular pressure at any point P is a result of the superposition of incident pressure waves P_{IN}, and reflected pressure waves P_{RE} as given in (*2.39*).

$$P = P_{IN} + P_{RE} \tag{2.39}$$

A central problem associated with wave reflection is that the measured pulse waveform at any location along the artery is the result of an interference pattern created by the superposition of incident and reflected pressure waves as they propagate throughout the arterial tree. Therefore, a specific waveform feature e.g. maximum value, in the measured waveform is not representative of either the incident or reflected waveform alone. The two primary implications of this phenomenon are that the pulse transit time and pulse wave velocity estimated from two measured waveforms could represent an apparent pulse wave velocity (c') not the actual pulse wave velocity (c) described in (*2.26*) and this apparent pulse wave velocity would be frequency dependent.

A simple solution to this problem is to calculate pulse transit time measurements using only the wave front or leading edge of the waveform prior to the arrival of any reflected waves at the measurement site. The wave front velocity during this initial period is representative of the actual pulse wave velocity that is governed only by the properties of the arterial wall and has

pressure dependence described by the expression in (*2.26*). This solution assumes that the reflected and re-reflected waves have been attenuated to a negligible magnitude at the onset of the new pulse wave at our measurement site. Implementation of this method will be described further in chapter 4. An interesting aspect of our device is that due to the peripheral location of our sensor the time difference between incident waveform onset and arrival of the reflected pressure wave will be very brief. Assuming a reflection site in the finger tip (*~5 cm*) and a pulse wave velocity of 7 m/s, this time difference may be as brief as 7 milliseconds for the waveform measured by the ring PPG sensor.

2.4 A LUMPED PARAMETER MODEL

Based on the equations and analysis presented in the preceding sections a very simple pulse wave velocity model can be developed for our device. The pulse wave velocity through the arterial segment monitored by our device will be represented using the symbol '*pwv*'. The expression in equation (*2.26*) can be simplified using the assumption that the pulse wave velocity at zero pressure (pwv_0) is constant as given in equation (*2.40*).

$$pwv\left(P_{tm}=0\right)=\sqrt{\frac{E_0}{\rho}\frac{h}{D}}=pwv_0 \tag{2.40}$$

The expression in (2.26) can be further simplified by defining the constant parameter k as given in (*2.41*).

$$k=\frac{a}{2} \tag{2.41}$$

The expressions in equations (*2.40*) and (*2.41*) can be combined with (*2.26*) to form a lumped parameter model for pulse wave velocity in the peripheral arteries as given in (*2.42*).

$$pwv(t)=pwv_0\exp\left(k\cdot P_{tm}(t)\right) \tag{2.42}$$

The relationship between pulse wave velocity and the pulse transit time (denoted using the symbol '*ptt*') across an arterial segment of length Δz is given in equation (*2.43*).

$$ptt(t)=\frac{\Delta z}{pwv(t)} \tag{2.43}$$

The expression in (*2.42*) can be transformed into an expression using equation (*2.43*) to form a lumped parameter model between pulse transit time and transmural pressure as given in equation (*2.44*).

$$ptt(t) = ptt_0 \exp\left(-k \cdot P_{tm}(t)\right) \tag{2.44}$$

Where we have implicitly assumed the relationship, $ptt_0 = \frac{\Delta z}{pwv_0}$.

The internal arterial pressure can be written as the sum of the arterial blood pressure $P_{bp}(t)$ and the pressure from height variation $\rho gh(t)$ as given in equation (*2.45*).

$$P_i(t) = P_{bp}(t) + \rho gh(t) \tag{2.45}$$

The expression for transmural pressure given in (*2.10*), can be substituted into the lumped parameter model in equation (*2.44*) as given in equation (*2.46*), where we have developed a two parameter model for our device that relates measured pulse transit time to arterial pressure and height variation.

$$ptt(t) = ptt_0 \exp\left(-k \cdot \left(P_{bp}(t) + \rho gh(t) - P_{ex}\right)\right) \tag{2.46}$$

CHAPTER 3
INSTRUMENTATION DESIGN & DEVELOPMENT

The goal of this chapter of the thesis was to detail the design and development process used to build a potentially wearable prototype PTT device that could be adaptively calibrated using relative height variation. The requirement of the device was a set of peripheral in-line pulse waveforms sensors that could accurately measure the transit time of a pressure pulse as it propagated between them and were co-located in a manner that the underlying pressure at the measurement site could be varied through vertical height change using natural human motion. Additionally, a sensor had to be developed to determine the height of the measurement site relative to the heart.

The main issues that are addressed in this chapter include; selection of a set of non-invasive pulse waveform transducers, development of an understanding of the operating principle of the transducers and their circuit requirements, selection of the optimal peripheral sensor locations based on a set of established criteria, evaluation of the effect of pulse transit distance on the operation of the device, design of the sensor housings used by the waveform sensors, and development & evaluation of an accelerometer based height sensor.

3.1 THE PHOTOPLETHYSMOGRAM

There are 3 primary transduction mechanisms that can be used to measure a non-invasive peripheral pulse waveform all three of these mechanisms are based on measurement of the time varying volumetric change (plethysmography) produced in the blood vessels underlying the sensor measurement site. The three mechanisms include; electrical impedance plethysmography (EIP), photoplethysmography (PPG), and skin surface plethysmography in which volumetric pulsations at the skin surface are measured with an external pressure transducer.

The photoplethysmogram (PPG) whose operation relies on two main components, a photodetector and a light emitting diode or LED, was selected as the pulse transducer used in our device. The decision to select this transducer was based on a number of features that it offered. Because both the LED and the photodetetctor are compact in size the PPG provides a localized pulse waveform that can be derived from a specific artery. The compact size allows the sensor to

be very small and unobtrusive and allows a narrow spacing between the in-line sensors which provides the capability to measure pulse transit time across a very short transit path. The arterial specificity allows us to measure volumetric variations in just a single target artery of our choice. The PPG provides pulse waveform signals that have a very high signal to noise ratio, an important feature for detecting subtle timing differences across a short transit path. The components required by the PPG sensor are extremely light weight and consume very little power. The typical operation current required by the LED is around 15-30 milliamps and both components can be supplied with a low voltage source on the order of 5 volts. The components of the PPG are also low cost, a medical grade LED and photodiode can each be purchased for less than $10.

The operating principle of the PPG transducer can be described using the cross-sectional sketch of the finger shown in Figure *3-1*.

The LED transmits a light of intensity I_0, and wavelength λ, into the tissue of the finger. The light passes through the finger and arrives at the photodetector with an intensity $I(t)$ that is less than the initial value emitted from the LED. This incident light causes a current flow in the photodiode that is converted to voltage using a trans-impedance amplifier. The amount of current flow depends on the surface area of the photodiode, and the intensity and wavelength of the light reaching the photodetector. The intensity level of light that reaches the photodetector can be described by the Beer-Lambert Law [31] which is given in equation (*3.1*), where α is the absorption coefficient of the material, l is the path length, and c the concentration of the absorbers in the light path.

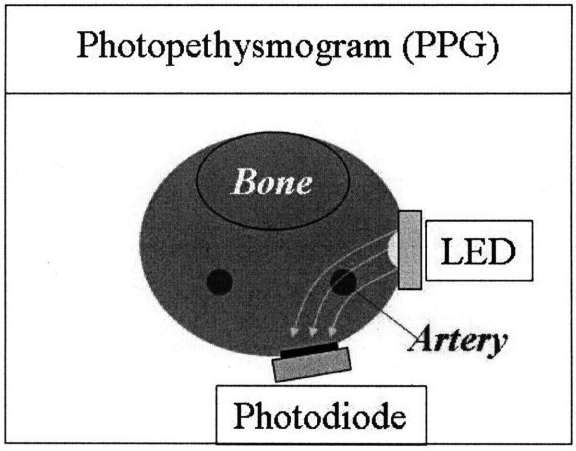

Figure 3-1. Operating principle of the PPG sensor applied to the digital artery of the finger

$$\%Transmission = 100 \cdot \left(\frac{I(t)}{I_0} \right) = 100 \cdot \exp(-\alpha lc) \qquad (3.1)$$

This equation reveals that the amount of light reaching the photodiode from the LED is inversely proportional to the arterial volume in the light path. Therefore as the arterial volume pulsates throughout the cardiac cycle so does the light intensity $I(t)$ and the voltage output from the transimpedance amplifier. The inverse relationship between a set of arterial blood pressure waveforms and the corresponding PPG signal is shown in Figure *3-2*.

The Beer-Lambert Law can be used to qualitatively explain the inverse relationship between arterial volume and the PPG signal. However, the actual intensity of light reaching the photodetector is governed by a much more complicated set of optical principles. Due to the heterogeneous composition of the tissue, optical effects such as scatter, reflection, and refraction affect the actual light intensity reaching the photodetector.

Each PPG sensor requires just three basic circuits. These three circuits include;

- A voltage controlled constant current circuit to power the LED
- A transimpedance amplifier circuit to convert photodetector current to measured voltage
- A low-pass filter to condition the measured voltage prior to data acquisition

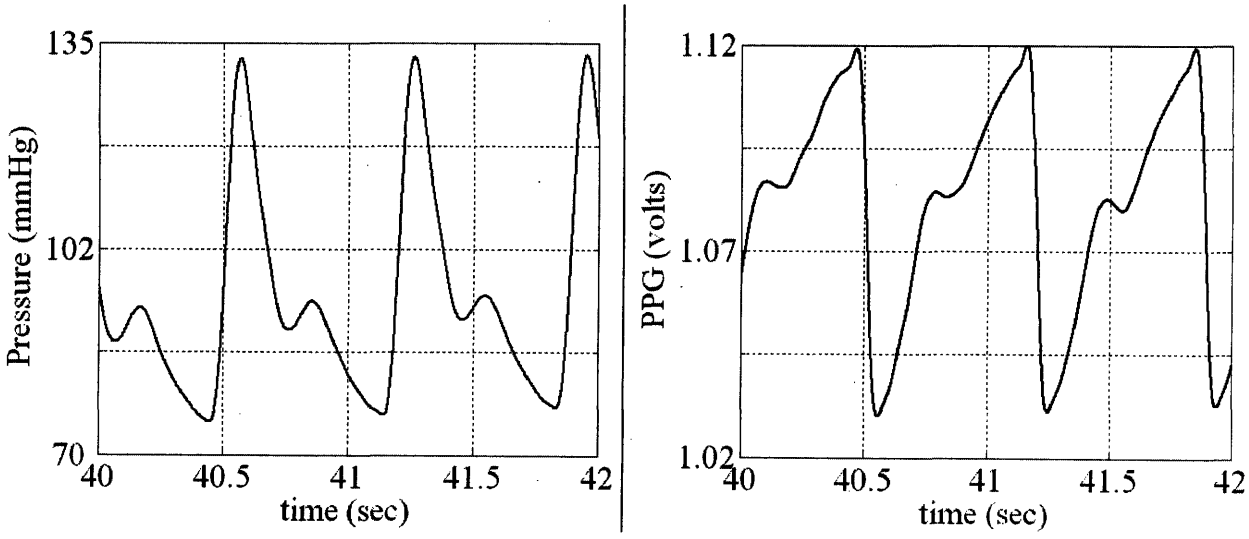

Figure 3-2. The measured PPG voltage signal is inversely proportional to the underlying arterial pressure waveform.

3.2 SENSOR MEASUREMENT SITE SELECTION

Based on our choice of the photoplethysmogram as the pulse transducer, two different questions had to be answered before building the prototype device. What peripheral arterial measurement sites should be monitored by our sensors and how closely can the sensors be spaced while maintaining the blood pressure estimation error below a prescribed threshold.

Potential arterial measurement sites for the PPG sensor include any location with a palpable artery that can be used to determine the pulse rate. The sites are generally locations where the artery lies close to the skin surface. Five different measurement sites were considered as potential sensor locations these sites included; A) the brachial artery at the bicep, B) the brachial artery just below the elbow joint, C) the radial artery at the wrist joint, D) the digital arteries in the finger, and E) the ulnar artery at the wrist joint. These locations are shown in Figure *3-3* along with the PPG sensors used to measure the signals.

The sensor sites were evaluated based on the following set of criteria; signal strength, does signal acquisition allows natural posture, ease of sensor placement, comfort, and wearability. PPG waveforms were measured at each of the locations.

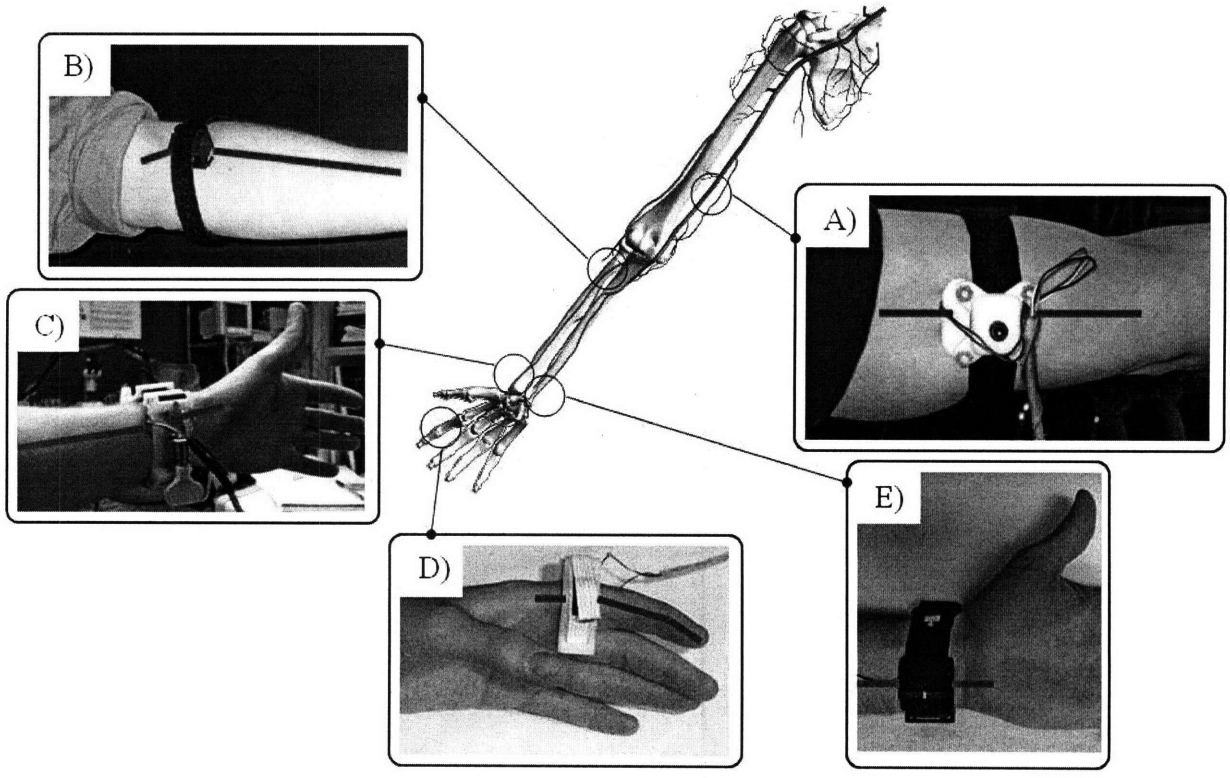

Figure 3-3. Potential PPG sensor site locations

Following extensive in lab human subject testing, which required the design and development of multiple prototype PPG sensor housings and attachment/pressurization mechanisms the sites were ranked based on these criteria. The ranking of the sites is shown in Table *3:1*, where 1 indicates the best potential PPG sensor location and 5 indicates the worst potential PPG sensor location.

Ranking	*Measurement Site*
1	D) Digital Artery at the finger
2	E) Ulnar Artery at the wrist
3	C) Radial Artery at the wrist
4	B) Brachail Artery at the elbow
5	A) Brachial Artery at the bicep

Table 3:1. Ranking of potential PPG sensor measurement sites (1 = best & 5 = worst)

Based on this analysis the optimal solution would be to co-locate the sensors along the digital artery of finger. However, a second important issue must be addressed regarding sensor site selection. What is the minimum length of the transit path between the two in-line sensors that would still allow accurate beat-to-beat blood pressure estimates? In other words, how close can we space the two in-line sensors, what are the limits of our current technology? The minimum transit distance is determined by two factors, the data sample rate required by the device and the PTT estimation error inherent in using in-line PPG sensors to determine the pulse transit time.

The sample rate required by our in-line device depends on the maximum pulse wave velocity, the length of the transit path, and the desired blood pressure resolution of the device. For example, to resolve the 1 *mmHg* pressure difference between 110 *mmHg* and 111 *mmHg* using pulse transit time measurements requires a specific pulse transit time resolution and the required resolution or sample rate will depend on the transit distance between the two sensors. Given some typical model parameters, the required sample rate can be determined as a function of pulse transit distance. The required sample rate as a function of the transit distance needed to resolve the difference between 110 *mmHg* and 111 *mmHg* is shown in Figure *3-4*.

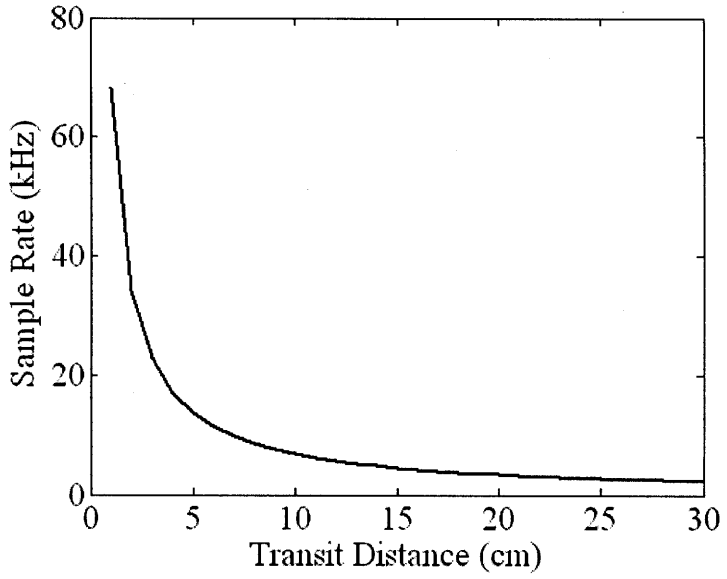

Figure 3-4. Required device sample rate as a function of transit distance.

We have assumed typical values for the model parameters, $k = 0.02$ mmHg^{-1} and $pwv_0 =$ 150 cm/sec. These pressure values were selected because they were assumed to lie at the extreme range of potential diastolic blood pressure values, where PWV would be at its maximum value. Based on the analysis shown in Figure 3-4, a 10 centimeter transit distance would require a sample rate of approximately 6.8 kHz and a transit distance of 1 centimeter would require a sample rate of 68.4 kHz. Given the clock speeds of today's microprocessors this sample rate is not a limiting factor in our design.

As a result of many different factors (e.g. signal noise, PPG shape variation, and physiologic parameter sensitivity) the pulse transit time values measured by our in-line PPG sensors will inherently contain some error. The influence that this error has on our ability to estimate blood pressure also depends on the transit distance between the two sensors. This is a trade-off that exists when using co-located in-line PPG sensors rather the traditional means of measuring PTT using and EKG sensor and a finger-tip PPG sensor which measures the pulse transit time across a very large distance.

The inherent pulse transit time error present when using in-line PPG sensors was determined experimentally using an ulnar artery PPG sensor and a digital artery PPG sensor. The experimental protocol was as follows. The ulnar artery PPG sensor and digital artery PPG sensor were attached to the test subject's left hand using an elastic band. Throughout the experiment the

subject's left hand was maintained in a stationary position resting on a table. A Finapres BP monitor was attached to the index finger of the left hand to provide continuous blood pressure measurements. PPG data and blood pressure data were measured continuously for approximately two minutes. At two different times during data acquisition a valsalva maneuver was performed to increase arterial blood pressure at the measurement site. Each of these maneuvers lasted approximately 5 seconds.

Prior to error estimation the PPG signals and blood pressure signal were filtered using a 4^{th} order butterworth low-pass filter with a cut-off frequency of 20 Hz. Pulse transit time was estimated from the PPG waveforms as the timing difference between the onset of the digital artery PPG waveform and the onset of the ulnar artery PPG waveform. A least squares identification technique was used to identify the model parameters $\hat{k}$ and $\hat{y}_0$ in equation (*3.2*) using the diastolic blood pressure $P_{bp}(t)$, estimated from the Finapres BP waveform and the measured pulse transit times. This linear formulation will be discussed in depth in Chapter 5.

$$\ln\left(\frac{1}{ptt(t)}\right) = \hat{k} \cdot P_{bp}(t) + \hat{y}_0 \tag{3.2}$$

Following identification, these two model parameters and the measured diastolic pressure were used to estimate the true pulse transit time (ptt_{true}) values as given in equation (3.3).

$$ptt_{true}(t) = \exp\left(-\hat{k} \cdot P_{bp}(t) - \hat{y}_0\right) \tag{3.3}$$

The inherent pulse transit time error in the in-line PPG sensors was estimated using the difference equation given in (*3.4*).

$$e(t) = ptt(t) - ptt_{true}(t) \tag{3.4}$$

A plot of the error estimated during a typical experiment is shown in Figure *3-5*. The mean pulse transit time error was 0.05 milliseconds and the standard deviation of the pulse transit time error was 1.6 milliseconds. This standard deviation value was representative of all three of the experiments performed to estimate PTT error and will be assumed to be the representative PTT error value in the remainder of this thesis. The mean error value was assumed to be zero milliseconds. This error analysis assumes that the Finapres BP measurement is representative of the true diastolic blood pressure. However, the Finapres BP may contain some error and the characterizing the effect of the Finapres error is outside the scope of this thesis.

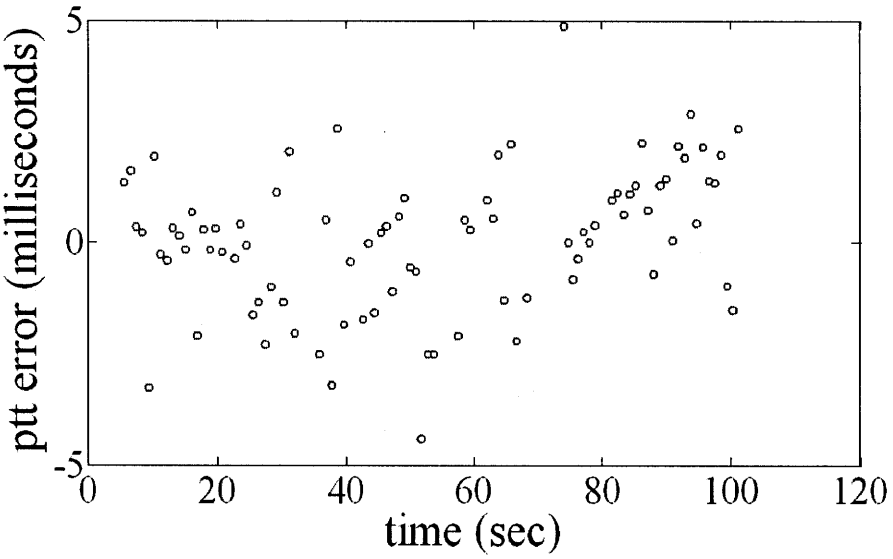

Figure 3-5. Estimated pulse transit time error measured between the ulnar artery and digital artery PPG sensors

Given this PTT error value an analysis was performed to determine the effect of transit distance on beat-to-beat blood pressure estimation error. In order to perform this analysis typical model parameter values were used; $k = 0.02\ mmHg^{-1}$, $pwv_0 = 150\ cm/sec$, and $P_{bp} = 77\ mmHg$. Using these model parameters and blood pressure a pulse wave velocity was determined for the artery as given in equation (*3.5*). This same PWV value was reported in McDonald's text [11] for the human radial artery based on experimental data.

$$pwv = 150\frac{cm}{\sec}\cdot\exp\left(0.02\frac{1}{mmHg}\cdot 77mmHg\right) = 700\frac{cm}{\sec} \tag{3.5}$$

For any given transit distance Δz, a true pulse transit time value could be estimated from this pulse wave velocity $ptt_{true} = \frac{\Delta z}{pwv}$. The estimated PTT error (σ_e =1.6 milliseconds) was added to the true pulse transit time determined for each transit distance. This augmented pulse transit time measurement was then used to estimate arterial blood pressure given the model parameter values listed above as given in equation (*3.6*).

$$\hat{P}_{bp} = \frac{1}{k}\left(\ln\left(\frac{1}{ptt_{true}+\sigma_e}\right) - \ln\left(\frac{pwv_0}{\Delta z}\right)\right) \tag{3.6}$$

The percent error between the actual and estimated blood pressure was determined using the expression given in equation (*3.7*).

$$\%\, P_{bp}\ Error = 100 \cdot \left(\frac{|\hat{P}_{bp} - P_{bp}}{P_{bp}} \right) \tag{3.7}$$

The results of this analysis are shown in Figure *3-6*. In order to determine a minimum transit distance for our sensors an error tolerance must be prescribed for our BP device. The British Society of Hypertension has developed a grading scale for NIBP monitors [38]. Their grading scale is shown in Table 3:2.

Grade	≤ 5 mmHg	≤ 10 mmHg	≤ 15 mmHg
A	60%	85%	95%
B	50%	75%	90%
C	40%	65%	85%
D	Worse than C		

Table 3:2. British Society of Hypertension's NIBP device grading scale

The error requirements for a grade "A" device demand that 60% of all the BP measurements made with the device fall within 5 mmHg of the true measurement. Achievement of this grade is nearly equivalent to the requirement that a standard deviation of the BP estimation error be less than or equal to 5 mmHg ($\sigma_{error} \leq 5$ mmHg).

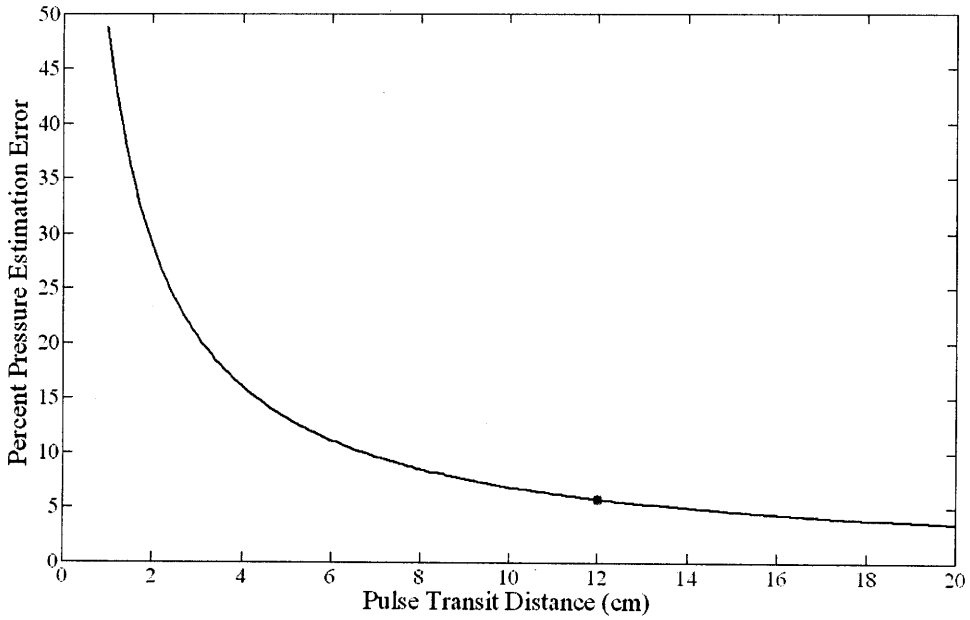

Figure 3-6. Blood pressure estimation error as a function of the transit distance between the in-line PPG sensors.

The transit distance at which the standard deviation of the error becomes greater than 5 mmHg is 10 centimeters. This analysis excludes co-locating the two sensors on the same finger ($\Delta z \sim$ 4-5cm), where the beat-to-beat estimation error would be approximately 10 mmHg. The next best alternative was to locate just one sensor at the digital artery and place the second sensor at the next highest rated location, the ulnar artery at the wrist. The transit distance between the sensor sites located at the ulnar artery and the digital artery at the base of the little finger is approximately 11-13 centimeters. The red dot indicates the average transit distance (12 cm) between the ulnar artery and digital artery PPG sensors. The standard deviation of the pressure estimation error at this distance is 5.8% which corresponds to 4.5 mmHg. This error is within the prescribed tolerance and these two sites will be selected for our device. The minimum sample rate required by the device at this distance is 6 kHz.

3.3 PPG SENSOR HOUSING DESIGN

There are four key factors that must be considered in the design of a PPG sensor used to measure arterial pulsations. These factors are the same regardless of PPG sensor measurement site.

- The angle between the photodetector and the LED
- The distance between the photodetector and the LED
- Pressurization of the sensor contact surface using tension (T) from a circumferential strap & sensor surface contact area
- LED intensity & the gain of the transimpedance amplifier

These four design elements are depicted graphically in Figure *3-7*.

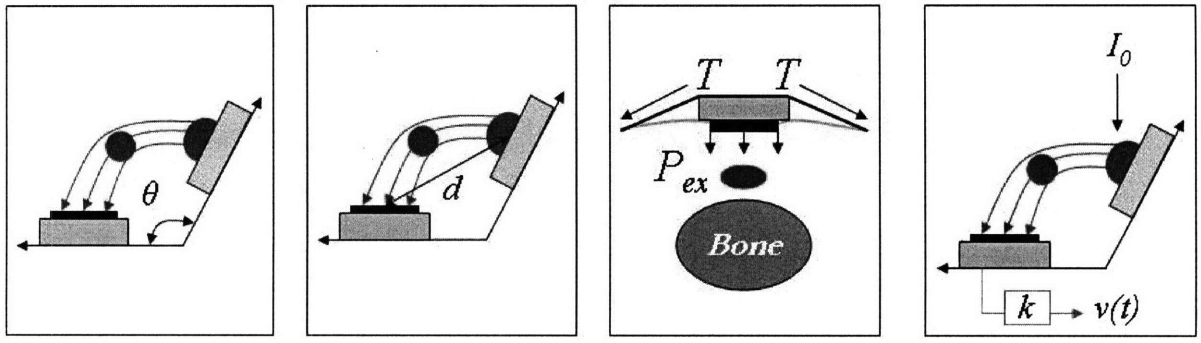

Figure 3-7. Key design elements used to develop a PPG sensor to measure arterial volume change

These design elements must be combined such that the PPG sensor has a high signal to noise ratio, the sensor housing can be easily attached and properly positioned by a wide variety of patients, and the sensor is comfortable and unobtrusive to the patient.

A timeline representing key events in development along with some of the major device prototypes is shown in Figure *3-8*.

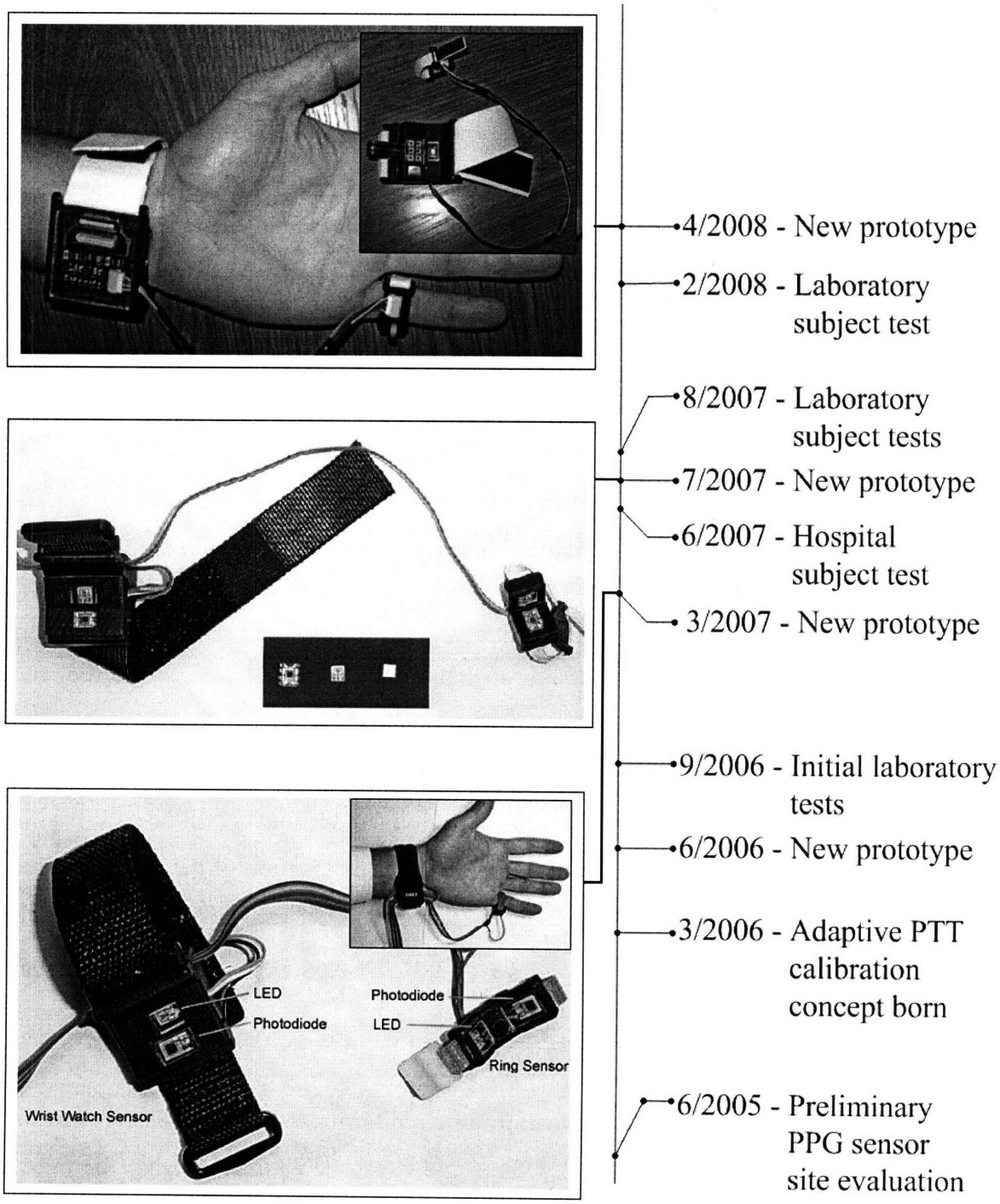

Figure 3-8. Timeline depicting milestones in prototype device design and testing.

The design of the ulnar artery and digital artery PPG sensors has been an iterative process performed throughout the course of the thesis and continues to evolve through laboratory human subject testing and based on new requirements imposed by the model identification algorithms. To date, the various prototype sensors have been successfully used to measure the effects of relative height variation on pulse transit time in over twenty different test subjects. These twenty test subjects have spanned a wide variety of sizes, from a 5'3" tall subject to a test subject that was 6'4" tall. They have included male and female subjects and test subjects from various races including Caucasian, Asian, and Latino patients. Additionally, the age of the test subjects has spanned a wide range from a 78 year female to a 22 year old male.

With each new prototype the four design parameters were altered to increase signal to noise ratio, minimize attachment issues, and improve comfort and wearability.

3.4 IMBEDDED HEIGHT MEASUREMENT SENSOR

The relative height of the device measurement site can be determined using a pair of 3-axis accelerometers, one located in the finger sensor housing and a second located at the bicep [32]. The concept of using a single 3-axis accelerometer imbedded in a wrist PPG sensor housing was explored as an alternative to the two accelerometer based height measurement methodology. The key assumption required to use a single 3-axis accelerometer to measure height is that the arm maintain a straight outstretched posture throughout the height change. A diagram of an arm and the key variables used in the single accelerometer based height estimation are shown in Figure *3-9*.

For simplicity the derivation of the height measurement technique will be described using just a single axis x, aligned along the length of the arm. The orientation of the other axes can be determined in a similar manner. The voltage output ($v_x(t)$) derived from the x-axis of the accelerometer in terms of the axis relative angle φ, to the gravity vector g is given in equation (*3.8*).

$$v_x(t) = M\cos\left(\varphi(t)\right) + v_0 \tag{3.8}$$

The values M and v_0 can be identified for our circuit prior to height measurement and are therefore assumed be known. The cosine of the angle φ can be estimated using the measured voltage output as given in equation (*3.9*).

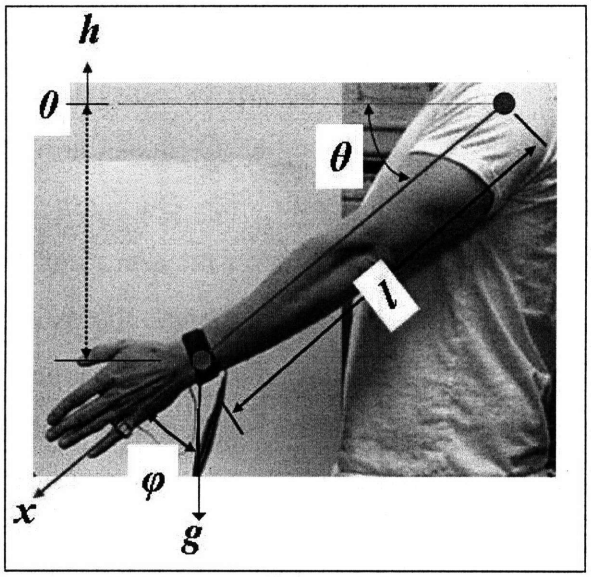

Figure 3-9. Diagram and variables used in single accelerometer height estimation.

$$\cos(\varphi(t)) = \frac{1}{M}(v_x(t) - v_0) \tag{3.9}$$

The height of the arm is given by the expression in equation (*3.10*) where *l* is the length of the arm between the pivot joint on the shoulder joint and the wrist sensor housing and the angle θ is shown in Figure *3-9*. The arm length *l* must be identified by having the patient initiate a known height variation prior to actual height estimation.

$$h(t) = l\sin(\theta(t)) \tag{3.10}$$

A simple geometric relationship exists between the two angles as given in equation (3.11).

$$\sin(\theta(t)) = -\cos(\varphi(t)) \tag{3.11}$$

The expressions in equations (*3.9*)-(*3.11*) can be combined to estimate the height of the wrist sensor using the x-axis accelerometer voltage as given in equation (*3.12*).

$$h(t) = -\frac{l}{M}(v_x(t) - v_0) \tag{3.12}$$

The other two axes can be used to adjust for error in the alignment of the x-axis accelerometer along the direction of the arm.

An experiment was performed in order to test the capability of our single accelerometer based height sensor. During the experiment data was collected from the 3 axis channels of the accelerometer. For reference, height was measured using a manometer type sensor that consisted

of an appropriate length of fluid filled elastic tubing connected to an external pressure sensor. The opposite end of the tubing was affixed to the wrist sensor housing. The pressure sensor was kept below the level of the wrist sensor housing at all times during the experiment. The wrist sensor was attached to the patient using an elastic strap. During the course of the experiment (~ 70 seconds) the patient was asked to raise and lower the arm to its highest and lowest position maintaining the elbow in a locked position and the arm in a fully extended straight posture.

The two sets of height measurements estimated during the experiment are shown in a plot in Figure *3-10*. The standard deviation of the error between the two height estimates was 2.1 cm which equates to about 1.6 mmHg. However, the majority of the error occurred between the two sensors at the extreme high and low values. This is likely caused by the non-ideal behavior of the shoulder joint at the extreme position where our assumption that the shoulder may be treated as a pin joint is no longer valid. If the patient's arm is kept away from these extremes during calibration the height measurement error is less than 1 mmHg and height measurement can be neglected as a source of error in our adaptive calibration procedure.

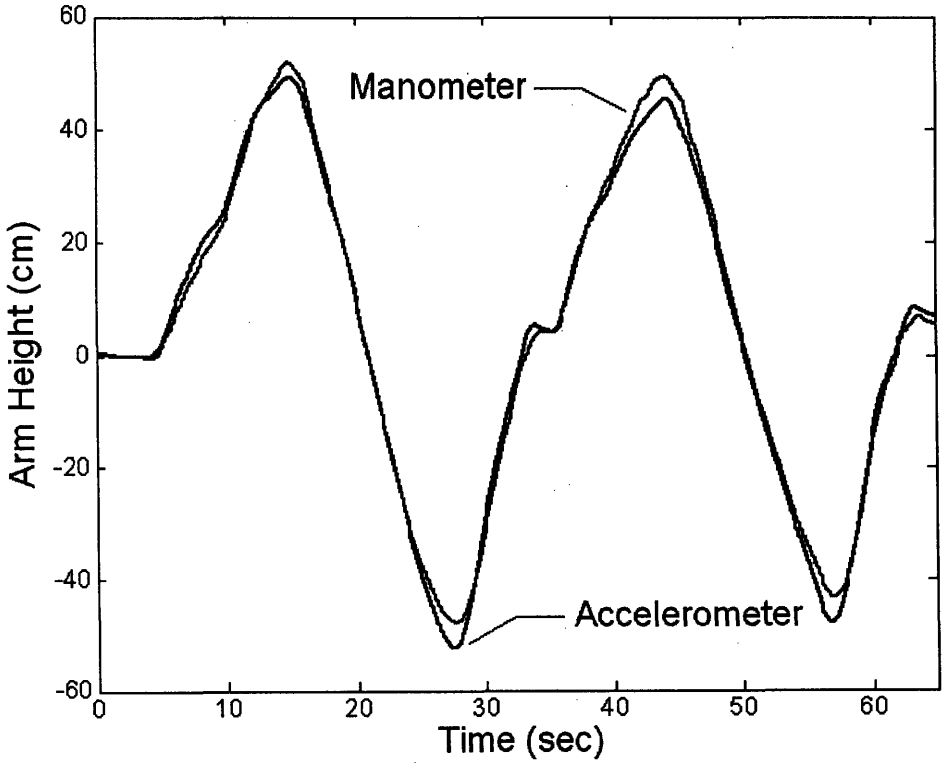

Figure 3-10. Comparison between height measurements made using a single 3-axis accelerometer imbedded in the wrist sensor housing and a manometer.

CHAPTER 4
PULSE TRANSIT TIME ESTIMATION

The goal of this chapter of the thesis is to describe the basic concepts and key elements that are involved when estimating pulse transit time from a pair of pulse waveforms. A review of the existing techniques that have been developed to estimate pulse transit time from blood pressure waveforms will be presented. The unique issues involved when estimating pulse transit time from a pair of PPG waveforms will be detailed. Finally, a few potential pulse transit time estimation techniques will be presented that may allow accurate PTT estimation using two PPG waveforms.

4.1 PULSE TRANSIT TIME ESTIMATION USING BP WAVEFORMS

Traditionally, the most common method of estimating pulse wave velocity using two blood pressure waveforms is to measure the time of travel of the "foot" of the wave over a known distance. The "foot" is defined as the point, at the end of diastole, when the steep rise of the next wave front begins [11]. The "foot" of the waveform is used because it is the portion of the transient waveform that is least affected by reflected waves, and thus is assumed to retain its identity largely unaffected by arterial pulse wave reflection. The model equations presented in Chapter 2 only apply to an incident pressure wave uncorrupted by reflection. Identifying the "foot" of the waveform with any precision especially when it is sampled at such high rates is difficult. Many techniques have been developed for identifying the arrival time of the "foot" of the blood pressure waveform. Some of the common methods include; estimating the arrival time of the waveform using the peak of the first derivative or peak of the second derivative of the waveform as the onset marker [11, 15, 33]. Another estimation technique involves extrapolating the wave front downward to an intersection with a straight line extrapolated from the last part of the diastolic curve [11]. The intersection of the two lines is used as an onset marker. Another technique utilizes a predetermined threshold as an onset marker, where the arrival time of the waveform is said to occur when the waveform reaches 1/5 of it total magnitude [11]. A final existing method used to estimate pulse transit time is performed by shifting the leading

waveform in time and estimating transit time as the time when the error between the two wave fronts is minimized [11]. These five techniques are summarized in Table *4:1*.

(1) Peak of the 1st derivative of the waveform

(2) Peak of the 2nd derivative of the waveform

(3) Intersection of extrapolated lines

(4) Threshold method

(5) Wave front minimization

Table 4:1. Common techniques used to estimate waveform arrival time for PTT estimation

4.2 PULSE TRANSIT TIME ESTIMATION USING PPG WAVEFORMS

Along with the superposition of incident and reflecting waves that complicate PTT estimation from the blood pressure waveform as discussed above, there are two additional sources of error when using PPG signals to estimate the transit time of the incident propagating wave they include signal noise and transmural pressure dependent waveform shape.

A common feature among the techniques presented above to mark waveform onset is that they depend on the shape of the pulse waveform therefore changes in the waveform shape will affect the location of the onset marker and influence the PTT measurement. The dependencies of these methods on waveform shape may cause errors when using PPG waveform signals to estimate PTT because the shape of the PPG waveform is not only determined by the arterial pulse wave but it is also influenced by the contact pressure being applied by the sensor housing to the underlying artery. Prior work has verified that contact force between the PPG photodiode and tissue will alter PTT estimates made using the ECG and PPG [33]. The loading conditions imposed by each of our PPG sensors will be unique and this difference may influence the estimated pulse transit time.

4.2.1 Technique dependent pulse transit time estimation

The pulse transit time value estimated from two in-line PPG sensors depends on the technique used to estimate waveform arrival time. This technique dependence results from the onset markers location on the wave front. The velocity of the propagating wave is pressure dependent, therefore as the arterial pressure increases throughout the systolic period of the cardiac cycle the velocity of the wave front will also increase. According to Nichols' text [11] if

the arterial transit path were long enough this pressure dependent wave velocity would eventually cause the propagating pressure wave to crest much like an ocean wave. Techniques that mark the onset of the waveform higher on the wave front will estimate a smaller pulse transit time due to the higher velocity of these regions. Another factor that influences the technique dependent pulse transit time is the unique shape of each of the measured PPG waveforms. The shape of the waveform is dependent on surface contact pressure being exerted on the tissue by the PPG sensor housing. The magnitude of this technique dependence is demonstrated using the two waveforms shown in Figure *4-1*.

The pulse transit times estimated using these three techniques are distinctly different in value. Selecting the waveform minimum as an indicator of arrival time produced the largest pulse transit time value, the second derivative peak located just above the minimum waveform value had the next largest PTT value and the peak of the first derivative which designated a point mid way up the wave front estimated the smallest pulse transit time value. The shape dependence of two derivative techniques can also be observed in Figure *4-1*. The location of the onset markers on each of the wave fronts is different and this shape dependence also contributes to the difference in estimated pulse transit time.

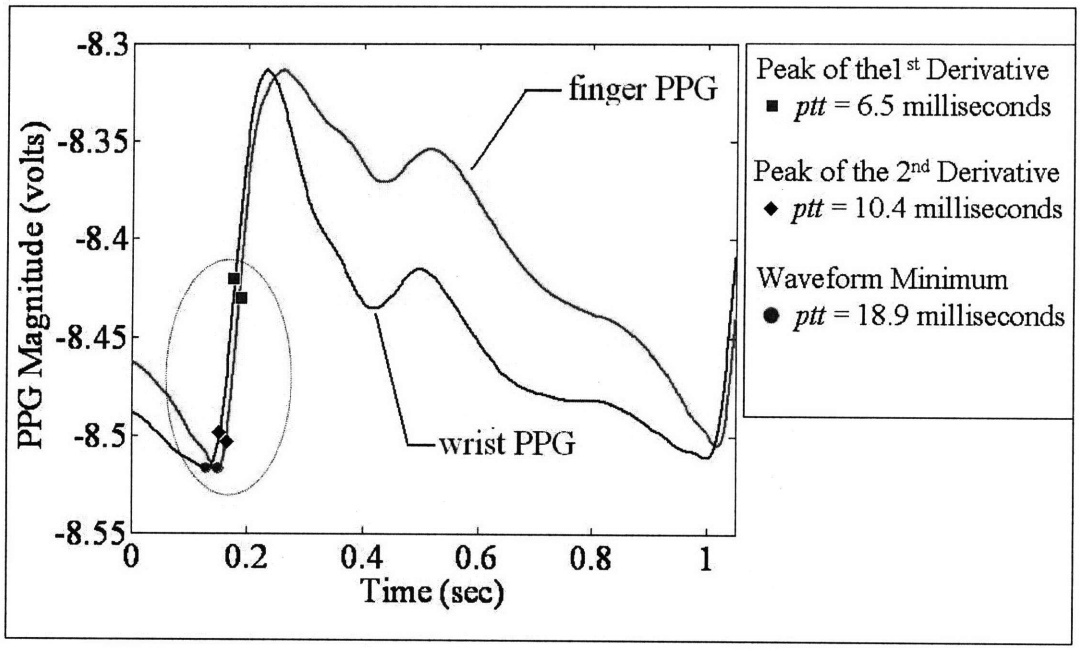

Figure 4-1. Estimated pulse transit time depends on the technique used to identify the arrival time of the PPG waveform.

Both the 1st and 2nd derivative marker on the wrist PPG signal occurs higher on the wave front than the corresponding markers on the finger PPG wave front this would phenomenon would also lead to a smaller estimated pulse transit time value using these techniques. This suggests that the onset markers should be selected at approximately the same level on each of the two wave fronts in order to accurately estimate the pulse transit time.

4.2.2 Understanding the External Pressure Dependence of the PGG Waveform

The appearance of the volumetric PPG signal is depends on 1) the shape of the arterial pressure waveform, 2) the magnitude of the arterial pressure pulse, and 3) the external pressure applied by the sensor housing. The primary mechanism through which these factors influence the shape of the PPG signal is through the non-linear arterial compliance. In order to accurately estimate the arrival time of the pressure pulse using the PPG waveform the effects that transmural pressure has on the identity of pressure waveform features in the measured PPG signal must be evaluated and understood. As a reminder, the transmural pressure acting across the arterial wall is given in equation (*4.1*), where P_{ex} is the external pressure acting on the artery. This external pressure is a function of the surface contact pressure applied by the PPG sensor housing.

$$P_{tm}(t) = P_{bp}(t) + \rho g h(t) - P_{ex} \tag{4.1}$$

The PPG signal is a measure of the volumetric pulsations in the artery over time. The arterial pressure-volume relationship is characterized by the non-linear arterial compliance of the vessel wall C_{wall}, which is dependent on the transmural pressure acting across the wall as given in equation (*4.2*).

$$C_{wall}\left(P_{tm}\right) = \frac{dV}{dP_{tm}} \tag{4.2}$$

A function describing the pressure dependent behavior of the non-linear arterial compliance is depicted in Figure *4-2*. This function was estimated using a model that was based on the sigmoidal pressure–volume relationship observed in the digital arteries of the finger [26]. This sigmoid model is given in equation (*4.3*).

$$V(t) = \frac{K}{1 + \exp\left(-aP_{tm}(t)\right)} \tag{4.3}$$

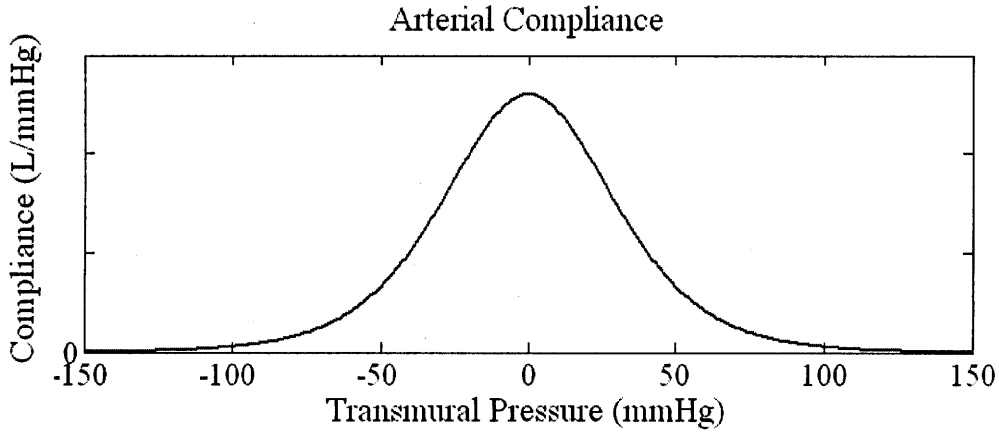

Figure 4-2. Pressure dependent behavior of the compliance of the arterial wall

This compliance model predicts that the maximum compliance value occurs at zero transmural pressure. Due to this non-linear compliance, when the mean arterial pressure value coincides with the zero transmural pressure point the volumetric pulsation in the underlying artery will reach its largest magnitude value and consequently the magnitude of the PPG signal will also reach its maximum value.

As a result of the non-linear arterial compliance the features of the pressure waveform are uniquely scaled, either exaggerated or attenuated, in the volumetric PPG signal depending on the transmural pressure value at which they occur. As the arterial pressure varies between its minimum diastolic and maximum systolic value, the range of transmural pressures spanned throughout the cardiac cycle depend directly on the external pressure imposed by the sensor housing.

Another mechanism through which external pressure can directly contribute to the appearance of the measured volumetric pulsation is through an upper pressure bound imposed on the artery by the external housing pressure. A distinction must be drawn between the contributions made to the PPG's appearance by the non-linear arterial compliance and the effects of waveform attenuation or clipping produced when the external pressure exceeds a certain threshold with respect to the internal arterial pressure. The illustration in Figure *4-3* displays how these two mechanisms may combine to determine the effective or observed magnitude of the pulsating arterial volume waveform.

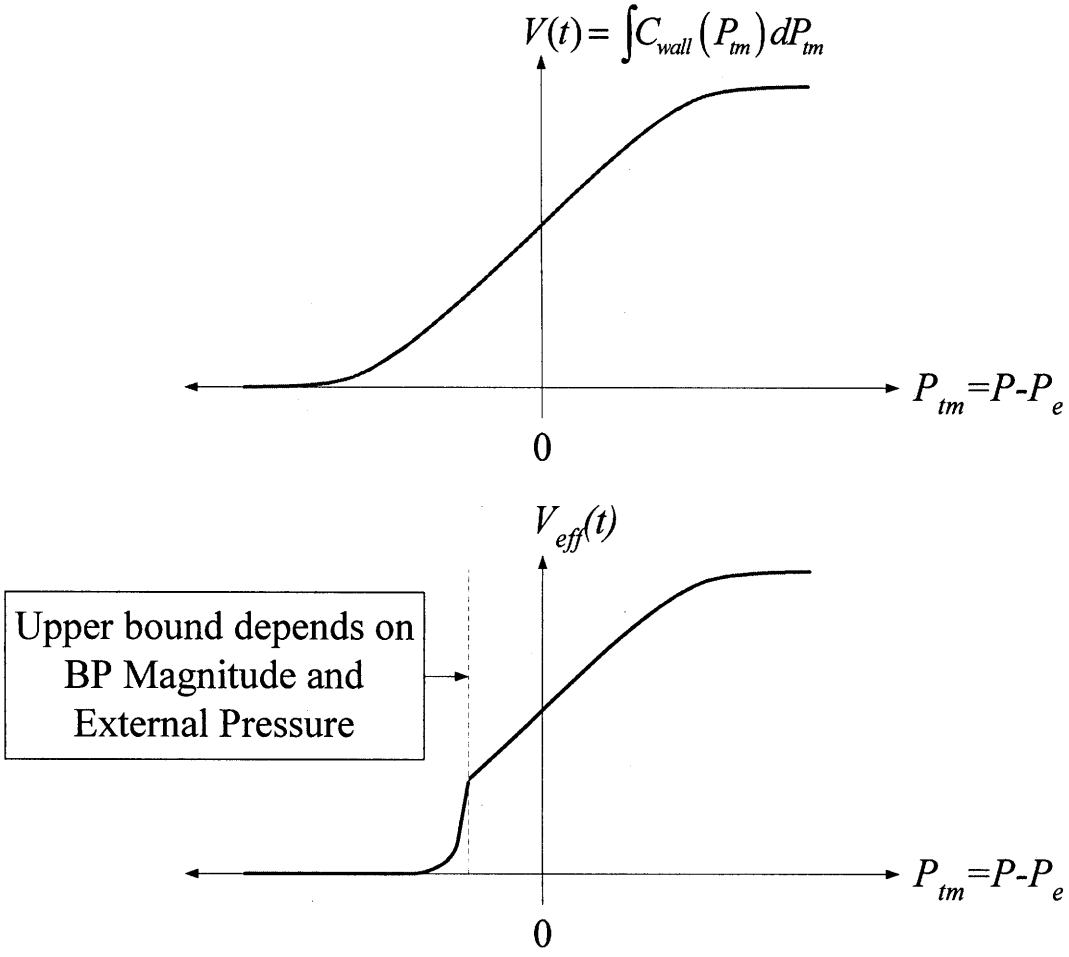

Figure 4-3. Variation in the arterial pressure volume relationship due to external loading

The effects of sensor contact pressure on the appearance of the PPG waveform were evaluated experimentally. The experimental protocol consisted of collecting a PPG waveform from the ulnar artery using our prototype wrist sensor. The PPG sensor was initially attached to the wrist using an elastic band which provided an initial external pressure $P_w(t = 0)$ to the artery. During the course of the experiment the external contact pressure applied by the wrist sensor housing was increased by applying a direct force to the exterior of the housing. The direct pressure applied to the wrist sensor was successively increased to 7 different values during 7 different experimental stages each approximately 30 seconds in length. The full wrist PPG data set containing all the waveforms measured during each stage is shown in Figure *4-4* and sample individual waveforms from each of the external pressure stages are shown in Figure *4-5*.

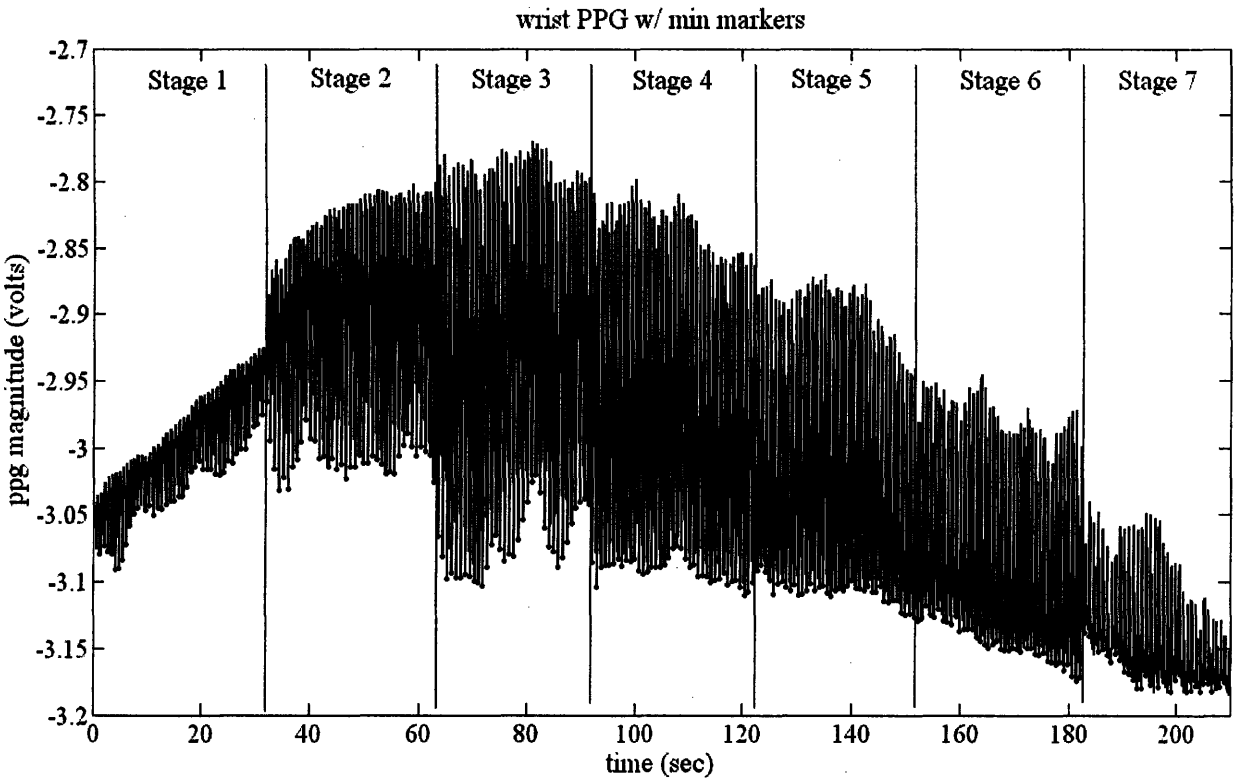

Figure 4-4. Wrist PPG waveform data measured given an increase in housing pressure during each successive stage

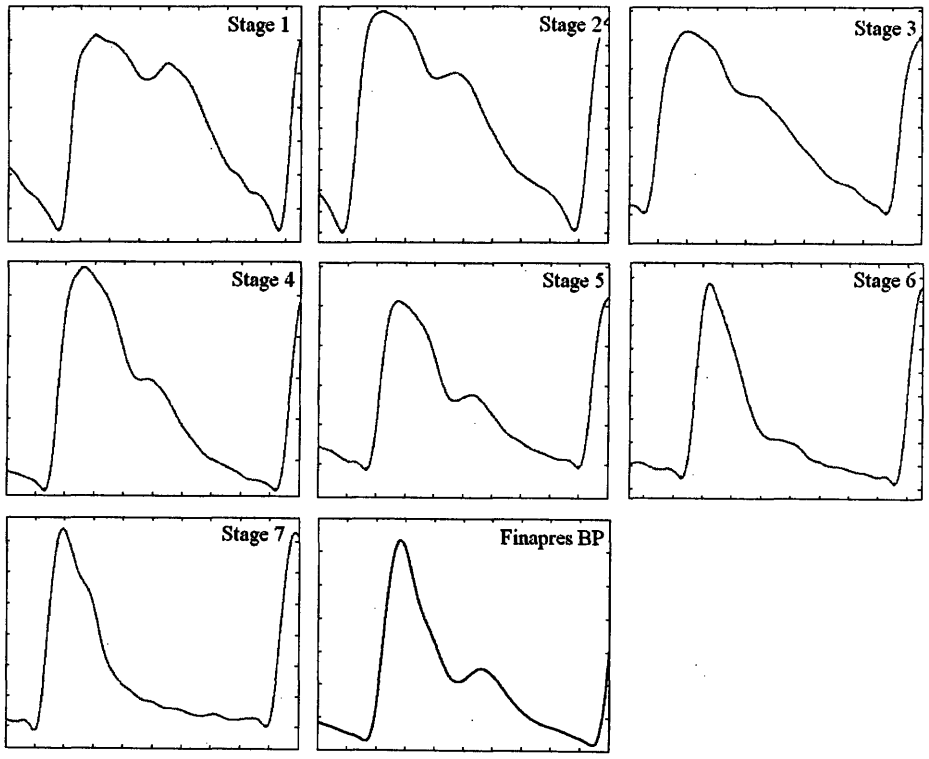

Figure 4-5. The effect of a multi-stage increase in external sensor pressure on the shape of the wrist PPG waveform

The evolution of the shape of the PPG waveform shown in Figure *4-5* demonstrates that as the mean transmural pressure of the waveform is decreased in each stage by the increases in external sensor pressure, various features of the blood pressure waveform are amplified or attenuated. Again this transformation is governed by the non-linear compliance of the arterial wall. Based on observation of the experimental waveforms it appears that during the first four stages of the experiment, features at the base of the BP waveform are being amplified while features near the peak of the BP waveform are being attenuated. This behavior is the result of the base of the waveform being close to or greater than the zero transmural pressure point and is explained by the larger arterial compliance value acting on the lower pressure range of the waveform. Conversely, as the base of the pressure waveform passes into the negative transmural pressure range the peak of the waveform lies in a pressure range with a higher arterial compliance and the peak is amplified. This behavior is clearly demonstrated in the peak of the PPG waveforms in stages 6 and 7. Also visible in stage 7 is the upper limit or threshold applied by the external pressure which completely attenuates the base of the pressure waveform.

The effect that this amplification and attenuation have on our pulse transit time estimates depends on the technique used to select an onset marker on the PPG waveform and the corresponding arrival time determined from this point. Only arrival time estimation techniques that are resistant to the effects of this amplification and attenuation should be considered for use in our device.

4.3 POTENTIAL PULSE TRANSIT TIME ESTIMATION TECHNIQUES

The first and simplest of the techniques presented in this section that can be used to reject the non-linear scaling changes in PPG waveform shape that are caused by transmural pressure variation is to select the minimum point of the waveform as the arrival time of the pulse wave. The minimum point occurs at the end of diastole immediately prior to the start of systole. This point will be at the same level of the wave front on both waveforms regardless of external sensor pressure and will negate the effects of waveform scaling. However, this location and minimum value may be the worst location in terms of signal noise rejection because of the small changes in PPG magnitude in this portion of the waveform.

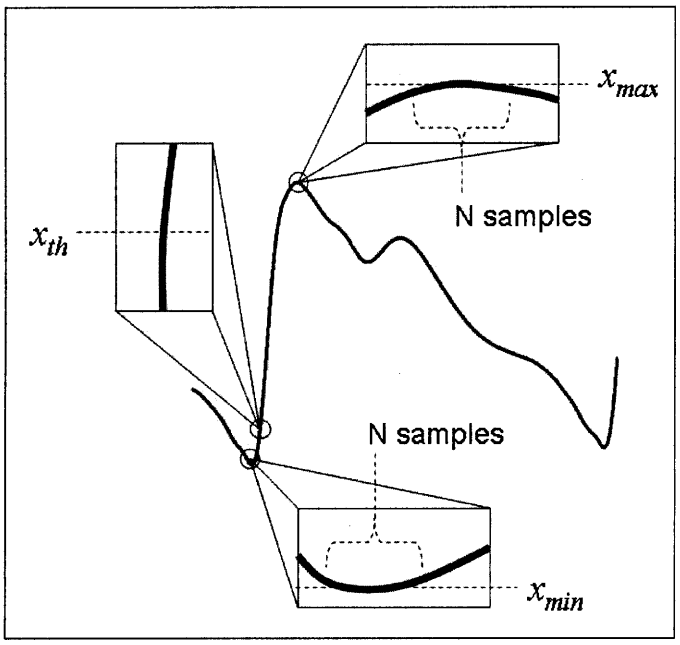

Figure 4-6. Pulse arrival time estimation using the waveform threshold averaging technique.

A second simple technique that may be more robust in terms of noise rejection than waveform minimum technique is a threshold averaging method. This technique is demonstrated in Figure 4-6. In this technique a mean minimum value is identified on the waveform by averaging the N smallest data samples in the waveform as given in equation (*4.4*). This averaging helps to remove the effects of noise on estimated minimum value.

$$x_{\min} = \sum_{t=M}^{M+N} x(t) \tag{4.4}$$

Similarly, a mean maximum value is identified on the waveform by averaging the N largest data samples in the waveform as given in equation (*4.5*).

$$x_{\max} = \sum_{t=P}^{P+N} x(t) \tag{4.5}$$

Prior to estimation a threshold is establish as a percentage of the overall magnitude of the waveform (*%mag*), typically the threshold is between 1-10%. The waveform threshold value x_{th}, used as the onset marker can then be determined on the waveform using the expression given in equation (*4.6*).

$$x_{th} = (\%mag) \cdot (x_{\max} - x_{\min}) \tag{4.6}$$

The threshold averaging technique is easy to implement, marks the onset of the two waveforms at the same height on the wave front, and can be used to mark the onset close to the waveform minimum while enjoying better noise rejection capabilities. However, because it is based on the magnitude of the waveform and on the rise time of the wave front it may be prone to error caused by shape variation.

A third technique that was considered by the author was an onset minimization method. This method is illustrated in *Figure 4-7*. In this method a representative onset marker data segment ($x_{on}[n]$) of length L is identified from the PPG sensor data. The onset marker is representative of the "foot" portion of the PPG waveforms in the data set. The onset marker data segment is then shifted in time across the PPG data set and the mean squared error between the onset marker data segment and PPG data is evaluated using the expression given in (*4.7*).

$$MSE[n] = \frac{1}{L}\sum_{k=0}^{L-1}\left(x[n+k] - x_{on}[k]\right)^2 \qquad (4.7)$$

The arrival time of the pulse waveform is considered to occur when the mean squared error value is at a minimum during each cardiac cycle

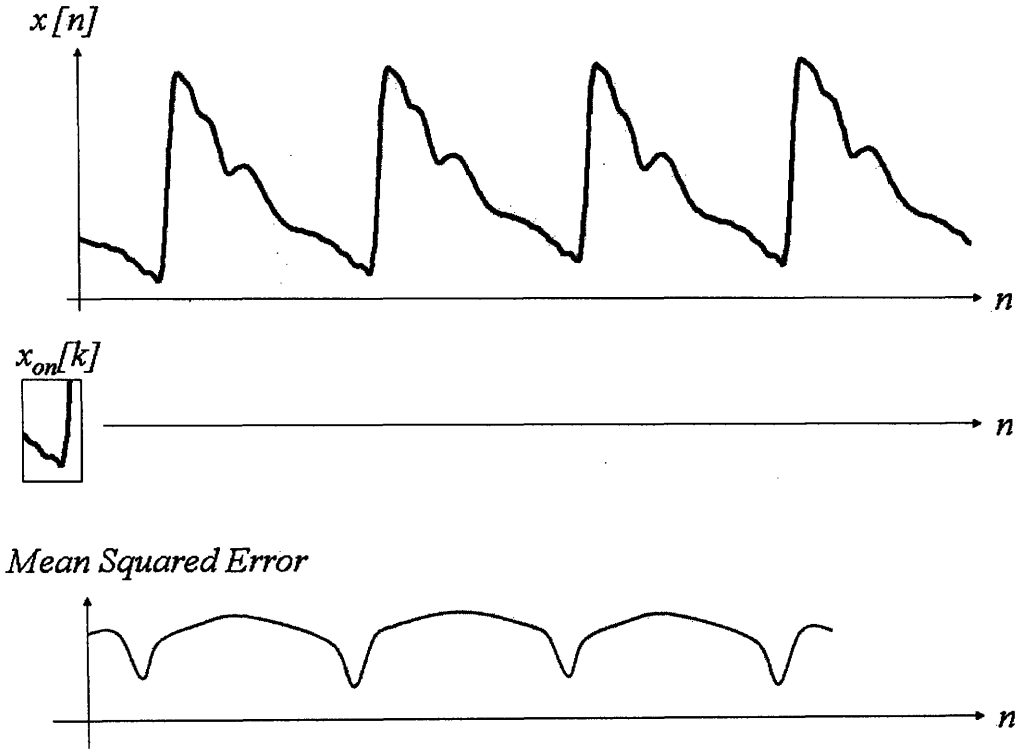

Figure 4-7. Pulse arrival time estimation using onset minimization

There are a number of techniques that can be used to identify a representative onset marker data segment from the foot portion of the PPG waveforms these include; waveform averaging, best fit criteria, and non-linear basis function approximation.

The main advantages to this method include; the marker is adaptive or can be updated over time, the arrival time estimation is robust against noise, and could be used to identify abnormalities in the waveform data if the minimum mean squared error is above some predetermined threshold. However, it is unclear how the effects of waveform scaling will affect the PTT estimates and it is not as simple to implement as the previous method requiring system identification and several parameters to be specified.

The advantages and disadvantages of these methods are shown in Table 4:2, where 1 represents the best performance in a category and 3 the worst performance.

Method	*Noise Rejection*	*Implementation Ease*	*Shape Adaptation*
Minimum Point	3	1	1
Threshold Averaging	2	2	3
Onset Minimization	1	3	2

Table 4:2 PPG arrival time technique comparison, 1 = best performance and 3 = worst performance

All of the methods listed in the table were applied to the PTT error analysis data sets described in Chapter 3. None of the methods demonstrated a significantly smaller standard deviation in measured PTT error than any of the others. Based on this analysis and the characteristics described in table *4:2* "Minimum Point" estimation appears to be the best arrival time identification technique.

CHAPTER 5
ADAPTIVE HEIGHT CALIBRATION

There are several key questions that that must be answered in order to use relative height variation to accurately identify the parameters of our device model. The first of these regards the sensitivity of our pulse transit time measurements to height variation, or can we accurately measure the variation in PTT caused by height variation and predict this response using our device model? Second, how sensitive are the parameters in our model to the effects of relative height change and can we accurately identify them given the typical error inherent in the measured PTT? Third, arterial blood pressure varies over time, how can the model parameters be identified given this unknown variation in the underlying arterial blood pressure. Finally, how can the system identification requirements be met using natural motion while still limiting the burden and complication of the calibration routine on the patient?

Although the primary goal of this chapter is to answer these questions and present a methodology and identification algorithm to calibrate peripheral pulse transit time measurements using relative height variation, these same methodologies and algorithms could be applied to other non-invasive arterial sensor modalities. Therefore, when appropriate the methodology will be extended to a general class of dynamic sensor systems. Further, the development of many of the concepts used in the algorithm is founded in linear system theory and a general formulation based on a dynamic system approach will promote a better understanding of the materials.

5.1 RELATIVE HEIGHT VARIATION & PULSE TRANSIT TIME

The goal of this section of the thesis is to establish our ability to measure the PTT change induced by height variation using our sensors and to validate the negative correlation between PTT and hydrostatic pressure variation predicted by our device model. Due to the non-linear relationship between pulse transit time and blood pressure the magnitude of PTT change induced by height variation is dependent on the initial magnitude of the patient's arterial blood pressure. Additionally, the non-linear elasticity of the arterial wall varies between different individuals and the observed PTT change induced by height variation will vary too. Therefore, extensive patient

testing would be required to fully quantify the range of PTT change induced by height variation a task which is outside the scope of this thesis.

Human subject testing was performed in the laboratory to observe the relationship between height variation and measured PTT. During the experiment, data was collected simultaneously from the wrist PPG sensor and finger PPG sensor which were attached to the test subjects using an elastic band. Additionally data was collected from a manometer type height sensor, comprised of a length of fluid filled tubing connected to an external pressure sensor. The opposite end of the tubing was affixed to the wrist sensor housing to measure the pressure variation at the measurement sites. During data collection test subjects were instructed to slowly vary the height of the sensor measurement sites by raising the sensor outfitted hand to heart level ($h \sim 0cm$) from its initial resting position hanging at their side ($h \sim -50cm$) pause at that position, and then lower the hand back to the side again, repeating this motion several times. Pulse transit time measurements were estimated as the timing difference between the onset of the finger PPG waveform and the onset of the wrist PPG waveform. A sample result of these experiments is shown in *Figure 5-1*.

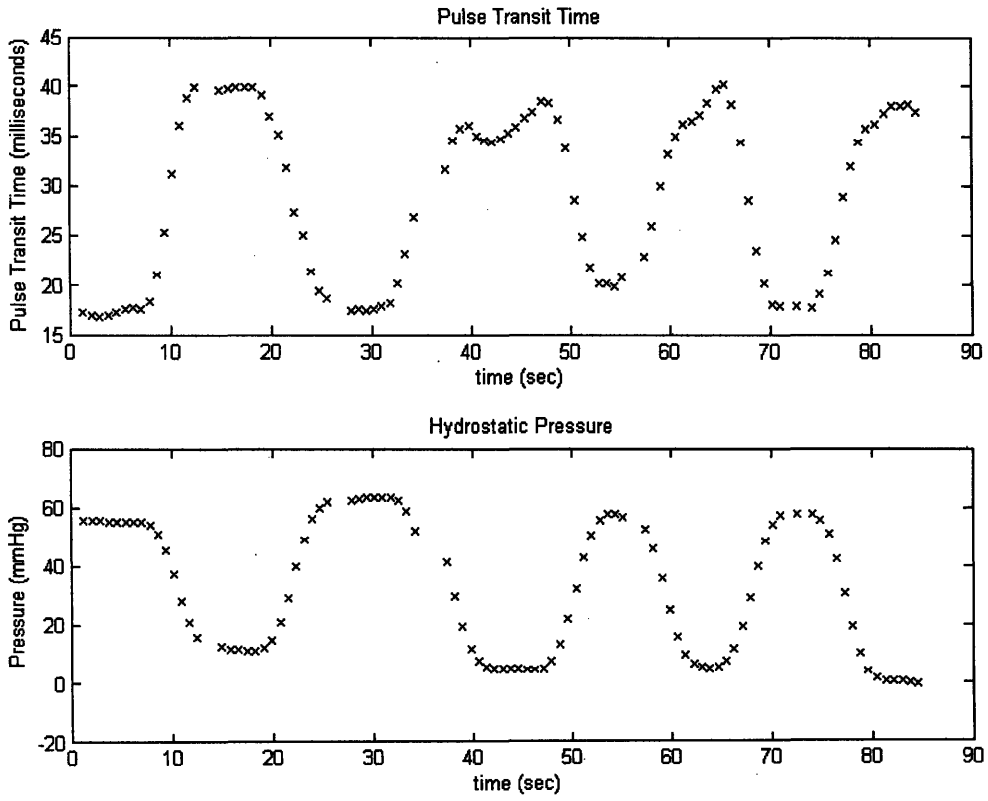

Figure 5-1. Observed alteration in pulse transit time caused by relative height variation.

Based on the results derived from three different individuals a height variation which increases the intravascular pressure at the sensor measurement site by 30 mmHg will produce an average decrease in pulse transit time of 26.5 milliseconds. The ability to resolve the pulse transit time changes induced by height variation is easily within the capability of our device. Furthermore, all three subjects demonstrated a negative correlation between hydrostatic pressure and PTT as predicted by our model.

5.2 PRINCIPAL EQUATIONS

Development of the system identification algorithm used to identify the parameters in our model begins with a proper formulation of the system equations.

A general dynamic model representing the relationship between a time varying transmural pressure, $P_{tm}(t)$ acting across the arterial wall at the sensor measurement site and a measured non-invasive sensor parameter $y(t)$, is given by equation (*5.1*), where $s(t)$ represents the transduction dynamics of the sensor modality and y_0 represents the steady-state zero pressure parameter offset.

$$y(t) = s(t) * P_{tm}(t) + y_0 \tag{5.1}$$

A block diagram representing this system is shown in *Figure 5-2*. Our device model relating pulse transit time to transmural pressure can be expressed in the form of equation (*5.1*) by applying a non-linear transformation to the pulse transit time measurements as given in equation (*5.2*) where $y(t) = \ln\left(\frac{1}{ptt(t)}\right)$ and $y_0 = \ln\left(\frac{1}{ptt_0}\right)$.

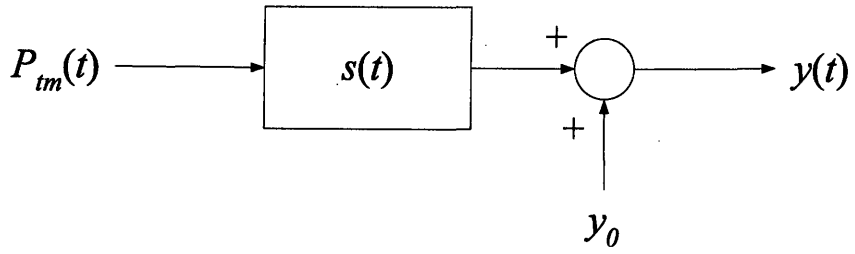

Figure 5-2. Block diagram depicting the dynamic relationship between transmural arterial pressure $P_{tm}(t)$ and a measured non-invasive sensor signal $y(t)$.

$$\ln\left(\frac{1}{ptt(t)}\right) = k \cdot P_{tm}(t) + \ln\left(\frac{1}{ptt_0}\right) \tag{5.2}$$

The transmural pressure in equation (*5.2*) can be expressed as the sum of arterial blood pressure $P_{bp}(t)$, and the pressure change induced by the relative height $h(t)$, of the measurement sites as given in equation (5.3), where we have assumed that the external pressure acting along the pulse transit path is negligible. This assumption will be addressed in more detail in later chapters in this thesis.

$$P_{tm}(t) = P_{bp}(t) + \rho g h(t) \tag{5.3}$$

The output of our linear system may be defined as the superposition of our model's response to arterial blood pressure and its response to relative height variation. In order to identify the parameters in our device model using height variation our system of equations must be reduced to an input-output relationship involving only the known height variation and its specific contribution to the measured PTT. Two potential methods exist for isolating the contribution to PTT from relative height change and eliminating the unknown arterial blood pressure from our system of equations, 1) a temporal differential formulation or 2) a zero-mean formulation.

For a general linear system as given in (*5.1*), a differential relationship can be defined between a set of temporally distinct inputs and outputs as given in (*5.4*) where τ is a positive real valued number. In the case of our PTT model, $s(t)$ is simply equal to k.

$$\Big(\big(P_{bp}(t) - P_{bp}(t-\tau)\big) + \rho g\big(h(t) - h(t-\tau)\big)\Big) * s(t) = y(t) - y(t-\tau) \tag{5.4}$$

An immediate consequence of this differential formulation is that the unknown zero pressure offset y_0, is eliminated from this system of equations and cannot be identified using this formulation. In fact, an inability to estimate an offset term is a natural consequence of utilizing a relative input change to identify our model parameters and is an unavoidable result of this type of system identification having an unknown input component.

The unknown arterial blood pressure given in (*5.4*) can be eliminated if $P_{bp}(t) = P_{bp}(t-\tau)$. This may occur if blood pressure is constant across the calibration period or if it is periodic in time having a frequency $f = \frac{2\pi}{\tau}$. By eliminating the unknown blood pressure we are left with a

simple input-output relationship between height variation and the measured variable and the model parameters can be identified using a least squares identification technique.

However, it is difficult to implement this differential formulation given the limitations imposed by the cardiovascular system. The heart rate varies over time ($f \neq constant$) potentially requiring a time varying parameter τ. The measured PTT has a non-uniform sampling rate which may influence the distribution of the data when divided temporally. Any data screening which might be used to eliminate poor measurements may effect the temporal distribution of our data. Clearly, the selection of the parameter value τ determines the richness of the data used to identify the model parameters and potentially their identified values. Presently, there exists no clear or optimal method to select the parameter τ.

As a result of this complexity, the differential formulation was abandoned in favor of a zero-mean formulation that is much easier to implement.

The mean of the measured output signal with L samples can be determined using equation (*5.5*).

$$\bar{y} = \left(\frac{1}{L}\right)\sum_{t=0}^{L-1} \ln\left(\frac{1}{ptt_m(t)}\right) \tag{5.5}$$

Using this mean value the measured output data can be transformed into a new zero-mean variable as given by equation (*5.6*).

$$\tilde{y}(t) = y(t) - \bar{y} \tag{5.6}$$

Similarly, the mean of the hydrostatic pressure data can be determined as in (*5.7*).

$$\bar{P}_h = \left(\frac{1}{L}\right)\sum_{t=0}^{L-1} \rho g h(t) \tag{5.7}$$

Again, using the calculated mean the measured hydrostatic data can be transformed into a new zero-mean variable as given by equation (*5.8*).

$$\tilde{P}_h(t) = \rho g h(t) - \bar{P}_h \tag{5.8}$$

The mean arterial pressure value is given by equation (*5.9*).

$$\bar{P}_{bp} = \left(\frac{1}{L}\right)\sum_{t=0}^{L-1} P_{bp}(t) \tag{5.9}$$

The arterial pressure can be transformed into a zero-mean variable using equation (*5.10*).

$$\tilde{P}_{bp}(t) = P_{bp}(t) - \bar{P}_{bp} \tag{5.10}$$

By exploiting the laws of linear convolution a linear system can be transformed using a linear zero-mean filter $H_{filt}(z)$ as given in (*5.11*) into a relationship between the zero mean variables given in (*5.8*) – (*5.10*) as shown in Figure 5-3.

$$H_{filt}(z) = 1 - \left(\frac{1}{L}\right)\sum_{n=0}^{L-1} z^{-n} \tag{5.11}$$

Similar to the differential formulation, the constant offset y_0 is lost from the zero-mean model equation that is given in (*5.12*) where $s(t)$ in our pulse transit time model is simply equal to the constant parameter k.

$$\tilde{y}(t) = s(t) * \tilde{P}_{tm}(t) = s(t) * \left(\tilde{P}_{bp}(t) + \tilde{P}_h(t)\right) = k \cdot \left(\tilde{P}_{bp}(t) + \tilde{P}_h(t)\right) \tag{5.12}$$

Under the assumption that the diastolic or mean blood pressure is constant or that its variation has a zero-mean value over our calibration period this formulation eliminates the unknown arterial pressure and establishes a relationship between just the measured zero mean height variation and zero mean output variable and the model parameters may be identified using a least squares technique. The only parameter that must be determined in the zero-mean formulation is the number of data samples used in the identification, a topic that will be considered in more depth later in this chapter.

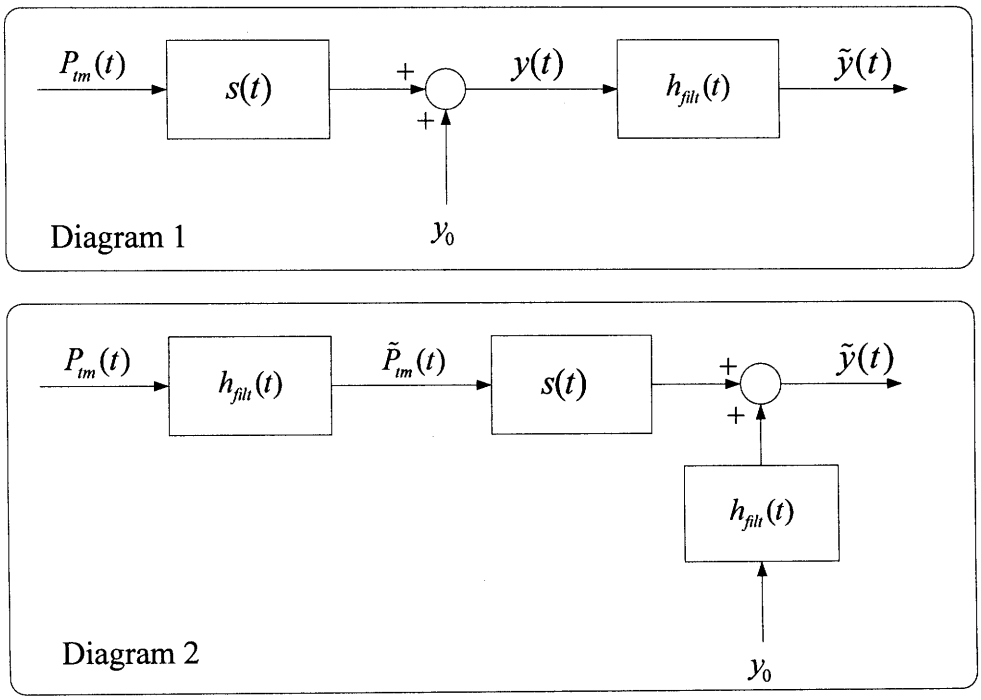

Figure 5-3. Transformation of a linear system with zero-mean output into an equivalent system with a zero-mean input (denoted by ~) using a linear filter

5.3 ADAPTIVE SYSTEM IDENTIFICATION

Unfortunately, the ideal assumptions that the diastolic pressure or mean pressure are constant throughout the calibration period or that their variation throughout the calibration period has a zero-mean value are not strictly true. Natural physiologic variation occurs in peripheral arterial blood pressure over time. This variation is produced by a variety of sources including cardiac output variability, time varying periodic pressure waves produced by respiration and vasomotor activity [18] which have a frequency range of between 0.25 Hz and 0.1 Hz and have a magnitude range of between *4-20 mmHg*, or additional variation resulting from changes in the patient's sympathetic activity. Therefore, it is likely that during the calibration period, $\tilde{P}_{bp}(t) \neq 0$ and that identification of the model parameter(s) using the expression in (*5.12*) requires a more sophisticated calibration algorithm that can cope with unknown blood pressure variation.

We have developed a calibration algorithm that allows identification of the model parameters in $s(t)$ directly from $\tilde{P}_h(t)$ despite the presence of an unknown pressure component $\tilde{P}_{bp}(t)$ if the frequency of the relative height change is properly selected. The foundation of the adaptive system ID algorithm is based upon the principles of adaptive noise cancellation [34].

Again, for a linear system superposition allows us to separate the contributions of the two input components $\tilde{P}_{bp}(t)$, and $\tilde{P}_h(t)$, in our zero-mean output $\tilde{y}(t)$ such that $\tilde{y}(t) = \tilde{y}_{bp}(t) + \tilde{y}_h$, given the definitions in (*5.13a*) and (*5.13b*).

$$\tilde{y}_{bp}(t) = s(t) * \tilde{P}_{bp}(t) = k \cdot \tilde{P}_{bp}(t) \qquad (5.13a)$$

$$\tilde{y}_h(t) = s(t) * \tilde{P}_h(t) = k \cdot \tilde{P}_h(t) \qquad (5.13b)$$

The block diagram shown in Figure *5-4* depicts the basic structure of the adaptive height calibration algorithm used to estimate the model parameter k in $s(t)$. Using the adaptive noise calibration framework it can be proven that the model parameter k, can be identified in a least squares sense by simply minimizing the error variance in the expression $\left(\tilde{y}(t) - \hat{k} \cdot \tilde{P}_h(t)\right)^2$, if the unknown blood pressure variation $\tilde{P}_{bp}(t)$, is not correlated with the pressure change $\tilde{P}_h(t)$, induced by the height change of the sensor measurement sites.

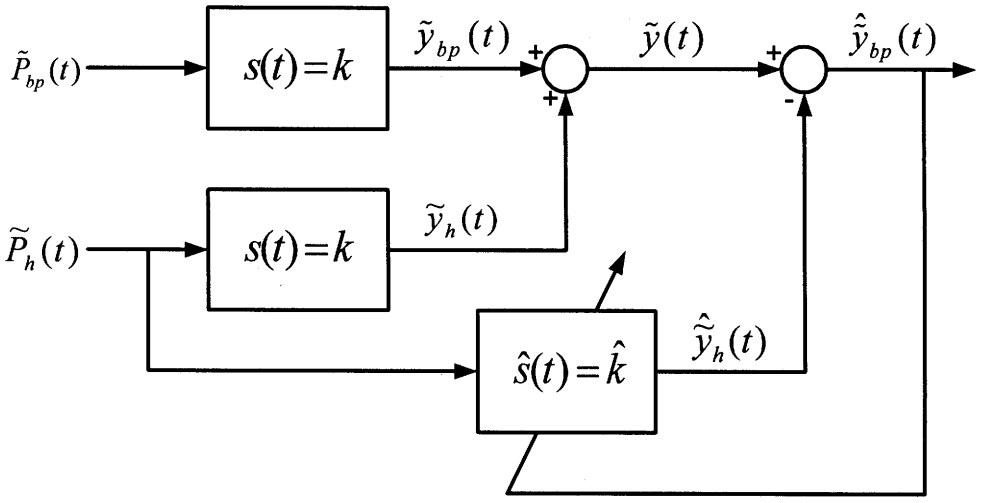

Figure 5-4. Block diagram depicting the adaptive height calibration algorithm.

The proof proceeds as follows. The square value of the estimated output produced by blood pressure variation $\hat{\tilde{y}}_{bp}(t)$ shown in Figure 5-4 is given in equation (*5.14*).

$$\left(\hat{\tilde{y}}_{bp}\right)^2 = \left(\tilde{y} - \hat{\tilde{y}}_h\right)^2 = \left(\tilde{y}_{bp}\right)^2 + \left(\tilde{y}_h - \hat{\tilde{y}}_h\right)^2 + 2\tilde{y}_{bp}\left(\tilde{y}_h - \hat{\tilde{y}}_h\right) \tag{5.14}$$

Taking expectations of both sides of the equation in (*5.14*) leads to (*5.15*).

$$E\left[\left(\hat{\tilde{y}}_{bp}\right)^2\right] = E\left[\left(\tilde{y}_{bp}\right)^2 + \left(\tilde{y}_h - \hat{\tilde{y}}_h\right)^2 + 2\tilde{y}_{bp}\left(\tilde{y}_h - \hat{\tilde{y}}_h\right)\right] \tag{5.15}$$

If the unknown arterial pressure variation is uncorrelated with the known height variation then so are their outputs and the expression in (*5.15*) can be reduced to that in (*5.16*).

$$E\left[\left(\hat{\tilde{y}}_{bp}\right)^2\right] = E\left[\left(\tilde{y}_{bp}\right)^2\right] + E\left[\left(\tilde{y}_h - \hat{\tilde{y}}_h\right)^2\right] \tag{5.16}$$

The signal power $E\left[\left(\tilde{y}_{bp}\right)^2\right]$ is unaffected when minimizing $E\left[\left(\hat{\tilde{y}}_{bp}\right)^2\right]$ by adjusting $\hat{s}(t)$ with respect to the $\tilde{P}_h$ input as in (*5.17*).

$$\min E\left[\left(\hat{\tilde{y}}_{bp}\right)^2\right] = E\left[\left(\tilde{y}_{bp}\right)^2\right] + \min E\left[\left(\tilde{y}_h - \hat{\tilde{y}}_h\right)^2\right] \tag{5.17}$$

Therefore, by designing $h(t)$ such that it is uncorrelated with $\tilde{P}_{bp}(t)$ we can identify the sensor transduction dynamics by minimizing the term $E\left[\left(\tilde{y}_{bp}\right)^2\right]$ and this is equivalent to minimizing the expression $E\left[\left(\tilde{y}_h - \hat{\tilde{y}}_h\right)^2\right]$ despite unknown variation in arterial blood pressure

during the calibration period.

Although we are unable to predict the frequency content of the pseudo-random fluctuations in $\tilde{P}_{bp}(t)$ during the calibration period and are forced to assume that they are uncorrelated with our height change, we can estimate the frequency of the periodic fluctuations occurring in the peripheral blood pressure prior to calibration by analyzing the frequency content of the measured PPG waveforms. Once the frequency content of the periodic oscillations is determined, an appropriate height variation protocol could be designed so that our input is uncorrelated with those oscillations. Alternatively, identifying the frequency content of these oscillations may allow us to exclude data from our calibration algorithm that was measured during periods when the frequency of the height change initiated by natural patient motion was correlated with the variation in arterial blood pressure.

This adaptive height calibration algorithm allows model parameter identification using natural motion given some mild conditions on that motion. The alternative to this type of algorithm would be to force the patient to move and then hold the sensor measurement sites at a certain vertical height long enough to average out the effects of periodic oscillation. This would require a burdensome calibration routine and still would not address any non-periodic fluctuations in the arterial blood pressure during the calibration period.

5.4 AHC IMPLEMENTATION

The goal of this section of the thesis is to characterize some of the fundamental implementation parameters in our adaptive height calibration algorithm. Specifically, what is the sensitivity of the estimated blood pressure to error in the identified calibration parameter and how is the variance of the identified model parameter affected by the duration of the calibration period?

The sensitivity of our estimated blood pressure to error in the identified model parameter k, is shown in Figure *5-5*. Average parameter values derived from human subject testing were specified for $k = 0.02\ mmHg^{-1}$, $P_{bp} = 80\ mmHg$ and $y_0 = 2$. The plot in Figure *5-5* demonstrates that for these parameter values a +-6% error in the identified model parameter k, will produce a +-5 *mmHg* error in the blood pressure estimates made using our device.

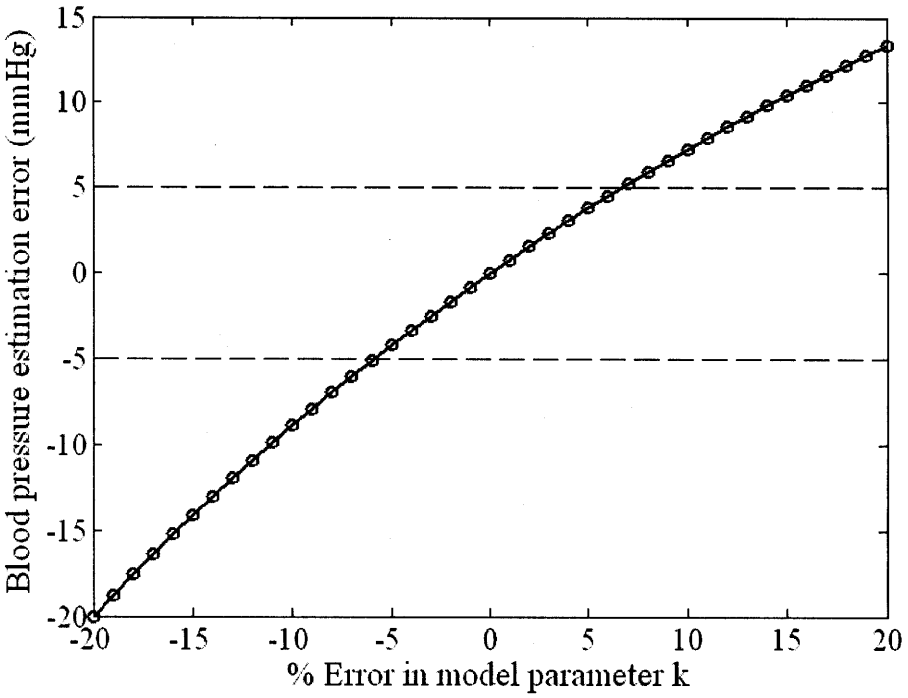

Figure 5-5. Blood pressure estimation error as a function of error in model parameter *k*.

Based on the error analysis presented in chapter 3 of this thesis there exists some uncertainty in every pulse transit time measurement made with our device. The standard deviation of this error, or uncertainty was determined to be 1.6 milliseconds. Due to this uncertainty we must expect that some error will be introduced into our identified model parameter. Based on system identification theory [35] the variance of our parameter error should approach some asymptotic minimum value. A simulation was used to quantify the relationship between the duration of the calibration period and the standard deviation of the error in the identified model parameter *k*. In the simulation the hydrostatic pressure was varied as a sinusoid at a frequency of 0.05 Hz or T = 20 seconds and a magnitude of 20 *mmHg*. A sinusoidal respiratory pressure variation was introduced into the arterial blood pressure at a frequency of 0.25 Hz and magnitude of 3 mmHg. The heart rate was assumed to have an average value of 60 beats per minute or 1 Hz. A pulse transit time measurement error was added to every pulse transit time value. This error was randomly drawn from a Gaussian distribution having a standard deviation of 1.6 milliseconds. The standard deviation of the error was determined for the different calibration period lengths after running the simulation at that time length 10,000 times. The values used in the simulation were the same used to generate Figure *5-5*.

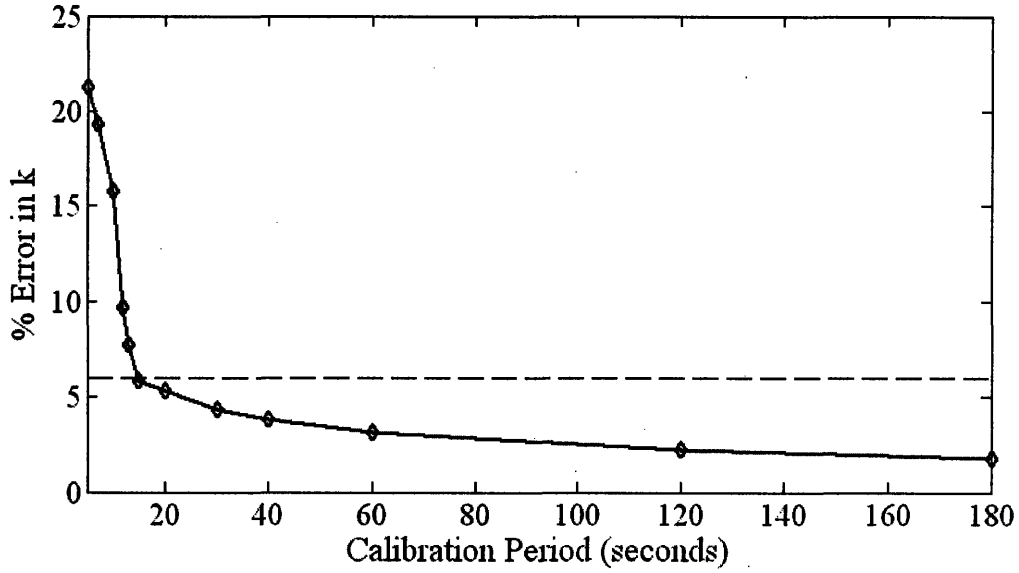

Figure 5-6. Relationship between model parameter error and calibration period length

These average parameter values were derived from human subject testing, $k = 0.02$ $mmHg^{-1}$, $P_{bp} = 80$ $mmHg$, and $y_0 = 2$. The results of these simulations are summarized in Figure *5-6* where the length of the calibration period is shown versus percentage error in the identified model parameter *k*, the percentage error reported in this plot represents the standard deviation in all the error values calculated for each period length from the 10,000 iterations. The 6% error threshold which represents the value where our BP estimation error is +- 5 mmHg is crossed when the duration of the calibration period is greater than 15 seconds.

CHAPTER 6
ADAPTIVE HEIGHT CALIBRATION HUMAN SUBJECT TESTING

The objective of this round of experimental testing was to evaluate the ability of our adaptive height calibration algorithm to accurately identify the model parameter k given simultaneous PTT and height measurements. Additionally, these experiments represented the first large scale tests of the wrist and finger PPG sensors and their ability to measure quality volumetric waveform signals across a wide variety of test subjects and utilize these waveforms to accurately estimate pulse transit time.

The Finapres blood pressure monitor, a BP device which is capable of providing a continuous non-invasive blood pressure measurement was also used to simultaneously collect data throughout the experiment in order to separately identify the model parameter k, for comparison with the results of the adaptive height calibration algorithm. The Finapres BP monitor estimates BP using the volume clamp method of Penaz [10]. The parameters of the device model were estimated from the Finapres BP data ($P_{bp,Fin}$) using a simple least squares identification technique applied to the linear device equation developed in chapter 5 and which is given in (*6.1*) for convenience.

$$y(t) = \hat{k}_{Fin} \cdot P_{bp,Fin}(t) + \hat{y}_0 \qquad (6.1)$$

6.1 EXPERIMENTAL PROTOCOL

Human subject data was collected in accordance with an experimental protocol approved by the Massachusetts Institute of Technology's Committee on the Use of Humans as Experimental Subjects (COUHES Approval No. 0403000233) and following Federal regulations for the protection of human subjects established by 45 CFR 46.

Throughout the duration of the experiment data was simultaneously collected from four different sensors; a PPG sensor located at the ulnar artery of the left wrist, a PPG sensor located along the digital artery at the base of the little finger of the left hand, a manometer type height sensor which consisted of a length of fluid filled tubing connected to an external pressure sensor.

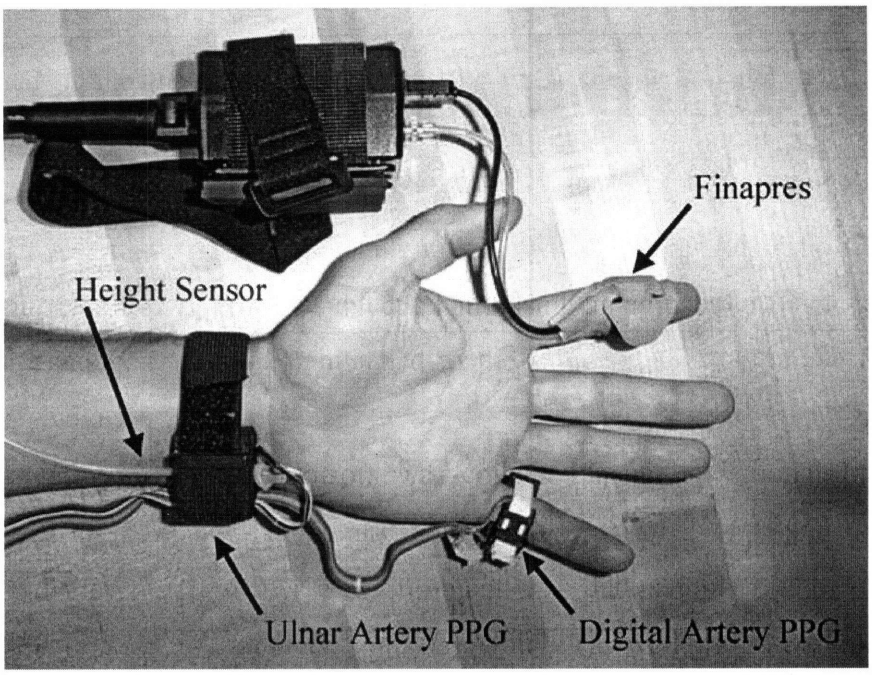

Figure 6-1. Sensor attachment configuration used in the adaptive height calibration tests.

The opposite end of the tubing was affixed to the wrist sensor housing. The Finapres blood pressure monitor was attached to the index finger of the left hand. A picture of this experimental set-up is shown in Figure 6-1.

The bulky pneumatic actuator housing utilized by the Finpres (also shown in Figure *6-1*) was loosely secured to the back of the subject's hand using an adjustable elastic strap. The cable required by the Finapres was loosely attached to the subjects arm just above the elbow joint using an adjustable nylon strap.

Data from the four sensors was collected using a National Instruments data acquisition board (NI-3452) that had a maximum sample rate of 2 *MHz* and using a program running in the LabView™ 7.1 software environment. The data sample rate of each of the four sensors was *20kHz* (*20kHz x 4 channels = 80kHz*), which was well within the maximum sample rate of our DAQ board.

The experimental protocol was performed as follows; throughout the experiment the test subjects remained seated in a chair, the subjects were initially asked to hold their left outstretched arm at heart level as shown in Figure *6-2*. This height was used to establish the zero level of the height sensor. After approximately 10-15 seconds in this position each subject was verbally instructed to lower their left hand to a predetermined height (height *C*) indicated by a

fixed height marker (not pictured in Figure *6-2*) located just beyond the fingertips of the left hand. The left hand was maintained at this height for approximately 10-15 seconds, after this period of time the subject was verbally instructed to raise the level of their hand above heart level to a second height (height *A*) indicated on the fixed height marker. The hand was maintained at this level for approximately 10-15 seconds, following this period of time the subject was verbally instructed to lower their left hand back to level *C* on the height marker.

This cycle of raising and lowering the patients left arm at 10-15 second intervals was continued throughout the course of the experiment. The total duration of each experiment was approximately 60-70 seconds. The height variation used in the experiment could be approximately described as a square wave with a frequency of 0.05 Hz to 0.033 Hz. This frequency range is lower than the frequency ranges associated with respiratory pressure variation ($f \sim 0.25$ *Hz*) and vasomotor waves ($f \sim 0.1$ *Hz*). The difference in height between the two positions *A* and *C* on the fixed height marker was 40 centimeters which corresponded to a relative pressure change at the measurement sites of approximately 30 *mmHg*. The fixed height marker was used to simplify the verbal instructions during the experiment and to insure that patients spanned a large enough pressure range through arm height variation. An example of the pressure change measured at the wrist by the height sensor during the course of one of the experiments is shown in Figure *6-3*.

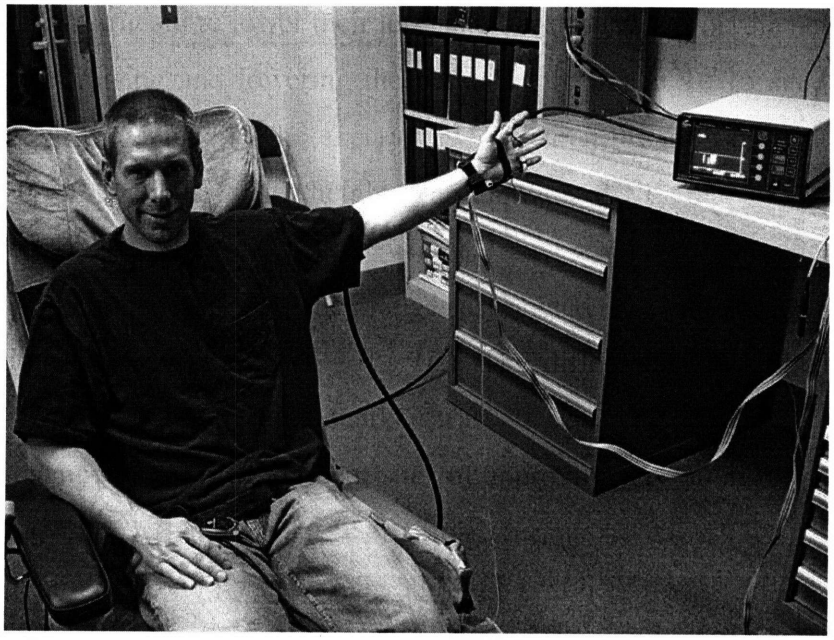

Figure 6-2. Photo of test subject during the initial phase of the AHC experimental protocol

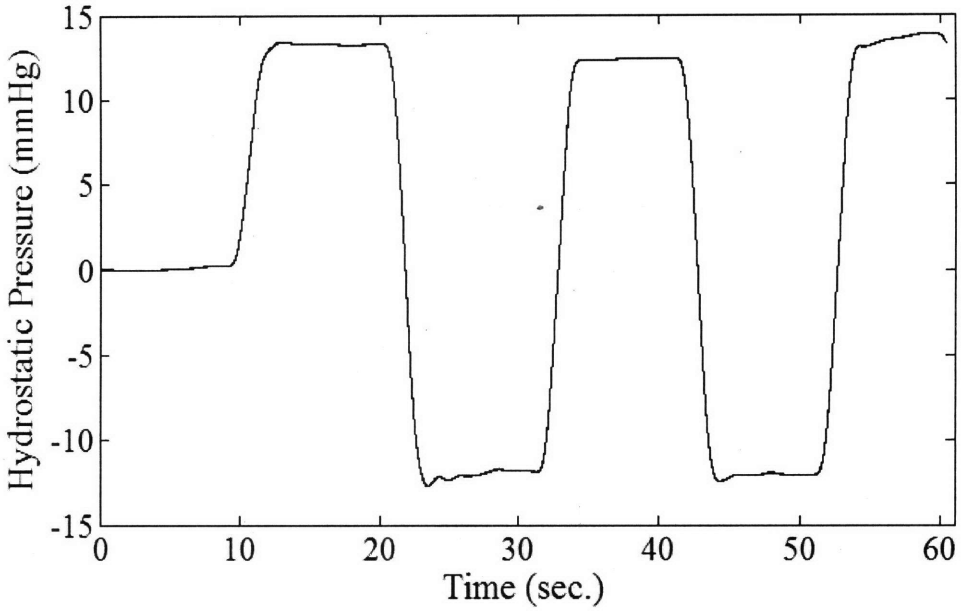

Figure 6-3. Experimental pressure variation measured at the wrist sensor during a human subject test

6.2 EXPERIMENTAL RESULTS

The adaptive height calibration protocol was performed in our laboratory at MIT on eight different subjects. Each of the subjects read and signed a COUHES approved consent form prior to participating in the experiment. A histogram displaying the ages of the test subjects is shown in Figure *6-4*.

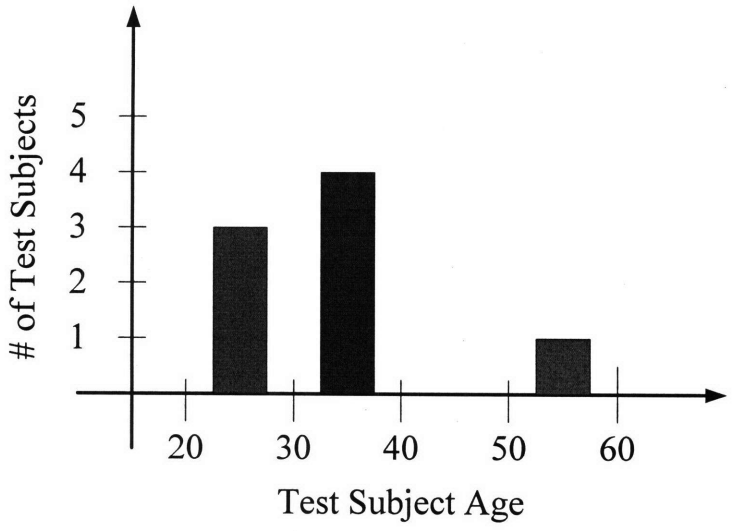

Figure 6-4. Histogram depicting the age distribution of the AHC test patient population

All data processing and analysis was preformed off-line using the MATLAB™ software environment following completion of the eight experiments. Prior to processing any of the data all four of the recorded sensor signals were low-pass filtered using a finite impulse response (FIR) filter with a cutoff frequency of 20 *Hz*. This cutoff frequency was chosen because the blood pressure waveform can be accurately represented using the first 10 harmonics [22]. The resting heart rate of all the patients in the study was less than 2 *Hz* thus the blood pressure and volumetric PPG waveforms should be accurately captured in a frequency spectrum below 20 *Hz*. An FIR filter was chosen because it has a linear phase across the band limited frequencies of our signals.

The pulse transit time ($ptt(t)$) between the two sensors was estimated as the timing difference between the arrival time of the finger PPG waveform and the arrival time of the wrist PPG waveform. The arrival time of each of the waveforms was estimated using the average threshold estimation technique described in Chapter 3 using a 1% threshold marker. Pulse transit time estimates that were less than 0 milliseconds and greater than 100 milliseconds were eliminated from the data set. These liberal limits were used to remove data that is obviously outside the range of possible PTT values measured between our sensors. In the future, more conservative limits may be established to screen errors from the data set.

The height ($h(t)$) that corresponded to each estimated pulse transit time value was determined from the measured output of our height sensor and was selected from the measured data set at the time corresponding to each finger PPG arrival time. To ensure the accuracy of the height sensor it was calibrated against a known height prior to every experimental session. The height data was converted to internal blood pressure assuming that the density of human blood is 1060 kg/m^3.

Diastolic blood pressure ($P_{bp,Fin}(t)$) was estimated from the blood pressure waveforms measured with the Finapres. The arrival time of the blood pressure waveform was determined using the same threshold technique and 1% threshold marker that was applied to the PPG waveforms. The diastolic pressure value was selected as the BP waveform value at the identified arrival time.

Unfortunately, throughout the testing period the Finapres BP monitor randomly performed auto-calibration routines. During these routines (lasting 1 – 5 seconds) the BP monitor did not provide BP waveform data. To allow a one-to-one comparison of PTT and BP data

throughout the measurement period any PTT data that was collected during these BP calibration periods was removed from the patient data set.

Adaptive height calibration was performed on each subject's data to identify the model parameter k ($\hat{k}_{AHC}$), using only the measured PTT data and height sensor data. A minimum of 30 seconds of the most correlated *PTT* data and height data derived from each subject were used to perform the identification technique. Causes of poor data correlation are discussed later in this chapter. From a data set that corresponded directly in time to that used in the adaptive height calibration algorithm the Finapres™ BP data and PTT data were used to identify the model parameters k ($\hat{k}_{Fin}$) and y_0 ($\hat{y}_0$) using a least squares estimation technique applied to equation (*6.1*).

The model parameter k, identified using adaptive height calibration ($\hat{k}_{AHC}$) and identified using the Finapres™ ($\hat{k}_{Fin}$) BP measurements is given for each patient in Table *6:1* along with the correlation ($r_{y,P}$) between the transformed PTT variable $y(t)$ and measured Finapres blood pressure data used in the identification.

Patient	$r_{y,P}$	$\hat{k}_{AHC}$	$\hat{k}_{Fin}$
1	0.81	0.0240	0.0238
2	0.53	0.0209	0.0183
3	0.75	0.0236	0.0232
4	0.91	0.0285	0.0281
5	0.85	0.0183	0.0182
6	0.93	0.0334	0.0342
7	0.55	0.0265	0.0255
8	0.79	0.0129	0.0132

Table 6:1. Experimental results form the adaptive height calibration human subject testing

The percent error between the two identified model parameters as defined in equation (*6.2*) is shown in Figure *6-5* for each patient.

$$\%\ error\ \hat{k} = 100 \cdot \left(\frac{|\hat{k}_{AHC} - \hat{k}_{Fin}|}{\hat{k}_{Fin}} \right) \qquad (6.2)$$

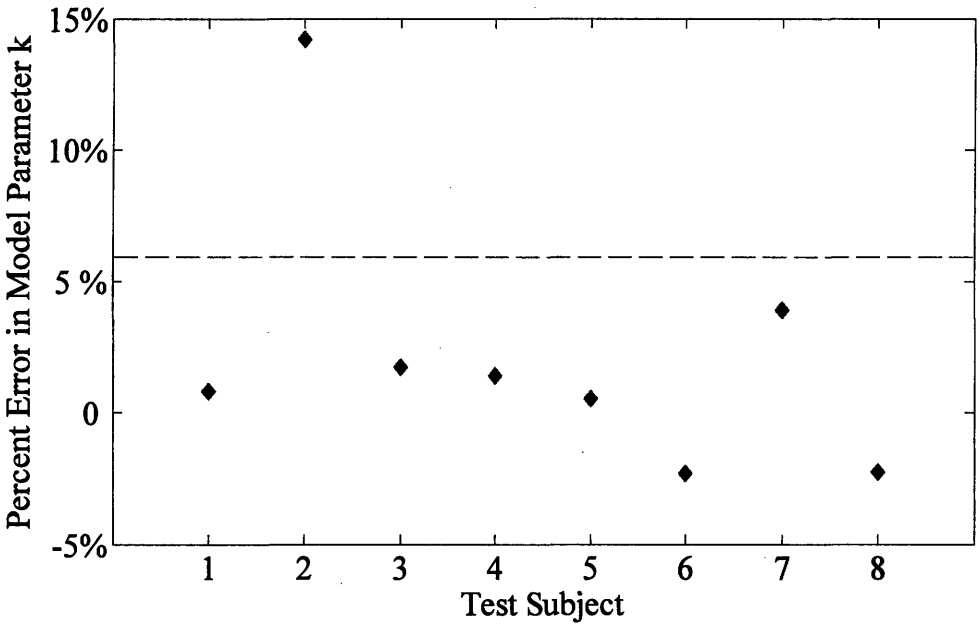

Figure 6-5. Percent error between the model parameter *k* identified using adaptive height calibration and the model parameter *k* identified using Finapres BP measurements

According to the analysis presented in Chapter 5, the expected blood pressure estimation error will be less than 5 *mmHg* if the error in the identified model parameter $\hat{k}$ is less than 6%. This 6% threshold is indicated in Figure *6-5* using a dashed horizontal line. It is clear from this plot that 7 out of 8 of the identified values fell below this threshold. The one patient (patient # 2) in which the identified parameter value was above this threshold demonstrated a poor correlation ($r_{y,p} = 0.53$) between the measured PTT variable and the Finapres blood pressure.

This set of experimental results demonstrates that the model parameter *k*, can be identified using the adaptive height calibration algorithm when it is applied to the PTT data measured with our device and the measured height of the sensor sites. Additionally, we have demonstrated that the parameter error in the overwhelming majority of test subjects is within the threshold required to limit the estimated blood pressure error below 5 *mmHg*.

In order to estimate blood pressure from a test subject's measured pulse transit time required identification of the zero pressure offset value y_0. Unfortunately it is not possible to identify this parameter using adaptive height calibration (AHC) alone. However, to demonstrate the potential of the model parameter identified using the AHC algorithm $\hat{k}_{AHC}$ to estimate blood pressure, we will combine the AHC identified model parameter with the Finapres BP data to first

estimate the unknown model offset y_0, and then estimate the diastolic blood pressure from the measured pulse transit time values. The model offset was identified using a least squares identification technique that minimized the error in the expression shown in equation (*6.3*) to identify $\hat{y}_{0,AHC}$.

$$\left(\left(\hat{k}_{AHC} \cdot P_{bp,Fin}(t) - \ln\left(\frac{1}{ptt(t)}\right)\right) - \hat{y}_{0,AHC}\right)^2 \tag{6.3}$$

Note that the model parameter $\hat{k}_{AHC}$ was previously identified using the AHC algorithm. Following identification of the model offset, diastolic blood pressure was estimated using the expression given in equation (*6.4*).

$$\hat{P}_{bp}(t) = \frac{1}{\hat{k}_{AHC}}\left(\ln\left(\frac{1}{ptt(t)}\right) - \hat{y}_{0,AHC}\right) \tag{6.4}$$

The estimated blood pressure can then be compared to the measured Finapres blood pressure. A sample result generated from this procedure is shown in Figure 6-6. The result is based on data derived from patient # 4. The horizontal bars indicate the error values that correspond to two standard deviations or 2σ.

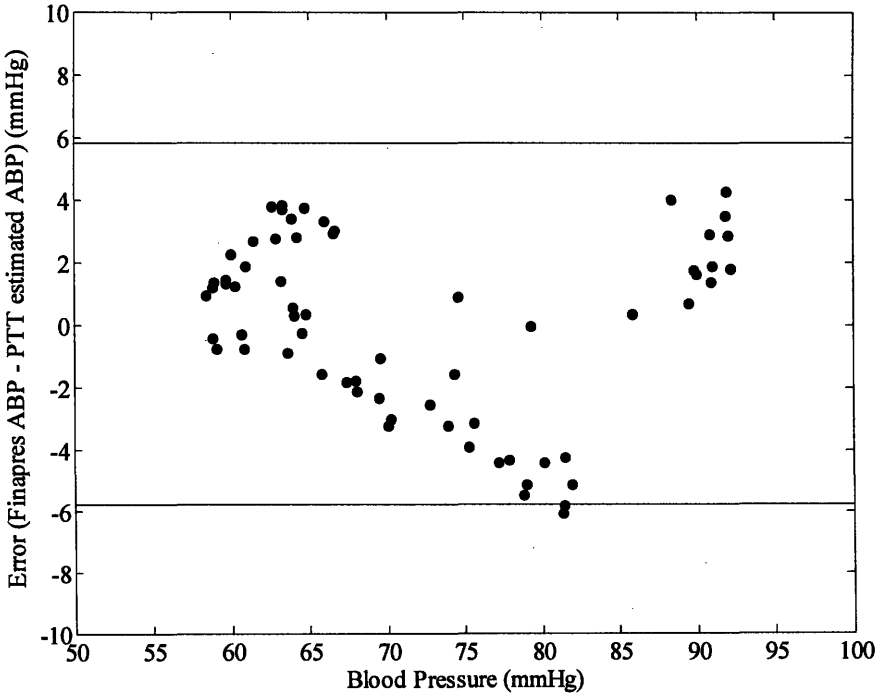

Figure 6-6. Sample human subject test result depicting the difference between PTT BP and Finapres BP.

The final step in the verification of the adaptive height calibration algorithm is to demonstrate that the algorithm can successfully identify the model parameter *k*, despite unknown changes in the arterial blood pressure, if those changes are uncorrelated with the height change. This capability can be verified using techniques normally employed in adaptive noise cancellation. The estimated contribution due to arterial blood pressure variation in our measured PTT variable is given in equation (*6.5*).

$$\hat{\tilde{y}}_{bp}(t) = \tilde{y}(t) - \hat{k}_{AHC} \cdot \tilde{P}_h(t) \tag{6.5}$$

A natural consequence of minimizing the squared error in (*6.5*) using a least squares technique to identify the model parameter $\hat{k}_{AHC}$ as is done in the adaptive height calibration algorithm is that the estimated signal $\hat{\tilde{y}}_{bp}(t)$ will be uncorrelated with the input signal $\tilde{P}_h(t)$ although this consequence does not imply this about the correlation between the estimated signal $\hat{\tilde{y}}_{bp}(t)$ and measured signal $\tilde{y}(t)$.

The actual value of the arterial blood pressure contribution to the PTT signal can be determined using the Finapres BP data from the expression in equation (*6.6*).

$$\tilde{y}_{bp}(t) = \hat{k}_{Fin} \cdot \left(\tilde{P}_{bp,Fin}(t) - \rho g \tilde{h}(t) \right) \tag{6.6}$$

If the two signals $\hat{\tilde{y}}_{bp}(t)$ and $\tilde{y}_{bp}(t)$, are equal or almost equal then our adaptive height calibration algorithm will have successfully identified the model parameter *k*, despite unknown, uncorrelated variation in the arterial blood pressure. A plot displaying the estimated and actual variation in PTT due to blood pressure variation for a sample test subject is shown in Figure *6-7*.

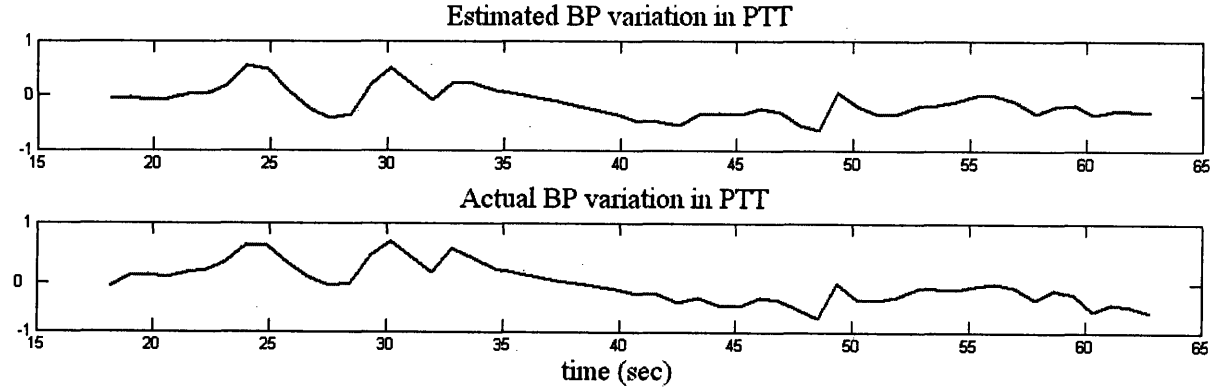

Figure 6-7. Actual $\tilde{y}_{bp}(t)$ and estimated $\hat{\tilde{y}}_{bp}(t)$ contribution to the measured PTT caused by unknown blood pressure variation throughout the calibration period

The plot was identified from the data measured in patient 4 from Table *6:1*. The plot demonstrates that actual and estimated signals are nearly identical and that we have succeeded in identifying the model parameter k, with less than 2% error despite unknown changes in arterial blood pressure.

6.3 EVALUATING CORRELATION BETWEEN MODEL PARAMETERS

Unfortunately, the adaptive height calibration algorithm does not allow identification of the zero pressure offset parameter y_0 used in our device model. Both of the parameters in this model represent physiologic characteristics of the vessel (e.g. wall stiffness) and fluid being monitored by our device. It is very likely that the sympathetic mechanisms that cause the model parameter k to evolve over time might also have an affect on the offset parameter y_0. A series of experiments were preformed in order to develop an understanding of how the two model parameters vary with respect to each other over time and begin to build a foundation upon which updates in model parameter k, might be used to adaptively update the parameter y_0.

The experimental protocol and data processing used in these experiments was the same used in the adaptive height calibration tests described in the preceding section of this chapter. However, all parameter model values reported in this section were identified using the measured pulse transit time data and Finapres blood pressure data.

In the first set of experiments parameter values were identified for the same individual at hourly intervals over a 9 hour period. The identified model parameter values and mean diastolic blood pressure values identified during these experiments are displayed in Figure *6-8*.

These experimental results demonstrate a strong negative correlation between the identified model k, and the identified model parameter y_0. The correlation coefficient between the two model parameters was -0.90.

Further testing was performed on multiple subjects to determine whether this negative correlation was demonstrated in other patients. Data collection and parameter identification was performed on three different subjects, at two different times, on two consecutive days. The 6 sets of model parameters identified during these tests are shown in Figure *6-9*. The patient numbers are in reference to the numbers in Table 6:1. These results presented in Figure *6-9* also display a negative correlation between the identified model parameter k, and the identified model parameter y_0.

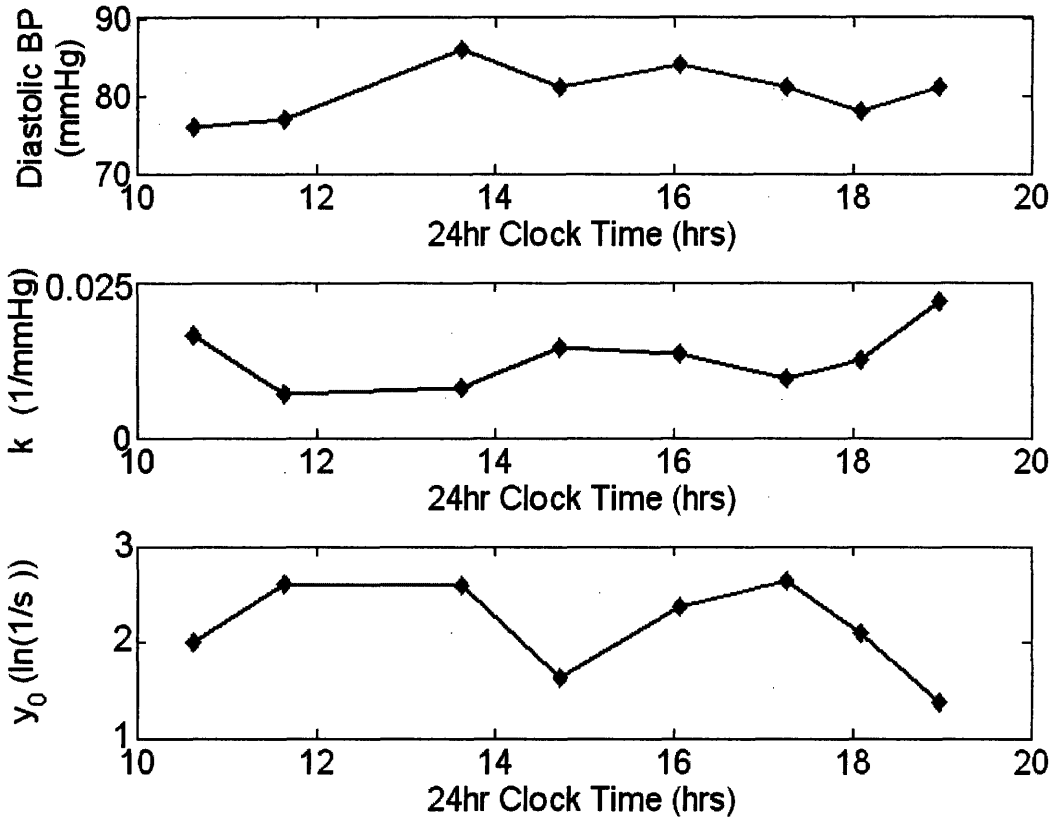

Figure 6-8. Variation in the identified model parameters k and y_0 over a 9 hour period

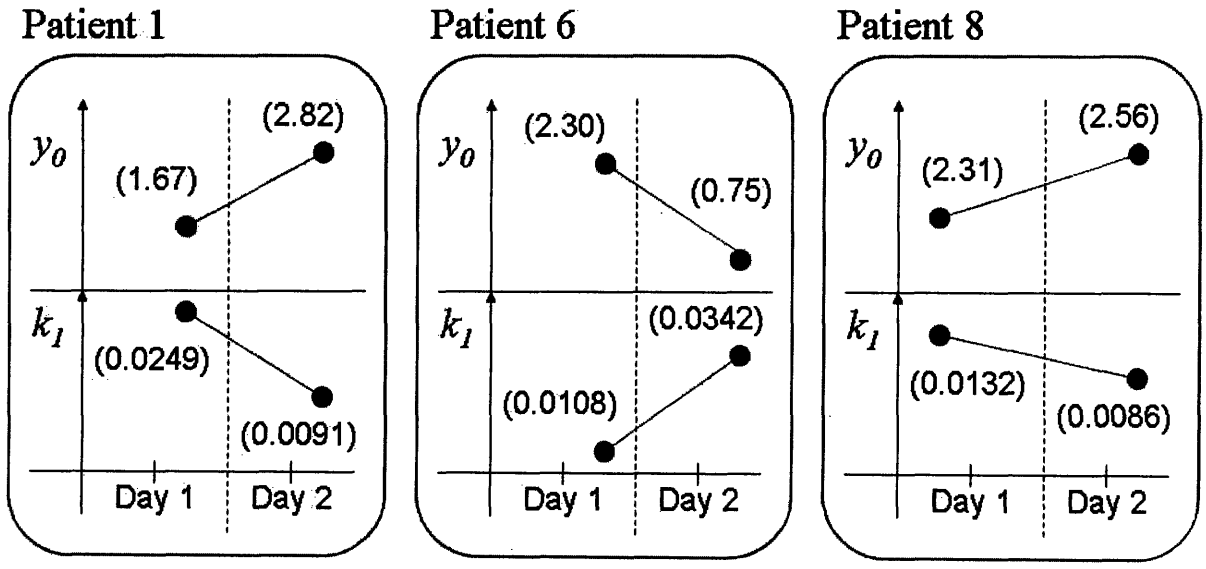

Figure 6-9. Model parameter variation observed in data collected on two consecutive days

Based on these experimental results, there appears to be a consistent relationship between the two model parameters. However, this relationship is not easily captured using simple polynomial models. Additional experimentation was required to determine the source of this variation and whether it was due to physiologic mechanisms or the result of local arterial conditions imposed by the sensors in our device. This topic will be explored in depth in the next chapter in this thesis.

6.4 DATA SCREENING

During processing and analysis of the data collected in these experiments, four primary sources were identified as causing abnormally poor correlation between the height variation and the variation in measured pulse transit time. These four sources include; variation in arterial blood pressure that is correlated with our height variation, low signal to noise ratio in the PPG signals, abnormalities in the foot of the PPG waveform, and motion of the joints proximal to the PPG sensors during the calibration period.

There exist several potential causes for correlated blood pressure change during our experiments. First, attaching the Finapres BP monitor to the same hand as the PPG sensors required the patient to raise and lower the heavy pneumatic actuator housing throughout the calibration period. This forced the muscles of the arm to be exerted and this isometric exercise may have increased BP with height variation. In future experiments requiring the Finapres this problem could be partly resolved by attaching the Finapres to the stationary hand opposite to the hand on which the PPG sensors are attached. Second, patients tend to anticipate the verbal instructions used to initiate height changes, this anticipation and the corresponding relaxation following height change may actually lead to some correlated blood pressure variation. This issue may be resolved by increasing a patient's familiarity and understanding of the calibration routine and it would not be a problem using natural patient mediated motion.

A low signal to noise ratio in the PPG signal makes it difficult to accurately identify a point of identity on the PPG waveform. The signal noise in the wrist PPG sensor and finger PPG sensor was identified from the respective sensor signals while the sensor was attached to a patient but misaligned such that it did not capture any arterial volume pulsation. The standard deviation in the signal noise present in the two PPG sensors used in these experiments was approximately 8 millivolts.

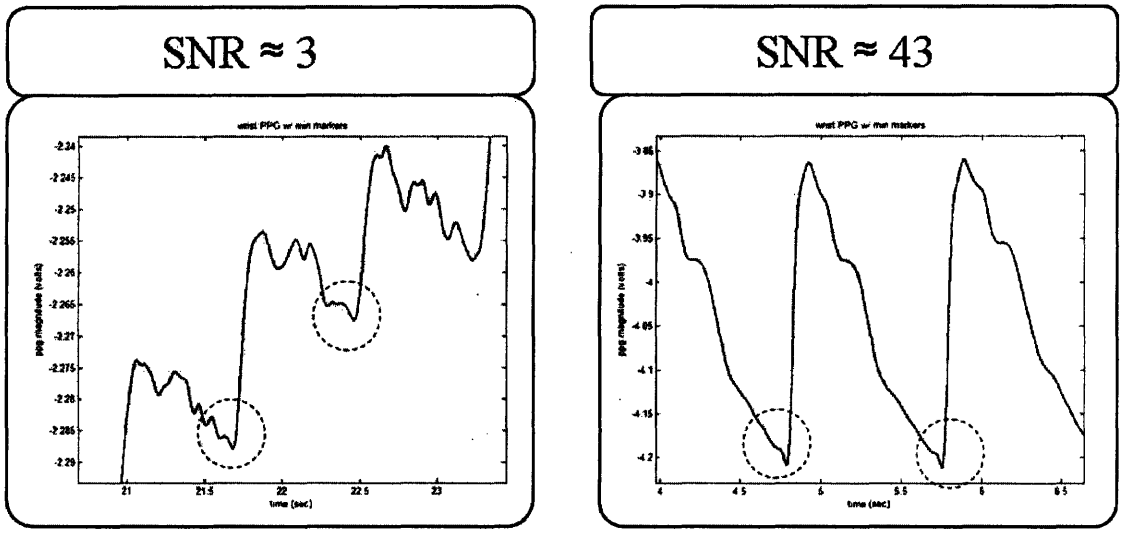

Figure 6-10. Pulse transit time error may result from measurements made from PPG waveforms with a low signal to noise ratio.

The amplitude of any filtered PPG signal was determined as the difference between the maximum voltage value measured during a specific cardiac cycle and the minimum voltage value measured during a specific cardiac cycle. Examples of filtered PPG waveforms having distinctly different signal to noise ratios are shown in Figure *6-10*. Based on experimental observation PPG waveforms demonstrating a signal to noise ratio (SNR) of less than 3 should be discarded from the data set.

Throughout the course of the experiment seemingly random abnormalities were infrequently observed in the foot of one of the PPG waveforms. An example of one of these abnormal onsets is shown in Figure *6-11* along side several normal onsets.

The cause of these abnormalities is unknown to the author but may be the result of motion artifact in the signal caused by an abrupt height change or contraction of the muscles surrounding the measurement site. Regardless of their origin a PTT estimate made from these abnormal onsets may produce an abnormally large variation in the estimated PTT value. However, the abnormal PTT value may still lie within the accepted range of normal PTT values. A screening mechanism which recognizes the wild transient fluctuations in PTT caused by these beats might include establishing a limit on the magnitude of variation between successive PTT measurements and discarding PTT data that falls outside these limits

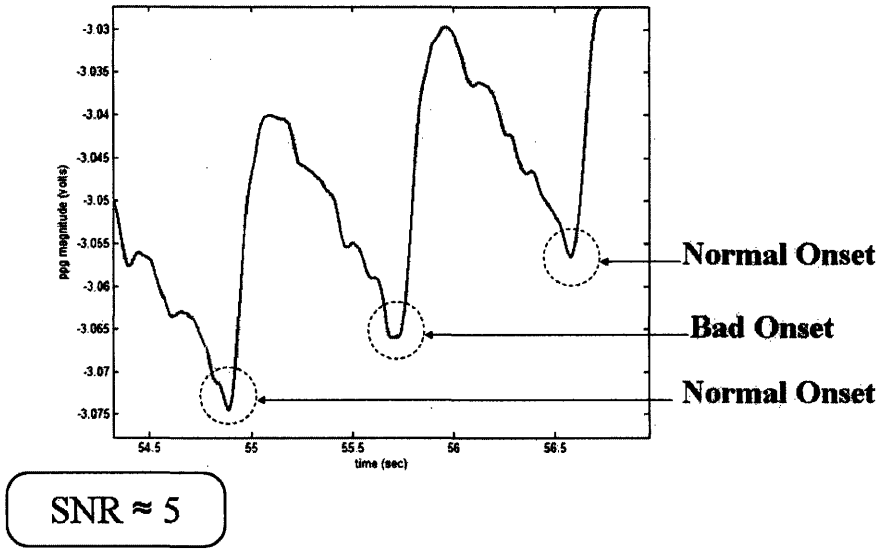

Figure 6-11. Pulse transit time error may result from signal abnormalities in the onset of the PPG waveform

The final source of error observed in these experiments was caused by motion of the joints proximal to the PPG sensor housing. This source of error will be explored in depth in the next chapter.

An additional screening mechanism that should be employed during adaptive height calibration is to observe the correlation between the transformed PTT variable $y(t)$ and the relative height variation $h(t)$. If the correlation between these two signals is low (less than 0.7) then the error in the identified model parameter k will most likely be high. Data segments within the calibration period that have very low correlation should be discarded from the data set. However, based on the analysis presented in chapter 5.4 a minimum data length of 15 seconds (or 15 samples) should always be used for the identification.

CHAPTER 7
MODELING THE EFFECTS OF SENSOR CONTACT PRESSURE ON MEASURED PULSE TRANSIT TIME

The goal of this chapter of the thesis is to augment our lumped parameter device model to include the effects of PPG sensor contact pressure on measured pulse transit time based on experimental observations and analysis.

Sensor contact pressure was on of the potential sources of error discovered during the adaptive height calibration laboratory testing. This chapter characterizes the magnitude of pulse transit time variation produced by sensor contact pressure. The 3 primary mechanisms through which sensor contact pressure influences the measured pulse transit time will be listed and evaluated through modeling and experimentation. An augmented device model will be proposed that characterizes the effect of sensor contact force on measured pulse transit time. Finally, in light of this new device model we will revisit the adaptive height calibration algorithm proposed in chapter 5 and explain the relationship between the model parameters k and y_0 observed in the experimental testing observed in chapter 6.

7.1 UNDERSTANDING THE INFLUENCE OF SENSOR CONTACT FORCE

The external pressure or contact force applied by the PPG sensor housing to the tissue at the measurement site influences the estimated arrival time of the measured PPG pulse waveform [33]. Variation of the external contact force at the measurement sites during calibration and/or BP estimation will alter the measured pulse transit time and serve as a source of error. The impact of external sensor force variation on the pulse transit times measured by our device may be especially significant because of the short pulse transit distance between our in-line PPG sensors and the error compounded by the use of two PPG sensors rather than just one. Therefore, it is important not only to quantify the effect that external force variation has on the pulse transit times measured by our device but also to understand the mechanisms of its influence in order to incorporate them into a system model of our sensors. This augmented system model will allow comparison of pulse transit times measured under the influence of different external sensor

pressures applied during attachment and improve the sensor calibration and estimation capability of our BP monitor.

7.1.1 Wrist Posture Test

The external contact pressure applied by the PPG sensor housing to the tissue can be varied by adjusting the posture of the joints proximal to the sensor measurement site. For example the external pressure applied by the wrist sensor housing can be altered by adjusting the angle between the palm and the forearm through rotation of the wrist joint. Similarly, the external pressure applied by the finger sensor housing can be altered by contracting or extending the joints of the finger. Therefore, any postural changes in these proximal joints during BP calibration or estimation periods may alter the measured pulse transit time and lead to error in the estimated BP.

The effect of postural change on the pulse transit time measurements estimated with our device was determined experimentally. The experimental protocol was as follows; two PPG signals were acquired simultaneously from the ulnar artery at the left wrist and the digital artery of the little finger of the left hand. Both the wrist and finger PPG sensors were attached to the subject with an elastic band producing an external sensor loading pressure P_w $(t=0)$ and P_f $(t=0)$ respectively. Throughout the experiment the left arm was supported by a table and kept at a constant height. The experiment was separated into two different stages, during stage one of the experiment $(0 < t < 30\ sec.)$ PPG measurements were collected with the external pressure of the wrist and finger PPG sensor held constant at the initial pressure provided by the elastic bands and with the palm and forearm co-linear to each other. During stage two of the experiment $(30\ sec. < t < 60\ sec.)$ the external sensor pressure applied to the measurement site by the wrist sensor, $P_w(t)$ was increased and held constant by altering the posture of the hand by rotating the wrist joint increasing the angle between the forearm and palm. Care was taken to keep the external pressure below the mean arterial pressure through observation of the wrist PPG waveform morphology. The external pressure applied by the finger sensor was held constant at the initial banded pressure during stage 2. The applied external sensor pressures along with the hand postures used in the protocol are illustrated in Figure *7-1*.

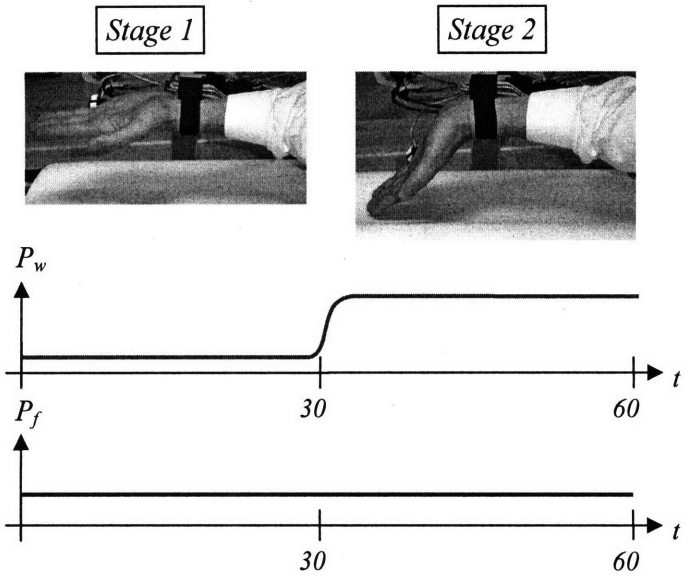

Figure 7-1. Experimental variation in external wrist sensor pressure using a change in hand posture

Pulse transit time (*ptt*) between the two sensors was estimated by subtracting the arrival time of the finger pulse waveforms from the arrival time of the wrist pulse waveform. In order to minimize the effects of waveform shape variation on our pulse transit time estimates the arrival time of the PPG pulse waveform was determined to be the minimum point of the waveform at the end of diastole occurring immediately before the rise of the next pulse wave. A mean pulse transit time was estimated for each stage.

Sample results from several of the experiments are presented in Table *7:1*. As these results suggest the change in pulse transit time caused by varying hand posture and thus the external pressure applied by the wrist sensor is significant. Because of its significance, successful operation of our device will require that posture of the proximal joints be held constant during BP calibration and estimation.

	Test 1	*Test 2*	*Test 3*
ptt_1 *(msec)*	37.2	33.9	32.6
ptt_2 *(msec)*	46.5	43.1	41.3
$\Delta ptt = ptt_2 - ptt_1$ *(msec)*	9.3	9.2	8.7
Percent Change	25.0%	27.1%	26.7%

Table 7:1. Average pulse transit time before (ptt_1) and after (ptt_2) an increase in external wrist sensor pressure

7.1.2 Direct Pressure Test

A second set of experiments were performed in order to eliminate any potential variation in pulse transit time that may have been caused by physiologic changes in the tissue surrounding the artery due to alteration in muscle, tendon or bone position as a result of altering wrist posture. This second set of experiments evaluated the impact that external sensor pressure variation has on pulse transit time measurements using a direct force applied to the sensor housing while the hand posture was fixed. The experimental protocol was as follows; two PPG signals were acquired simultaneously from the ulnar artery at the left wrist and the digital artery of the little finger of the left hand. A continuous blood pressure measurement was also collected using the Finapres™ blood pressure monitor attached to the index finger of the left hand. Both the wrist and finger PPG sensors were attached to the subject with an elastic band providing an external sensor loading pressure to the sensor contact surface $P_w(t)$ and $P_f(t)$ respectively. Throughout the experiment the left arm was supported in a fixed position. The experiment was separated into two different stages, during stage one of the experiment ($0 < t < 30$ *sec.*) PPG measurements were collected with the external pressure of the wrist and finger PPG sensor held constant at the initial pressure provided by the elastic bands. During stage two of the experiment (30 *sec.* $< t <$ *60 sec.*) the external sensor pressure applied to the measurement site by the wrist sensor, $P_w(t)$ was increased and held constant by applying a direct force to the sensor housing. Care was taken to keep the external pressure below the mean arterial pressure through observation of the wrist PPG waveform morphology. The external pressure applied by the finger sensor housing was held constant at the initial banded pressure during stage 2. The applied external sensor pressures used in the protocol are illustrated in Figure *7-2*.

Pulse transit time (*ptt*) between the two sensors was estimated by subtracting the arrival time of the finger pulse waveform from the arrival time of the wrist pulse waveform. In order to minimize the effects of waveform shape variation on our pulse transit time estimates the arrival time of the PPG pulse waveform was determined to be the minimum point of the waveform at the end of diastole occurring immediately before the rise of the next pulse wave. A mean pulse transit time was estimated for each stage.

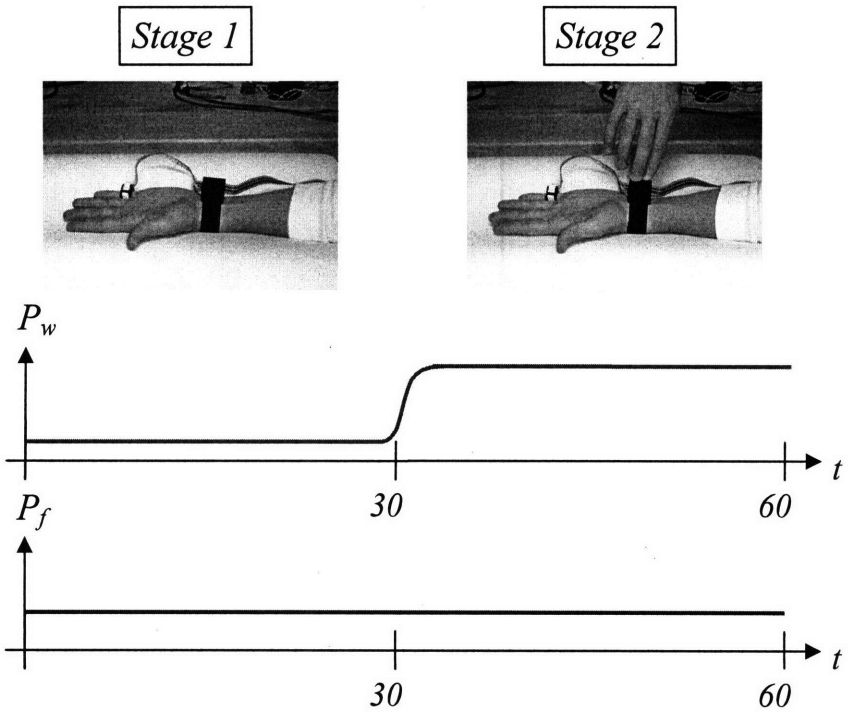

Figure7-2. Experimental variation in external wrist sensor pressure using direct pressure on sensor housing

Sample results from several of the experiments are presented in Table *7:2*. As these results suggest the change in pulse transit time caused by varying wrist sensor pressure is significant. Because of its significance, successful operation of our device will require the effect of external sensor pressure on our *ptt* measurements to be modeled and parameterized if *ptt* measurements are to be compared for a subject between different applications of the device under different loading conditions.

	Test 1	*Test 2*	*Test 3*
ptt_1 *(msec)*	23.6	22.3	20.4
ptt_2 *(msec)*	35.4	32.8	30.3
$\Delta ptt=ptt_2-ptt_1$ *(msec)*	11.8	10.5	9.9
ptt percent change	50.0%	47.1%	48.5%
$\Delta MAP= MAP_2 - MAP_1$ *(mmHg)*	2.9	8.5	2.5

Table 7:2. Average pulse transit time and mean arterial pressure (*MAP*) before (ptt_1) and after (ptt_2) an increase in external wrist sensor pressure.

Further, a comparison of the results presented in Table *7:1* and *7:2* which were derived from the same subject reveal that the difference in pulse transit time between the two stages caused by direct pressure and posture change are the same order of magnitude. The discrepancy between the mean *ptt* magnitudes in the two experiments may be attributed to the height difference of the measurement sites relative to the heart during data collection.

7.1.3 External Sensor Force & Transmural Pressure

An understanding of the mechanisms through which external sensor force acts to influence the arrival time of the PPG pulse waveform begins with a simple model of the anatomy of the sensor measurement sites. An idealized anatomical model of the PPG sensor measurement site is shown in Figure *7-3a* and *7-3b* and consists of three primary components, the sensor housing (grey) with elastic band used to attach it to the subject, a bone providing a solid support (yellow), and the artery being observed by the PPG which lies between the housing and the bone (red). Upon sensor attachment the elastic band and sensor housing apply a force to the skin at the contact surface of the sensor. This contact force compresses the tissue underlying the sensor between the bone and sensor housing. This compression produces an increased external pressure, P_e in the tissue surrounding the artery. As depicted in Figures *7-3a* and *7-3b* the greater the contact force, F_c (indicated by the darker shade of blue in Figure *7.3b*) the more the tissue is compressed under the sensor housing, creating a larger external pressure surrounding the artery (indicated by the darker shade of orange in Figure *7.3b*). Therefore the external force applied to the measurement site by the housing alters the external pressure P_{ex}, surrounding the artery and determines in part the transmural pressure acting across the arterial wall. The expression for transmural pressure is given again in equation (*7.1*) where P_i represents intra-arterial pressure.

$$P_{tm}(t) = P_i(t) - P_{ex}(t) \qquad (7.1)$$

This suggests that any physiologic variable measured by our sensors that is dependent on transmural arterial pressure at the sensor measurement site will be affected by the external force applied to by the sensor housing.

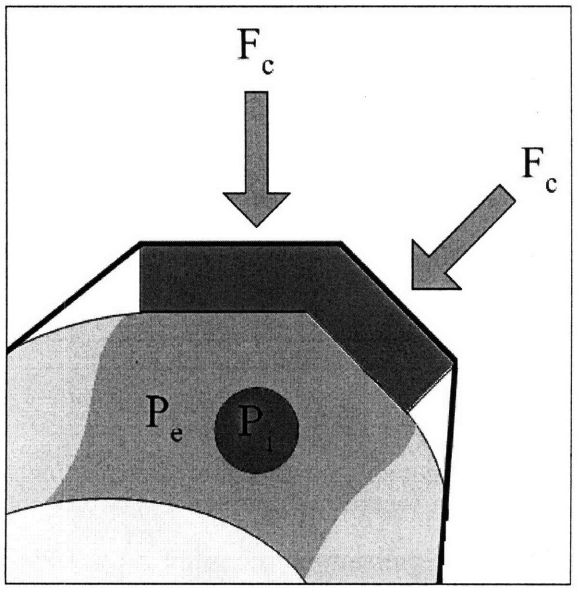

Figure 7-3a. Measurement site anatomy subject to a small sensor contact force, F_c.

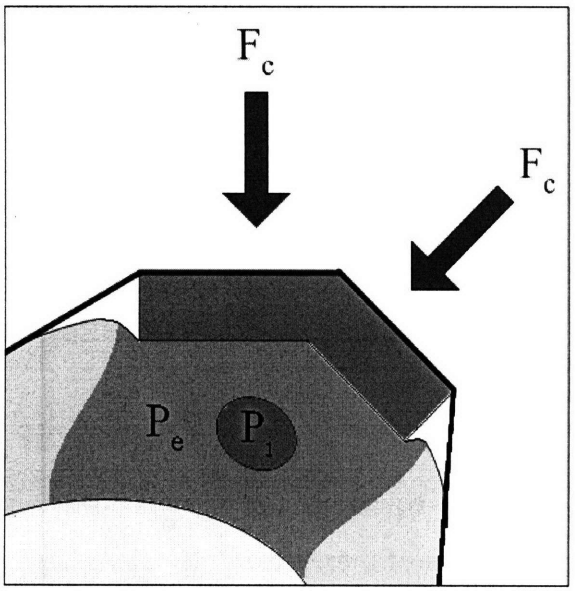

Figure 7-3b. Measurement site anatomy subject to a large sensor contact force, F_c.

The idealized anatomical model in Figure *7-3* illustrates and predicts the role that external sensor force plays in our system, however the actual anatomy underlying the sensor measurement site is far more complex. The anatomy is a three dimensional network of heterogeneous tissue types including, dermal tissue, adipose tissue, muscle tissue, tendons, ligaments, and bone each having unique mechanical properties (e.g. stiffness) and orientation relative to the sensor housing, properties which may be altered through muscular contraction and postural changes in the wrist and finger joints. Additionally, the external pressure applied to the measurement site by the sensor housing may not be uniformly distributed across the contact surface. This non-uniform contact pressure along with the heterogeneous tissue composition may result in a complex three dimensional external pressure field surrounding the artery. However, the experimental analysis and model development presented in the remainder of this chapter assumes that this pressure field can be approximated using a single valued external arterial pressure surrounding the vessel. The validity of this assumption and its role as a potential source of error may be a subject of investigation for future work.

There are three primary mechanisms through which an alteration in external sensor force and the corresponding change in transmural arterial pressure influence the estimated arrival time of the PPG waveform and *ptt*. These three mechanisms include; 1) alteration to the shape of the volumetric PPG waveform used to identify pulse arrival time 2) alteration in the phase delay

between the periodic pressure waveform and the volumetric PPG waveform, and 3) alteration in the velocity of the pressure pulse wave between the two measurement sites. The first mechanism was described in depth in chapter 4 where the problem on non-linear scaling of the pressure wave was addressed by selecting the PPG waveform minimum as the onset marker to identify pulse arrival time. The other two mechanisms will be discussed in depth and explored experimentally in the following sections.

7.2 EXTERNAL PRESSURE DEPENDENT PPG PHASE DELAY

The equations for wave velocity and transit time presented in chapter 2 govern the transmission of a pressure pulse along an artery. However, the pulsations recorded by the PPG signal are determined by the volumetric variation in the artery underlying the measurement site. The compliance of the arterial wall characterizes the pressure-volume relationship in the artery and this relationship is known to exhibit viscoelastic behavior such as hysteresis and creep [22]. Therefore, the function relating transmural arterial pressure $P_{tm}(t)$, to arterial volume $V(t)$, is a dynamic process $g_{wall}(t)$, and the dynamics of this process may influence the onset or arrival time of our volumetric PPG signal $v_{PPG}(t)$. In addition to serving as an input to our dynamic system the magnitude of the transmural pressure also modifies the non-linear compliance of our dynamic process. A block diagram of this relationship is displayed in Figure *7-4*.

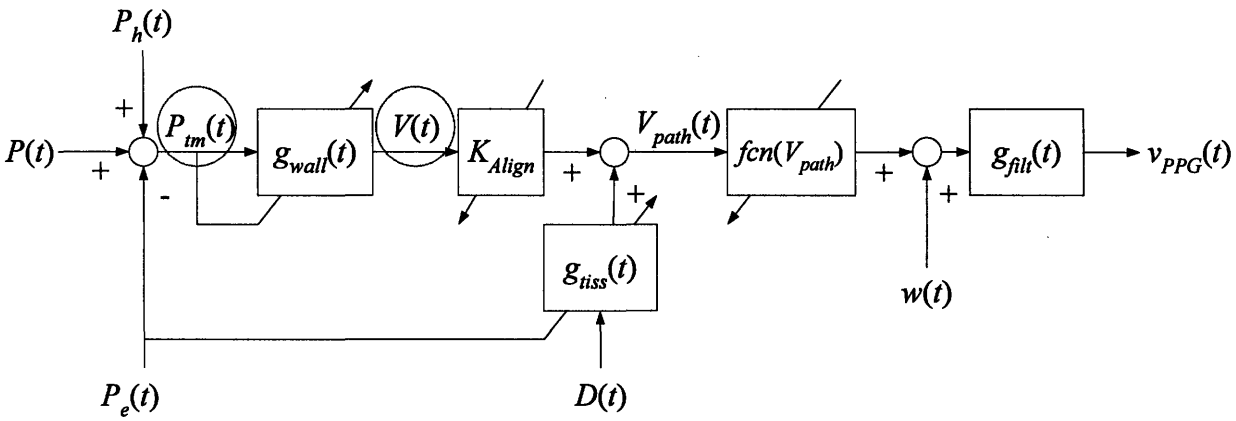

Figure 7-4: Block diagram displaying the dynamic relationship between arterial pressure *P*, external arterial pressure P_e and the measured PPG signal v_{PPG}

The input term $D(t)$ represents the volume of tissue and extra-arterial fluid in the optical path that attenuate light intensity reaching the photodiode from our LED, this volume may also be modified by the external pressure. The term $V_{path}(t)$ represents the total volume of light absorbers in the optical path, and $fcn(V_{path})$ is an algebraic function relating the volume of light absorbers to the measured PPG voltage. The term $w(t)$ represents the noise in our signal and $g_{filt}(t)$ the low-pass filter used to remove the filter noise. In this section we are focused on the relationship between transmural pressure acting across the arterial wall and arterial volume.

For a periodic arterial pressure the dynamics of the arterial wall may cause the arterial volume to lag behind arterial pressure inducing a phase delay in the periodic arterial volume. Typically, this phase delay $\phi(\omega)$, is only a function of the frequency ($\omega = 2\pi f$) of the input signal and depending on the input frequency, the arrival time of the PPG waveform (t_{PPG}) may be delayed compared to the arrival time of the pressure waveform (t_P) at the measurement site. However, due to the non-linear compliance of the artery the magnitude of this delay is not only frequency dependent but also dependent on the transmural pressure acting across the arterial wall as shown in equation (*7.2*).

$$t_{PPG}(\omega, P_{tm}) = t_P + \frac{|\phi(\omega, P_{tm})|}{\omega} \tag{7.2}$$

The effect that PPG phase delay has on the pulse transit time estimated from our in-line PPG sensors is given in equation (*7.3*).

$$ptt = (t_P(z_C) - t_P(z_A)) + \frac{1}{\omega}\left(|\phi(P_{tm}(z_C))| - |\phi(P_{tm}(z_A))|\right) \tag{7.3}$$

A model of the arterial pressure-volume relationship can be used to develop some intuition regarding the potential effect that the pressure dependent phase delay may have on the arrival time of our volumetric PPG signal. A simple model capable of representing the viscoelastic behavior of arterial wall is the Voigt model shown in Figure *7-5*. The model contains a non-linear spring with stiffness, μ that is dependent on transmural pressure, and a parallel damper, η.

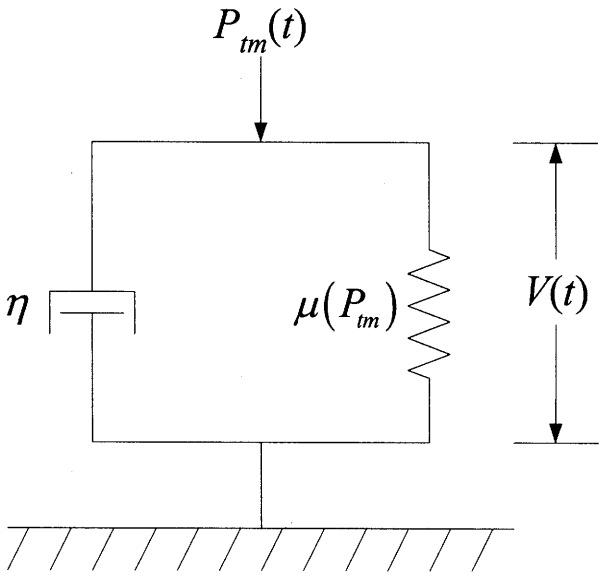

Figure 7-5. Voigt model used to describe the dynamic behavior of the arterial pressure-volume relationship

The differential equation that describes the pressure-volume relationship in this model is given in equation (*7.4*).

$$\mu(P_{tm})V(t)+\eta\dot{V}(t)=P_{tm}(t) \tag{7.4}$$

Because we are only concerned with the phase dependence of the foot or base of the pressure waveform insight about phase delay can be gained from the model through linearization of the pressure dependent stiffness about the minimum transmural pressure in the cardiac cycle (P_{foot}). The transfer function $G_{wall}(s)$ of the linearized model is given in equation (*7.5*).

$$G_{wall}(s)=\frac{1}{\eta s+\mu(P_{tm}=P_{foot})} \tag{7.5}$$

The magnitude of the phase delay of this dynamic model is given in equation (*7.6*).

$$\left|\phi(\omega,P_{foot})\right|=\arctan\left(\frac{\omega\eta}{\mu(P_{foot})}\right) \tag{7.6}$$

A sketch of the non-linear arterial stiffness is shown in Figure *7-6*. The potential effect that a change in external pressure can produce in phase delay can be evaluated from this figure.

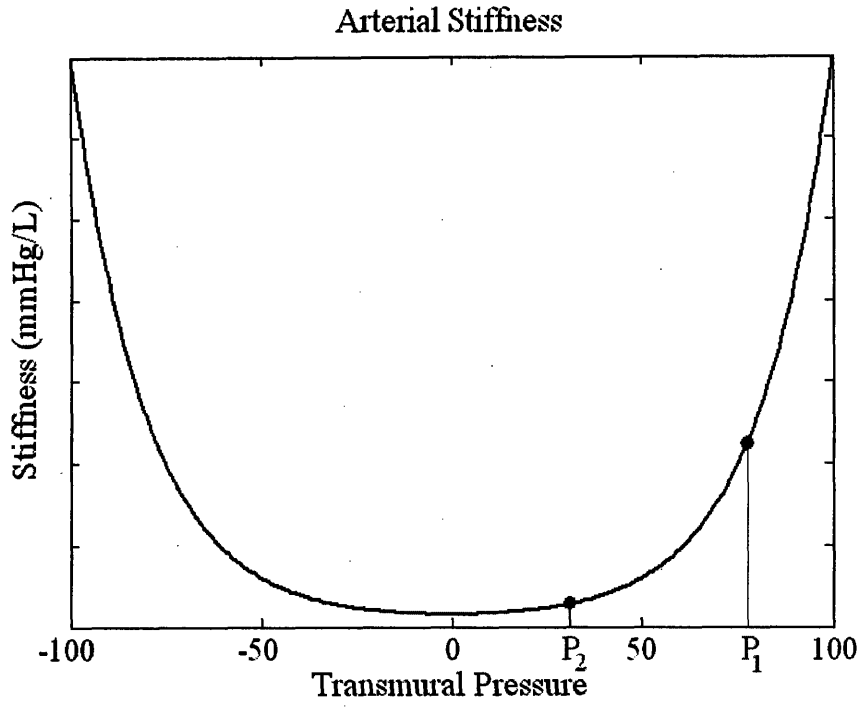

Figure 7-6. Sketch of the pressure dependent arterial stiffness, μ

Given the assumption that the initial value of the base of the pressure waveform is located at, $P_{foot} = P_1$ and then following an increase in external pressure the base arrives at a new transmural pressure value, $P_{foot} = P_2$ the relationship between the stiffness values at these two pressures is given in equation (*7.7*).

$$\mu(P_1) > \mu(P_2) \tag{7.7}$$

The relationship between the magnitudes of the phase delay produced in the arterial volume waveform for these two external pressures can be determined from equation (*7.7*) and is given in equation (*7.8*).

$$\left|\phi(\omega, P_1)\right| < \left|\phi(\omega, P_2)\right| \tag{7.8}$$

As equation (*7.8*) demonstrates if the magnitude of the arterial stiffness is diminished the magnitude of the phase delay is increased.

To understand the effect that phase delay has on the pulse transit times measured by our sensors we will assume that the transmural pressure change described above occurs at the wrist sensor measurement site. To isolate the effect of phase change on *ptt* we have assumed that the arrival time of the pressure waveform at both sensor locations remains constant with external pressure change however, this assumption is strictly speaking not true. We have also assumed

that the phase delay at the finger sensor remains constant. The change in measured pulse transit time due to the pressure dependent change in phase delay at the wrist sensor is given in equation (*7.9*).

$$\Delta ptt = ptt_2 - ptt_1 = \frac{1}{\omega}\left(\left|\phi(P_1)\right| - \left|\phi(P_2)\right|\right) < 0 \qquad (7.9)$$

This equation suggests that an increase in external pressure will increase the phase delay in the wrist PPG signal which would cause the pulse transit time measured between our two sensors to decrease. Based on the experimental data previously presented in section 7.1.1 in the *Wrist Flex Test* and section 7.1.2 in the *Direct Pressure Test* the pulse transit time consistently increased following an increase in external sensor pressure. These experimental observations along with the analysis presented in this section suggest that the change in the pressure dependent phase delay is small at the low frequencies of our input pressure waveform and this mechanism can be neglected from our device model.

7.3 EXTERNAL PRESSURE DEPENDENT PULSE WAVE VELOCITY

Contact force dependent variation in pulse wave velocity along an arterial segment underlying a PPG sensor housing was first described by Teng and Zhang [36] In their paper they proposed that the external pressure applied to the digital arteries by their finger tip PPG sensor reduced transmural pressure in the these arteries which in turn increased the pressure dependent compliance of the arterial wall and lowered the pulse wave velocity through the pressurized arterial segment. Their pulse transit time estimates were determined as the timing difference between the peak of the QRS complex of the EKG waveform and the onset of a PPG waveform measured at the fingertip.

However, their experimental protocol and conclusion were based on the pressurization of the finger tip PPG sensor used to determine the arrival time of the pulse waveform. Because factors that effect the volumetric PPG signal are also altered with contact force it is the author's opinion that their methodology may have failed to uniquely identify the contribution of pulse wave velocity change in their *ptt* measurements.

In this section we will explore the relationship between external sensor pressure and pulse wave velocity for our in-line PPG sensor architecture. The contribution that velocity change makes to the pressure dependent variation in the measured *ptt* will be experimentally

evaluated for our PPG sensor housings. Finally, a novel model will be developed to incorporate the effects that external sensor pressure has on wave velocity at the measurement sites and on our measured pulse transit time.

The external arterial pressure applied by our two sensor housings increases the external pressure at these locations. As a pressure pulse propagates along the arterial path between the two sensors it must pass through the pressurized arterial segments underlying the measurement sites. An illustration of the distributed external pressure found along the arterial path observed by our in-line PPG sensors is shown in Figure 7-7. In the figure the measurement point of the ulnar artery PPG waveform is denoted as z_A and the measurement point of the digital artery PPG waveform is denoted as z_C. The external arterial pressure surrounding the unloaded arterial segments is assumed to be negligibly small (or atmospheric).

7.3.1 Finger Band Test

A set of experiments were designed to investigate the effects of external pressure variation on the velocity of the propagating pressure pulse between our two sensors. An important goal of the experiment was to evaluate the effects of external pressure variation on pulse wave velocity without varying the external pressure applied by either of the sensors used to measure the pulse transit time.

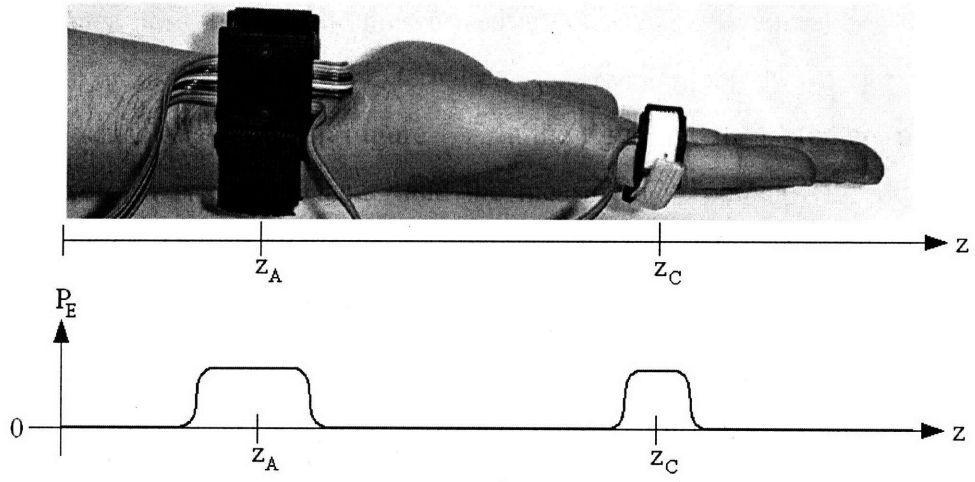

Figure 7-7. Sketch of the distributed external pressure along the arterial transit path observed by our in-line PPG sensors.

The protocol of the experiments was as follows, two PPG signals were acquired simultaneously from the ulnar artery at the left wrist and the digital artery of the little finger of the left hand. A continuous blood pressure measurement was recorded using the Finapres blood pressure monitor attached to the index finger of the left hand. Both the wrist and finger PPG sensors were attached to the subject with an elastic band providing an external sensor loading pressure of $P_w(t=0)$ and $P_f(t=0)$ respectively. The initial pressure applied by both sensors was held constant during the entire experiment. Throughout the experiment the left arm was supported in a fixed position. The experiment was separated into two different stages, during stage one of the experiment ($0 < t < 30$ *sec.*) PPG measurements were collected with an elastic band wrapped around the base of the little finger, exerting an external pressure on the digital artery segment just prior to the segment monitored by the ring sensor. The experimental configuration used in Stage 1 of the experiment is pictured in Figure *7-8* along with the corresponding transmural pressure distribution of the arterial path between the two sensors. At the onset of stage 2 of the experiment (t = 30 seconds) the band was instantly removed from the finger such that during the second stage of the experiment (30 *sec.* $< t < 60$ *sec.*) no external pressure was applied to the base of the digital artery by the band. Care was taken to keep the external pressure applied by the band below the diastolic pressure through observation of the finger PPG waveform morphology.

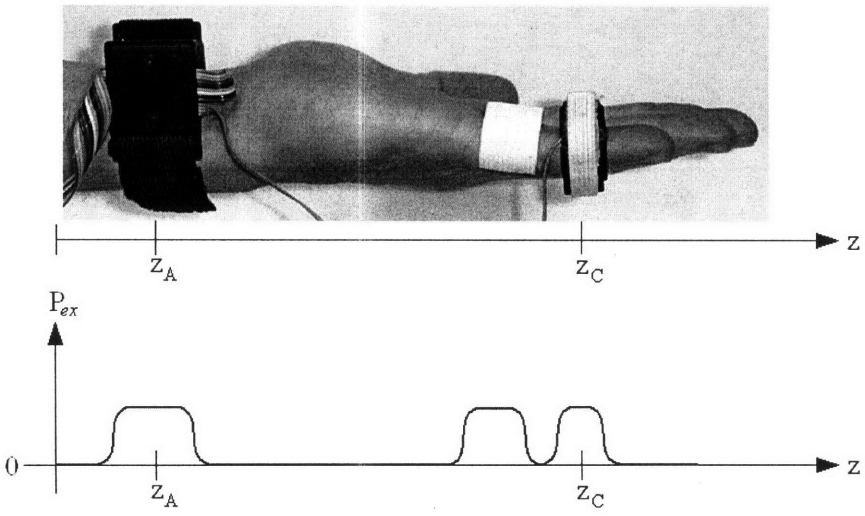

Figure 7-8. Experimental configuration used during stage 1 of the *Finger Band Test* experiment along with the distributed external pressure along the arterial path observed by the two sensors

The mean results from six different *Band-Test* experiments performed on a healthy male subject are presented in Table *7:3*.

	Mean	Standard Deviation
$\Delta ptt = ptt_2 - ptt_1$ (*msec*)	-10.4	4.3
$MAP_2 - MAP_1$ (*mmHg*)	-6.1	5.2
Wrist: $\|PPG_2\| - \|PPG_1\|$ (*millivolts*)	1.1	6.3
Finger: $\|PPG_2\| - \|PPG_1\|$ (*millivolts*)	16.5	28.6

Table 7:3. The differences in pulse transit time (*ptt*), mean arterial pressure (*MAP*), and PPG magnitude (|*PPG*|) before (stage 1) and after (stage 2) removal of an elastic band from the little finger.

A positive correlation was observed between the external pressure variation in the arterial segment underlying the elastic band and the variation in measured pulse transit time, as external pressure decreased with the release of the band, pulse transit time also decreased. With the elastic band attached to the finger the external pressure acting on the arterial wall was increased and the measured pulse transit time was largest during stage 1 of the experiment. During stage 2 of the experiment, with no elastic band around the finger, the external pressure was smaller in this arterial segment than it had been in stage 1 and the pulse transit time was also smaller compared to its stage 1 value. As indicated in Table *7:3*, in nearly all of the experiments performed the mean arterial pressure measured by the Finapres tended to slightly decrease between the two stages. This decrease would suggest an increase in pulse transit time in stage 2 but in fact the opposite effect was observed. This further demonstrates that removal of the band and the corresponding change in external pressure at this site was the dominant mechanism influencing *ptt*.

Unfortunately, removal of the elastic band appeared to have some impact on the finger PPG signal. Both the D.C. portion of the PPG signal and A.C. portion of the PPG signal changed following removal of the band. As expected the D.C. value decreased in the inverted PPG signal following band removal, indicating that while attached the band caused some venous pooling in the finger distal to the banded site at the sensor location and after release of the band the volume in the distal segment underlying the sensor measurement site decreased. An example set of finger PPG waveform data measured during one of the Finger band tests is shown in Figure *7-9*.

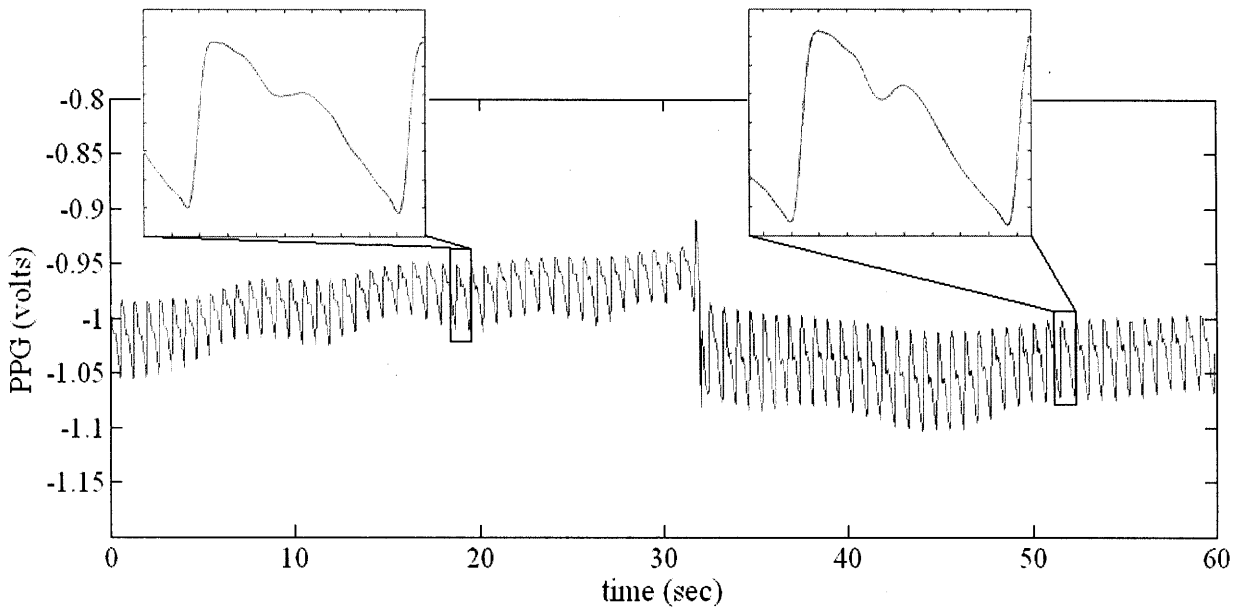

Figure 7-9. Example finger PPG data set measured before (t < 30) and after (t > 30) band removal during the *Finger Band Test.*

Although the magnitude of the Finger PPG signal did consistently increase between the two stages the magnitude of the increase was very small compared with the increase in magnitude demonstrated by the wrist and finger sensor following direct pressurization of the sensor housing. Direct pressurization of the wrist or finger sensor housing can induce a magnitude change of as much as 100-200 millivolts. When viewed form this perspective the average 16 millivolt change demonstrated between the two stages of this experiment is extremely small and probably did not have had a major impact on the experimental outcome. None the less a change did occur and this change prompted further experimental analysis of the effects of sensor contact pressure on pulse transit time.

7.3.2 Direct Pressure EKG Test

A second set of experiments were performed to specifically evaluate the effect that pressurization of our wrist sensor housing has on the velocity of the propagating pressure pulse along the arterial path between our two sensors. The experimental protocol was as follows; an EKG signal, an ulnar artery PPG signal at the left wrist, and a digital artery PPG signal at the little finger of the left hand were measured simultaneously. Both the wrist and finger PPG sensors were attached to the subject with an elastic band providing external pressures to the

measurement sites, $P_w(t=0)$ and $P_f(t=0)$ respectively. Throughout the experiment the left arm was supported in a fixed position. The experiment was separated into two different stages, throughout stage one of the experiment ($0 < t < 30$ *sec.*) PPG and EKG measurements were collected with the external pressure of the wrist and finger PPG sensor held constant at the initial pressure provided by the elastic bands. At the onset of stage two of the experiment ($t = 30$ *sec.*) the external sensor pressure $P_w(t)$, applied by the wrist sensor to the measurement site was increased by applying a direct force to the sensor housing. This direct force was held constant and applied throughout stage two of the experiment (30 *sec.* $< t < 60$ *sec.*). Care was taken to keep the external wrist sensor pressure below the mean arterial pressure through observation of the wrist PPG waveform morphology. The external pressure applied by the finger sensor housing was held constant at the initial stage 1 pressure during stage 2. The applied external sensor pressures used in the protocol are the same as illustrated in the previous Figure *7-2*.

To eliminate any potential *ptt* variation caused by the pressure dependence of the wrist PPG signal, the change in pulse transit time between the two stages was observed in *ptt* measurements estimated from the difference of the arrival time of the finger PPG waveform minimum and the peak time of the QRS complex of the EKG waveform. Therefore, we can evaluate the effect on *ptt* produced by an increase in wrist sensor contact force by increasing the external pressure along a segment of the arterial path leading to the finger PPG signal, without altering the contact pressure of the finger sensor used to estimate pulse onset. If the magnitude and morphology of the finger PPG signal remain constant across both stages of the experiment than an increase in pulse transit time must be the result of a decrease in pulse wave velocity through the externally pressurized arterial segment.

A sample experimental result of the pulse transit times measured between the finger PPG and EKG before and after wrist sensor pressurization for a healthy male subject is shown in Figure *7-10*. To simplify data processing and to eliminate any transient effects that may occur due to subject movement during the start of the experiment and immediately following external pressurization of the wrist sensor, measurements from the first 10 seconds of each stage were discarded. Stage 1 *ptt* measurements are displayed in Figure *7-10* using an "x" and stage 2 *ptt* measurements are displayed using a "o".

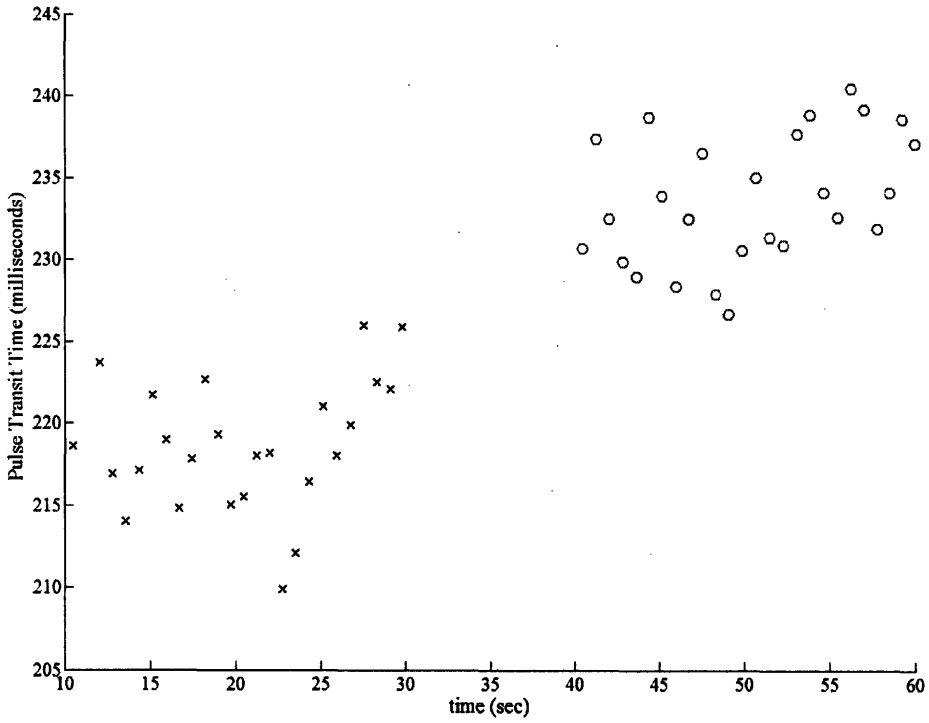

Figure 7-10. Pulse transit time estimates for a male subject derived from the EKG and finger PPG before (t < 30 sec.) and after (t > 30 sec.) direct wrist sensor pressurization

A 15 millisecond increase was observed in the mean *ptt* following pressurization of the wrist sensor, changing from a mean stage 1 *ptt* of 218.7 milliseconds to a mean stage 2 *ptt* of 233.7 milliseconds. The change in *ptt* observed following housing pressurization was directly correlated with the change in external pressure in the arterial segment underlying the housing.

The finger PPG signal and wrist PPG signal measured during this experiment are shown in Figure *7-11* and Figure *7-12* respectively. The change in mean finger PPG magnitude between the two stages was less than 3% or 8 millivolts and the morphology of the finger PPG before and after pressurization remains essentially constant as shown in the figure. In contrast to the finger PPG signal, the wrist PPG signal undergoes a significant change in both magnitude exhibiting a nearly 300% increase a change of 100 millivolts and waveform morphology following pressurization of the wrist sensor housing.

The behavior demonstrated in the sample experiment shown in these figures was typical of the wrist sensor pressurization response observed in the ptt measurements derived from the finger PPG and EKG waveform.

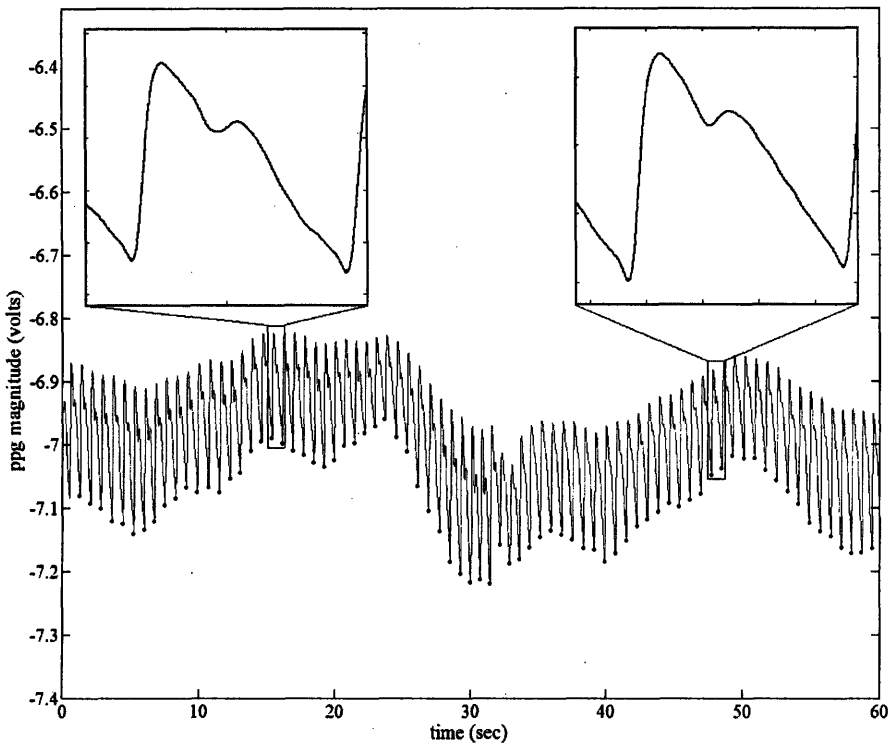

Figure 7-11. The measured finger PPG signal before (t < 30 sec.) and after (t > 30 sec.) direct wrist sensor pressurization

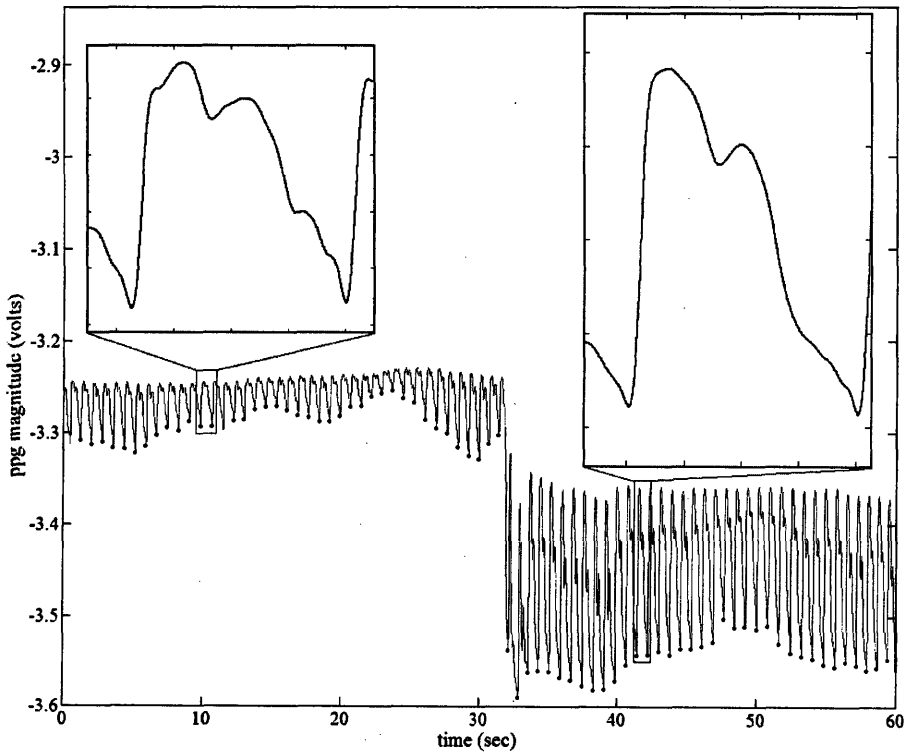

Figure 7-12. The measured wrist PPG signal before (t < 30 sec.) and after (t > 30 sec.) direct wrist sensor pressurization

The direct correlation between pulse transit time change and external pressure change was consistently demonstrated in multiple tests performed on different subjects. The average of three test results for a healthy male test subject (Patient 1) and healthy female test subject (Patient 2) are displayed in Table *7:4*.

	Patient 1	Patient 2
Mean ptt_1 (*msec*)	217.6	229.9
Mean ptt_2 (*msec*)	233.3	235.2
Mean Δptt (*msec*)	15.7	5.2
σ_{ptt} (*msec*)	1.1	1.5
Change in finger PPG magnitude	9.1%	13.5%
Mean arterial pressure (*mmHg*)	101	73

Table 7:4. Average pulse transit time values before (stage 1) and after (stage 2) wrist sensor pressurization derived from three *Direct Pressure EKG Test* performed on two different patients

An additional relationship that can be observed in the data in Table *7:4* was the correlation between mean arterial pressure and the magnitude of the pulse transit time change caused by increasing external pressure at the wrist sensor. This behavior can be attributed to an ability to apply a larger external pressure change in an individual with a higher mean pressure while still maintaining the external pressure at or below the level of the mean arterial pressure.

7.3.3 Multi-stage Direct Pressure EKG Test

The relationship between external sensor force, arterial blood pressure, and pulse transit time was investigated further by observing the effects of multiple step changes in sensor contact force on pulse transit time measurements and PPG magnitude. The experimental protocol used in these tests was similar to the two-stage *Direct Pressure Test* described in the previous experiment. However, instead of limiting the experiment to two external pressure stages the test consisted of 6 different stages in which contact force on the wrist sensor was increased at each successive stage and held constant for a 30 second period. A sketch of the external sensor pressures implemented in the protocol is shown in Figure *7-13*.

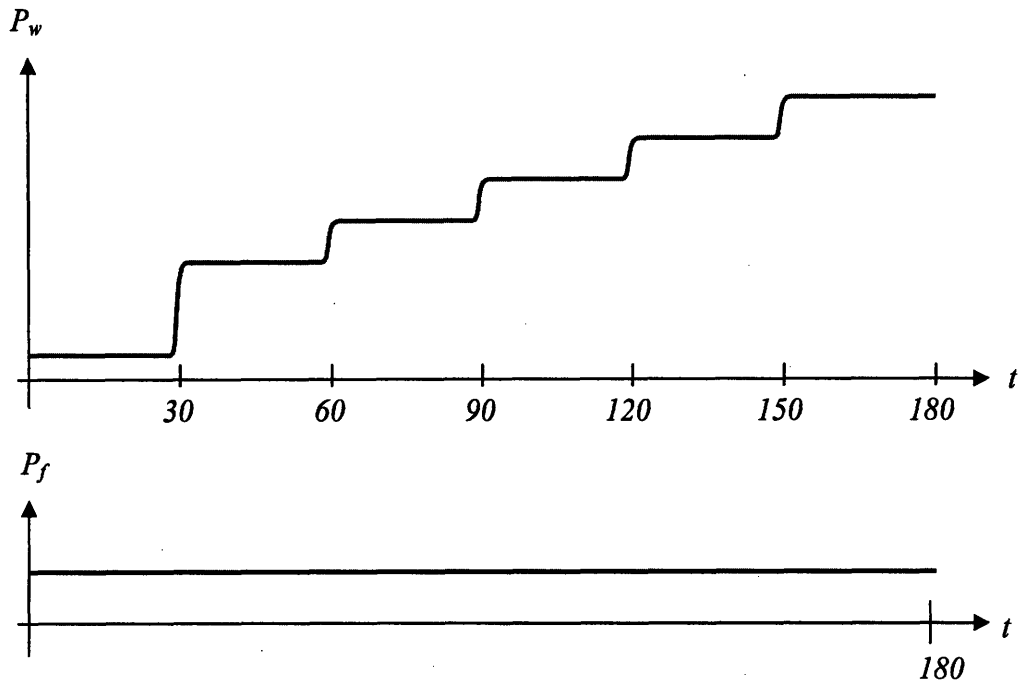

Figure 7-13. Multi-stage variation in external wrist sensor pressure using direct pressure applied to the wrist sensor housing

Pulse transit times were estimated during each stage as the timing difference between the minimum of the finger PPG waveform and the peak of the QRS complex of the EKG waveform. A mean pulse transit time, wrist PPG magnitude, and finger PPG magnitude were estimated using the last twenty seconds of data measured during each stage of the experiment. A set of sample results from these experiments are presented in Figure *7-14*.

According to the non-invasive blood pressure measurement method of oscillometry the point of maximum arterial pulsation occurs when the external arterial pressure is equal to the mean arterial pressure [10]. Further, the magnitudes of these volumetric pulsations are a function of the transmural pressure dependent arterial compliance. Based on Figure *7-14* the maximum arterial pulsation, or maximum wrist PPG amplitude, occurs during stage three of the experiment which suggests that the external wrist sensor pressure is at or near mean arterial pressure. The pulse transit time data is directly correlated with the wrist sensor PPG amplitude data. This correlation suggests that 1) the change in pulse transit time is a function of the magnitude of transmural pressure applied to the ulnar artery by the wrist sensor housing and 2) this relationship, like PPG magnitude, appears to be governed by the non-linear compliance of the vessel wall.

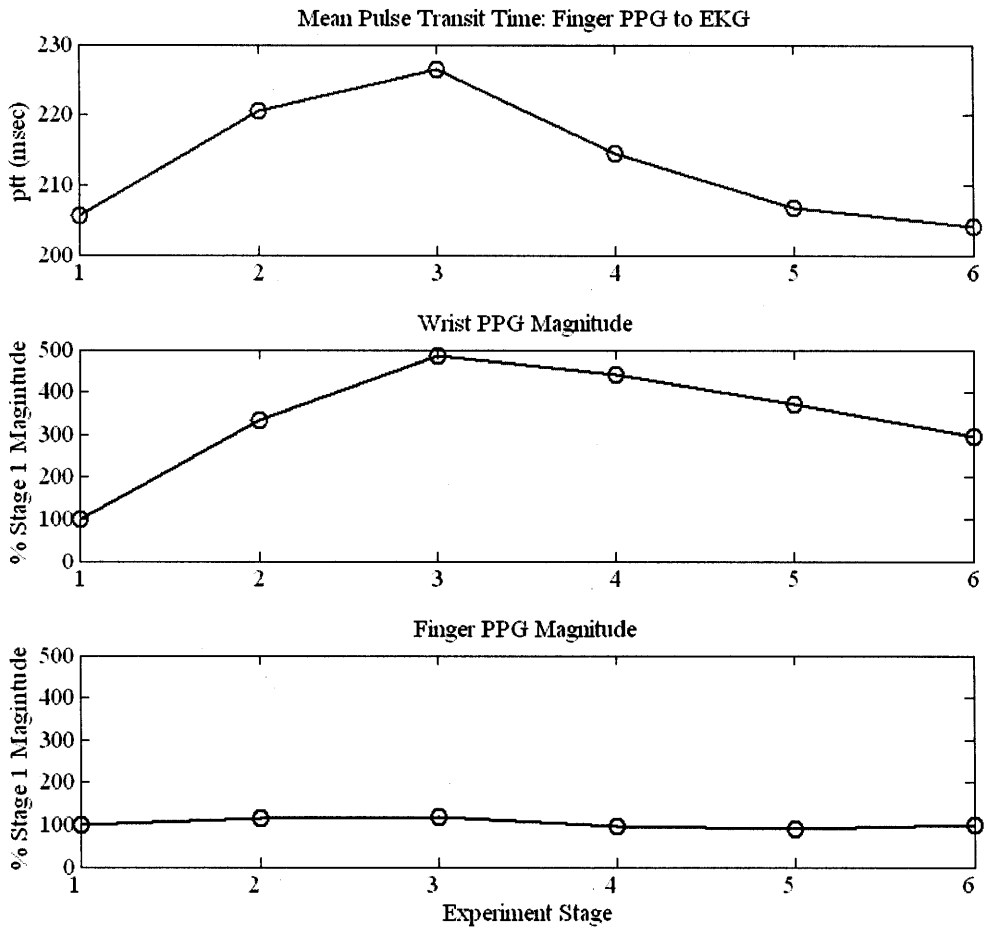

Figure 7-14. Pulse transit time and PPG magnitudes for a healthy male subject in response to a multi-stage increase in external wrist sensor pressure.

The results presented in this section demonstrate that a reduction in transmural pressure imposed by the wrist sensor housing on an intermediate arterial segment of the transit path plays a significant role in determining the velocity of the propagating pulse along this path. Further, we demonstrated that the magnitude of the change in pulse wave velocity depends on the transmural pressure of the arterial segment and that the change in pulse wave velocity appears inversely correlated to the non-linear compliance of the arterial segment underlying the sensor housing.

7.3.4 *A Distributed PTT-BP Model*

Because of its significant influence, the dependence of pulse wave velocity on external arterial loading conditions imposed by the sensor housings must be incorporated into the *PTT-BP* model to allow accurate BP calibration and estimation using our in-line sensors.

The distributed transmural arterial pressure is given in equation (*7.10*) where $P_i(z,t)$ represents the pressure inside the vessel and $P_{ex}(z,t)$ the external pressure outside of the vessel.

$$P_{tm}(z,t) = P_i(z,t) - P_{ex}(z,t) \tag{7.10}$$

Under the assumption that the internal arterial pressure is constant along the length of the arterial path $\left(\frac{\partial P_i}{\partial z} = 0\right)$ a distributed pulse wave velocity model can be developed from the model derived in chapter 2 in equation *2.42* as given in equation (*7.11*).

$$pwv(z,t) = pwv_0 \exp\left(k \cdot P_{tm}(z,t)\right) = pwv_0 \exp\left(k \cdot \left(P_i(t) - P_e(z,t)\right)\right) \tag{7.11}$$

The distributed pulse wave velocity predicted by this model along the arterial path observed by our in-line PPG sensors is shown in Figure *7-15*.

Based on equation (*7.11*) the pulse transit time between the two sensors may be found by integrating the inverse pulse wave velocity along the arterial path as given by equation (*7.12*).

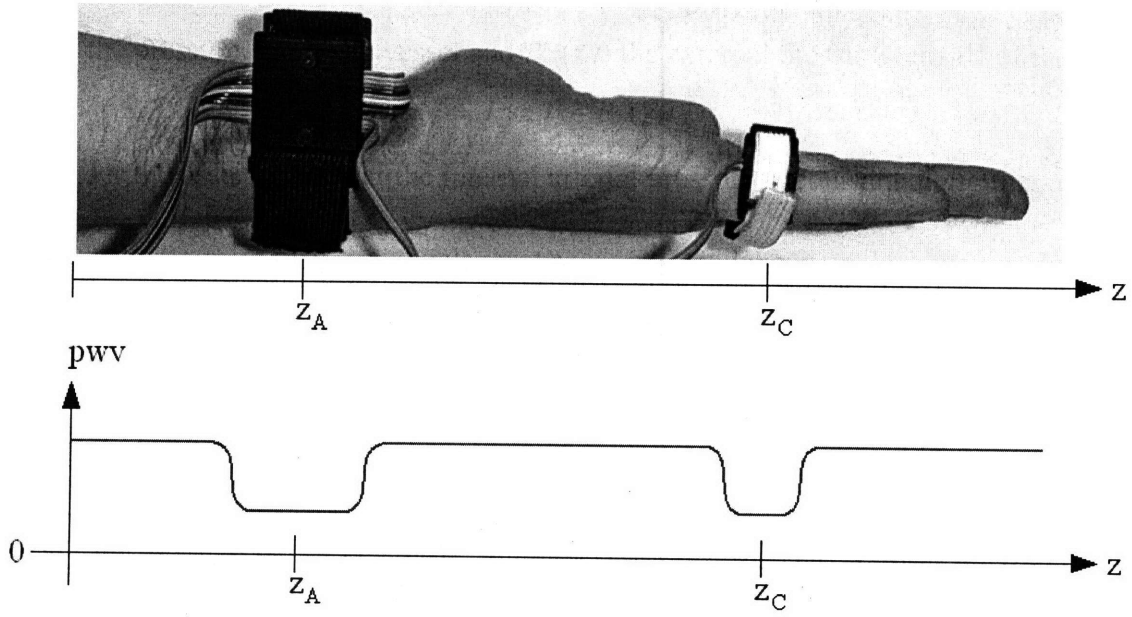

Figure 7-15. Distributed pulse wave velocity along the arterial path observed by our in-line PPG sensors

$$ptt = \int_{z_A}^{z_C} \frac{1}{pwv_0} \exp\left(-k \cdot \left(P_i(t) - P_e(z,t)\right)\right) dz \tag{7.12}$$

The distributed *ptt* equation given in (*7.12*) requires integration of a continuous pulse wave velocity function along the arterial segment between the two measurement points. Identification of this continuous distributed function is not possible using non-invasive sensors. Therefore, in order to incorporate the loading effect of the sensor housings into our *PTT-BP* model the arterial path between the two sensors will be subdivided into sections that have an approximately uniform transmural pressure. The new model will consist of three arterial segments, an initial arterial segment (segment A) under the influence of the external pressure applied by the wrist sensor housing, a middle arterial segment (segment B) having a negligible external pressure, and a third arterial segment (segment C) under the influence of the external pressure applied by the finger sensor housing. This new *ptt-BP* model is given in equation (*7.13*).

$$ptt = \left(\frac{\Delta z_A}{pwv_0}\right)\exp\left(-k \cdot P_{tm,A}\right) + \left(\frac{\Delta z_B}{pwv_0}\right)\exp\left(-k \cdot P_{tm,B}\right) + \left(\frac{\Delta z_C}{pwv_0}\right)\exp\left(-k \cdot P_{tm,C}\right) \tag{7.13}$$

The transit distances, Δz_A, Δz_B, Δz_C across these arterial segments must be selected such that the two expressions in equation (*7.14*) are equal.

$$\left(\frac{\Delta z_A}{pwv_0}\right)\exp\left(-k \cdot P_{tm,A}\right) + \left(\frac{\Delta z_B}{pwv_0}\right)\exp\left(-k \cdot P_{tm,B}\right) + \left(\frac{\Delta z_C}{pwv_0}\right)\exp\left(-k \cdot P_{tm,C}\right) = \int_{z_A}^{z_C} \frac{1}{pwv_0} \exp\left(-k \cdot P_{tm}(z)\right) dz \tag{7.14}$$

A block diagram showing the lumped parameter model used to predict the pulse transit time measured with our device is shown in Figure *7-16*. The model augments the model proposed in chapter 2 based on the distributed pulse wave velocity along the transit path that is imposed by the contact force applied by the PPG sensor housings.

Using some simple algebraic manipulation of the lumped parameter model presented in equation (*7.13*) can be used to transform this equation into the familiar linear representation given in chapter 5 as shown in equation (*7.15*)

$$\ln\left(\frac{1}{ptt(t)}\right) = k \cdot \left(P_{bp}(t) + \rho g h(t)\right) + \ln\left(\frac{pwv_0}{\Delta z_A \exp\left(k \cdot P_{ex,A}\right) + \Delta z_B + \Delta z_c \exp\left(k \cdot P_{ex,C}\right)}\right) \tag{7.15}$$

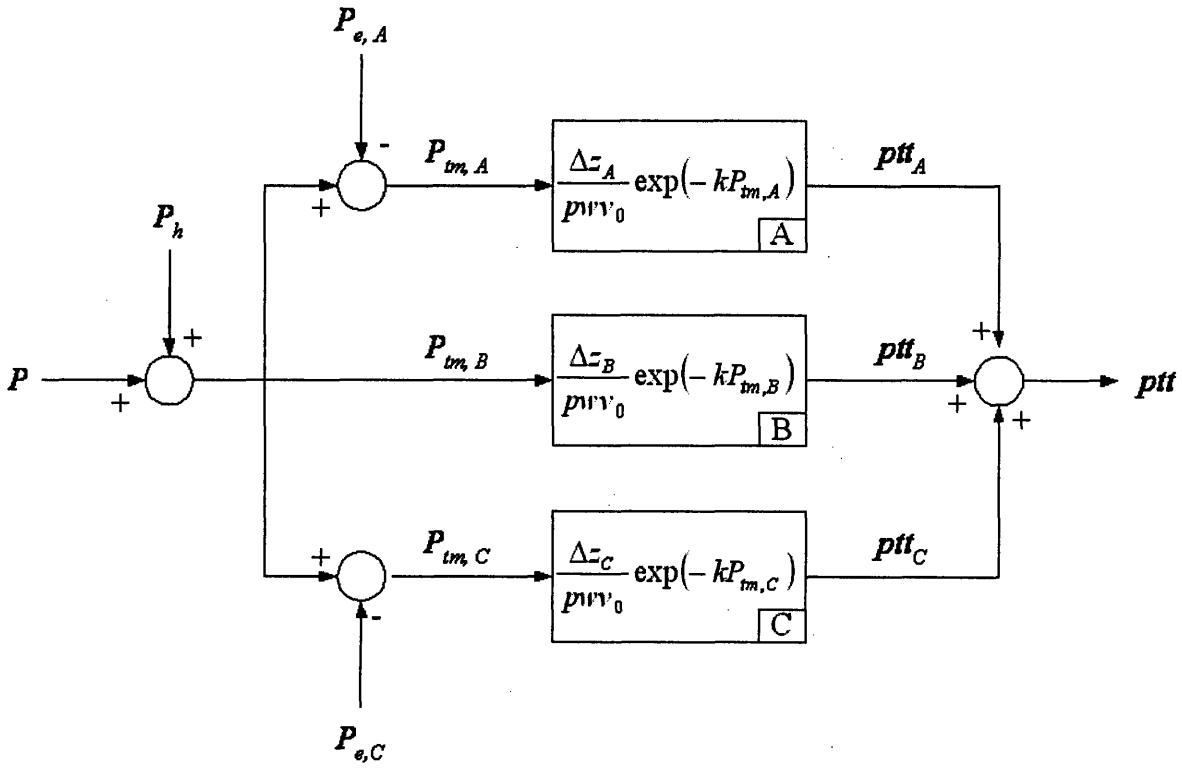

Figure 7-16. Block diagram of the lumped parameter device model that includes the effects of sensor contact pressure

The offset y_0 of our linear model is now defined not only in terms of the zero pressure pulse wave velocity and pulse transit distance but now also in terms of the model variable k and the external pressures applied to the arteries by the sensor housings as given in equation (*7.16*).

$$y_0 = \ln\left(\frac{pwv_0}{\Delta z_A \exp\left(k \cdot P_{ex,A}\right) + \Delta z_B + \Delta z_c \exp\left(k \cdot P_{ex,C}\right)}\right) \tag{7.16}$$

Clearly, the adaptive height calibration algorithm presented in chapter 5 is still valid given the new augmented model assuming the external pressures applied by the sensor housings are held constant during the calibration period. If these external pressures are not constant, and the variation in these pressures is correlated with height change the algorithm will fail to accurately identify the model parameter k.

The new augmented model also explains the negative correlation observed between the model parameter k and the model parameter y_0 in the experiments presented in chapter 6. Also the offset term's dependence on external senor pressure explains why simple polynomial models used to try and predict y_0 using k failed.

CHAPTER 8
FULL PTT CALIBRATION USING EXTERNAL ARTERIAL PRESSURE VARIATION

The goal of this chapter of the thesis is to describe a unique set of calibration tools that can be used to augment our adaptive height calibration algorithm in order to identify the unknown zero pressure offset in the lumped parameter device model. This calibration technique is based on the influence that external sensor pressure exerts on our system which was detailed extensively in Chapter 7. As this chapter will reveal the effects of external sensor contact pressure can be utilized as a tool for the purpose of system identification rather than serving only as an additional layer of complication in the calibration procedure.

This chapter begins by describing the basic concept of using external pressure change for pulse transit time calibration. A method will then be presented to utilize relative height variation to estimate the pressure difference acting across the arterial wall. Several examples will be presented in an increasing order of complexity to illustrate how these tools can be combined to achieve full calibration and allow blood pressure estimation. Finally some general analysis of the full calibration algorithm will be presented.

8.1 EXTERNAL ARTERIAL PRESSURE AS A CALIBRATION TOOL

The basic concept of using external arterial pressure variation as a calibration tool can be understood using the block diagram shown in Figure 8-1, which describes the relationship between transmural pressure and pulse wave velocity.

From this diagram it is apparent that external pressure applied to the artery ($P_{ex}(t)$) can be used to change pulse wave velocity along the arterial segment under the influence of the external pressure and therefore alter the measured pulse transit time through this arterial segment.

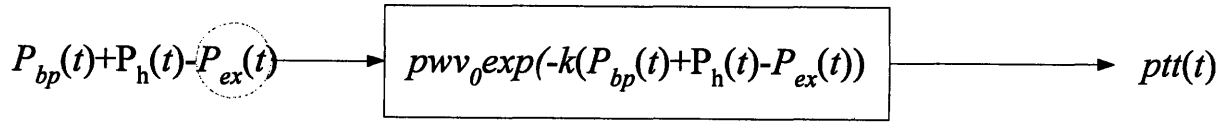

Figure 8-1. External arterial pressure (P_{ex}) variation as a means to calibrate pulse transit time (*ptt*).

However, similar to when using relative height change as a means of calibration, the contribution made to the measured pulse transit time by the arterial blood pressure is unknown and identification of parameters using external pressure would require some type of differential formulation that would seemingly once again lead to the loss of our offset from the identification equations. However, as one can observe from the diagram in Figure *8-1*, knowledge of the actual arterial blood pressure $P_{bp}(t)$ is not required to identify the model parameters governing the arterial segment rather it is the pressure difference acting across the arterial wall that is required. Any differential formulation that utilizes the known pressure difference across the wall allows direct substitution of this term into the exponential equation and identification of the zero pressure pulse wave velocity. Identification of pwv_0, using a known pressure difference lies at the foundation of the techniques described in the chapter.

8.2 TRANSMURAL PRESSURE ESTIMATION USING RELATIVE HEIGHT VARIATION

The transmural pressure (P_{tm}) acting across the arterial wall at the PPG sensor measurement site can be estimated using the amplitude of the PPG sensor signal along with hydrostatic pressure variation based on the principle of oscillometry. This technique has been previously implemented by Shaltis and Asada on the digital artery of the index finger using PPG sensor signals [19].

According to experimental studies on the arteries of animals and humans the compliance of the arterial wall is pressure dependent and its maximum compliance occurs when the pressure acting across the arterial wall is zero ($P_{tm}=0$) [10, 28]. At this value the intravascular pressure (P_i) equals external pressure (P_{ex}) as given in (*8.1*).

$$P_i = P_{ex} \tag{8.1}$$

However, the intravascular pressure is not constant rather it is a periodic function of time in which pressure varies throughout the cardiac cycle. Therefore, if the external pressure is constant and has a magnitude on the order of intravascular pressure the relationship in (*8.1*) will only be valid at specific times during the cardiac cycle.

Based on the pressure dependent compliance of the artery and the time varying intravascular pressure, the principle of oscillometry asserts that the amplitude of the volumetric

pulsations in the artery are maximum when the mean intravascular pressure is equal to the external pressure acting on the artery wall [10]. The mean intravascular pressure is defined as the sum of the mean value of the periodic arterial pressure waveform (P_m) plus the hydrostatic pressure offset as given by (*8.2*).

$$P_m + P_h = P_{ex} \tag{8.2}$$

As discussed in Chapter 3, the measured PPG signal is a function of the volume of blood present in the light path between the LED and the photodiode. Based on the principle of oscillometry the maximum amplitude of the periodic PPG signal occurs when the condition given in (*8.2*) is achieved. As opposed to standard oscillometry our method identifies this equilibrium point by altering internal rather than external arterial pressure by varying the hydrostatic pressure underlying the sensor. The procedure is easily explained through the use of a sample case study.

The pressure plot in Figure *8-2* graphically displays pressures values for a typical patient that are relevant to our calibration technique such as, the minimum or diastolic pressure (P_d), the mean arterial pressure (P_m), and the maximum or systolic pressure (P_s). The pressures in this figure will be referred to throughout the development of our identification algorithm.

Assume that the external pressure being applied to the artery by the PPG sensor housing (P_e) is equal to the constant value P_1 as shown in Figure *8-2*. The equilibrium point in equation (*8.2*) can be identified by raising and lowering the measurement site of the PPG sensor above and below the level of the heart and estimating the height (h_1) where the maximum PPG signal amplitude occurs. The range of intravascular pressure values spanned by a typical patient through hydrostatic variation are also depicted in Figure *8-2* with a minimum intravascular pressure value reached of $P_m+P_{h,min}$ and a maximum intravascular pressure value of $P_m+P_{h,max}$.

The pressure difference (ΔP_1) between the mean arterial pressure (P_m) and the external arterial pressure (P_1) can be identified from the maximum PPG amplitude as given in (*8.3*).

$$\Delta P_1 = P_m - P_1 = \rho g h_1 \tag{8.3}$$

Similarly if the external pressure applied to the artery (P_{ex}) by the PPG sensor housing is reduced to a different constant value (P_2) as depicted in Figure *8-2* the same hydrostatic variation procedure can be used to identify a new height (h_2) corresponding to the maximum PPG amplitude.

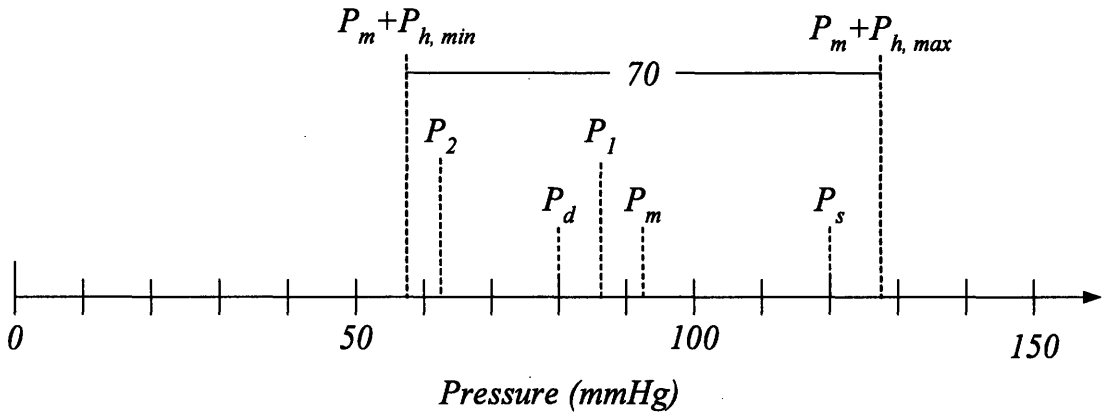

Figure 8-2. Typical intra-arterial and extra-arterial pressure values for a patient wearing our PPG sensors

This new pressure difference (ΔP_2) is given by (*8.4*).

$$\Delta P_2 = P_m - P_2 = \rho g h_2 \tag{8.4}$$

8.3 FULL CALIBRATION OF A LUMPED PARAMETER MODEL

The identification algorithm proposed in this section assumes that the pressure gain term (k) in our calibration equation was identified using the adaptive hydrostatic procedure described in chapter 5 and the pressure difference (ΔP_i) between mean arterial pressure and external arterial pressure was estimated using the method described in section *8.2*. Additionally, in order to simplify the initial description of the algorithm in this section we will assume that the height of the arm is held constant at the level of the heart ($P_h=0$) during identification of the zero pressure pulse wave velocity (pwv_0) and initial estimation of the arterial pressure (P_{bp}). However, this assumption will be removed in section *8.6* and all of the calibration algorithms combined into a parallel identification protocol.

The development and explanation of the identification and estimation algorithm presented in this section follows a sequential pattern beginning with a simple unrealistic sensor configuration and proceeding to the development of the algorithm for our more complicated actual sensor configuration. Throughout the analysis we will neglect edge effects and assume that the pulse transit distances (Δz_i) can be accurately measured.

8.3.1 Single elastic band with a uniform external pressure

Consider pulse wave propagation along an arterial segment (e.g. the lower arm) enclosed within an external elastic band. The elastic band compresses the tissue surrounding the arterial segment producing a constant external arterial pressure, P_{ex} along the length of the band. Photoplethysmograph sensors embedded at both ends of the band estimate the pulse transit time (*ptt*) of the pressure wave as it travels over the distance Δz as show in Figure *8-3*. We will assume that the PPG sensors have negligible width.

Assume that the external arterial pressure (P_{ex}) is equal to the constant value P_1. As described in section *8.2* the pressure difference ΔP_1, can be identified using hydrostatic variation to find the height (h_1) corresponding to the maximum PPG amplitude (Δx_{max}). The relationship between the measured pulse transit time and the transmural pressure acting on the arterial segment is given by (*8.5*).

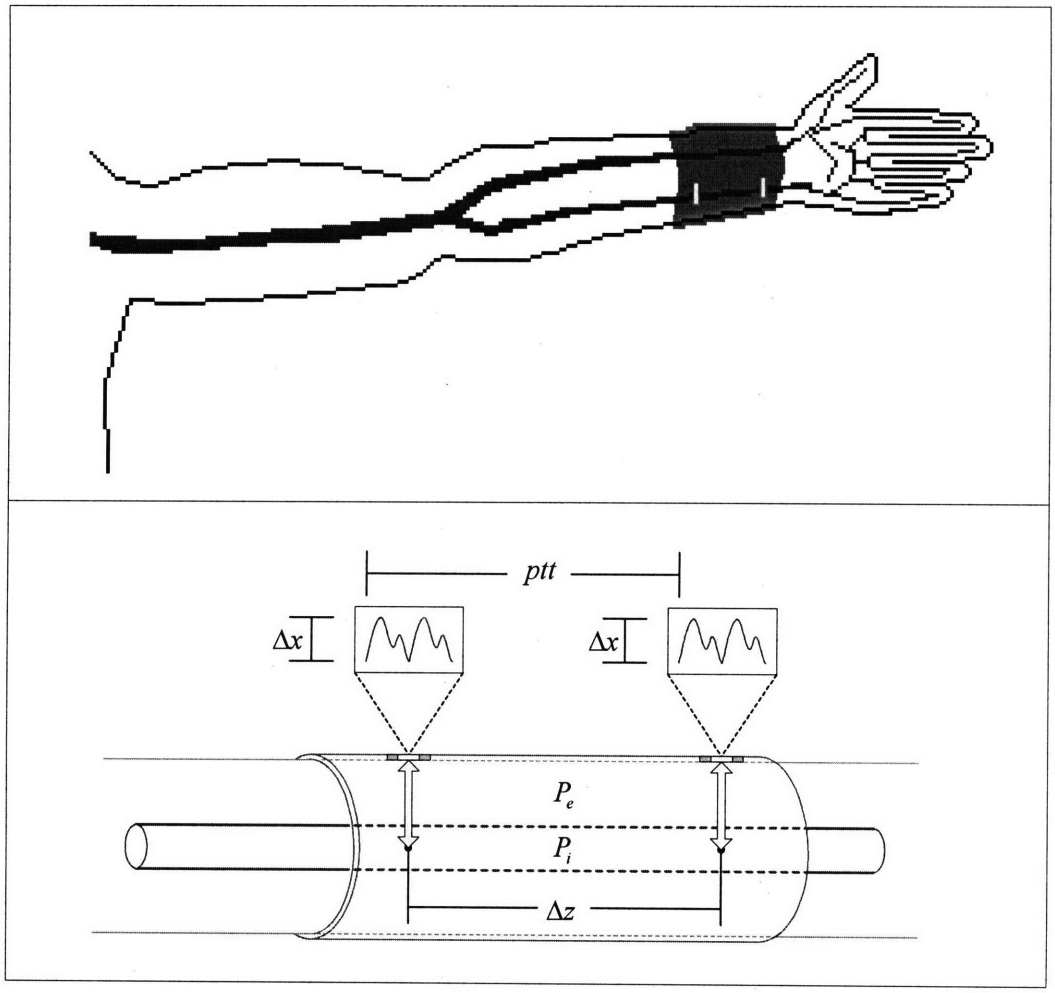

Figure 8-3. Pulse wave propagation through an artery under a uniform external pressure

$$ptt = \frac{\Delta z}{pwv_0}\exp(-k\Delta P_2) \tag{8.5}$$

The only unknown quantity in (*8.5*) is the zero pressure pulse wave velocity term, pwv_0 which can easily be solved for in this simple equation.

Following identification of the zero pressure pulse wave velocity, equation (*8.5*) can be rearranged in order to estimate mean arterial pressure P_m as given in (*8.6*).

$$\hat{P}_m = \frac{1}{k}\left(\ln\left(\frac{1}{ptt}\right) - \ln\left(\frac{pwv_0}{\Delta z}\right)\right) - P_1 \tag{8.6}$$

Unfortunately, the value of the external arterial pressure (P_1) is unknown and unidentifiable from our set of equations. Measurement of this value is not possible using our device architecture and would require an additional, expensive micro-pressure sensor and a number of assumptions relating skin surface pressure and external arterial pressure. It is therefore not possible to estimate mean arterial pressure using a single band with a uniform external arterial pressure.

8.3.2 Single elastic band with two different external pressures

Consider pulse wave propagation along an arterial segment (e.g. the lower arm) partially enclosed within an external elastic band. The elastic band compresses the tissue underlying it producing a constant external arterial pressure, P_{ex} along the length of the band. A single photoplethysmograph sensor is embedded in the band near the leading edge while a second PPG sensor is placed a known distance past the lagging end of the elastic band. The two PPG sensors are used to estimate the pulse transit time (*ptt*) of the pressure wave as it travels through the artery under the elastic band (segment *A*) a distance Δz_A, and through the unloaded artery (segment B) a distance Δz_B as show in Figure *8-4*. We will assume that the PPG sensors have negligible width and that the external pressure in the unloaded artery segment B, is equal to zero ($P_{ex,\,B}=0$).

A two stage procedure is required to identify the zero pressure pulse wave velocity of the artery being monitored using this sensor configuration. In the first stage pulse transit time measurements (ptt_1) are collected while the elastic band applies a constant external arterial pressure ($P_{ex,A}$) equal to an unknown value P_1.

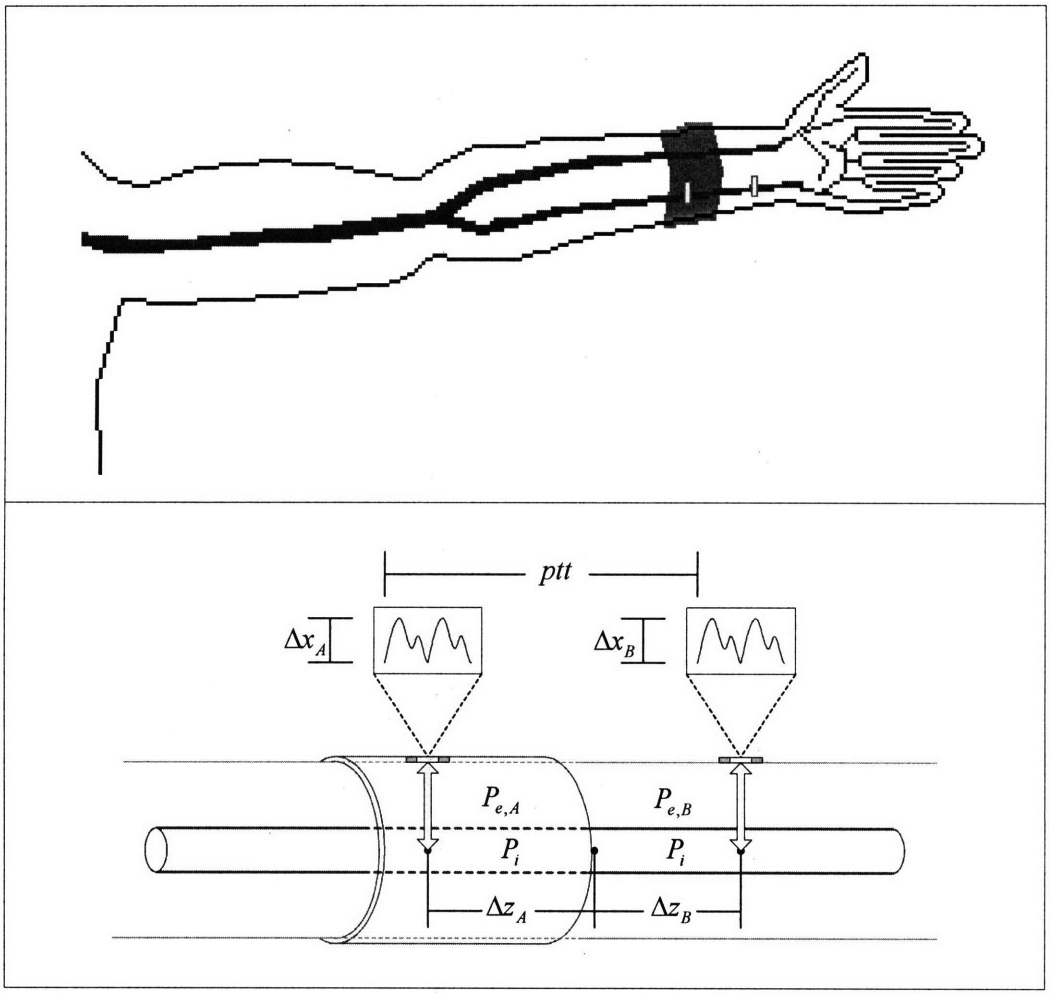

Figure 8-4. Pulse wave propagation through an artery under two external pressures

Again, as described in section *8.2* the pressure difference ΔP_1, can be identified using hydrostatic variation to find the height (h_1) corresponding to the max PPG amplitude ($\Delta x_{A,\,max}$). In the second stage the tension in the elastic band is adjusted and pulse transit time measurements (ptt_2) are collected while the elastic band applies a constant external arterial pressure ($P_{ex,A}$) equal to an unknown value P_2. The pressure difference ΔP_2, can be identified during this stage using the technique from section *8.2*.

The relationship between the measured pulse transit time and the transmural pressures acting on the arterial segment for each stage of the procedure are given by (*8.7a*) and (8.7*b*).

$$ptt_1 = \frac{\Delta z_A}{pwv_0}\exp(-k\Delta P_1) + \frac{\Delta z_B}{pwv_0}\exp(-kP_i) \qquad (8.7a)$$

$$ptt_2 = \frac{\Delta z_A}{pwv_0}\exp(-k\Delta P_2) + \frac{\Delta z_B}{pwv_0}\exp(-kP_i) \tag{8.7b}$$

Under the assumption that the intravascular arterial pressure remains approximately constant throughout both stage 1 and stage 2, the difference between the pulse transit times measured during each stage can be used to identify pwv_0, this difference is given in (*8.8*).

$$ptt_1 - ptt_2 = \frac{\Delta z_A}{pwv_0}\left(\exp(-k\Delta P_1) - \exp(-k\Delta P_2)\right) \tag{8.8}$$

The expression in (*8.8*) can easily be rearranged to solve for the zero pressure pulse wave velocity, pwv_0 as given in (*8.9*).

$$pwv_0 = \frac{\Delta z_A}{ptt_1 - ptt_2}\left(\exp(-k\Delta P_1) - \exp(-k\Delta P_2)\right) \tag{8.9}$$

An important aspect of this relationship and of the identified pwv_0 is that the zero transmural pressure point used to identify these terms corresponds to the mean arterial pressure, in other words in our model we have defined $P_i = P_m$.

An initial estimate of mean arterial pressure can be made using this sensor configuration because the external pressure in arterial segment B is zero. Under the assumption that the mean arterial pressure is constant throughout stage 2 of the procedure we can estimate the pulse transit time (ptt_A) of the wave across arterial segment A as in (*8.10*).

$$ptt_A = \frac{\Delta z_A}{pwv_0}\exp(-k\Delta P_2) \tag{8.10}$$

The transit time of the pressure pulse across arterial segment B can be estimated as the difference between the measure pulse transit time and the transit time across segment A as given in equation (*8.11*).

$$ptt_B = ptt_2 - ptt_A \tag{8.11}$$

The model used to define the pulse transit time in segment B is given in (*8.12*).

$$ptt_B = \frac{\Delta z_B}{pwv_0}\exp(-kP_m) \tag{8.12}$$

The mean arterial pressure can be estimated directly from (*8.12*) as given in (*8.13*).

$$P_m = \frac{1}{k}\left(\ln\left(\frac{1}{ptt_B}\right) - \ln\left(\frac{pwv_0}{\Delta z_B}\right)\right) \tag{8.13}$$

Given this initial estimate of mean arterial pressure the value of the external pressure ($P_{ex,A}$) can be estimated from the identified pressure difference as in (*8.14*).

$$P_{e,A} = \hat{P}_m - \Delta P_2 \tag{8.14}$$

Future estimates of the mean arterial pressure value can be made using the equation given in (*8.15*) under the assumption that the external pressure applied by the elastic band during stage 2 remains constant during the estimation period.

$$\hat{P}_m = \frac{1}{k}\left(\ln\left(\frac{1}{ptt}\right) - \ln\left(\frac{pwv_0}{\Delta z_A \exp\left(kP_{e,A}\right) + \Delta z_B}\right)\right) \tag{8.15}$$

An important aspect of this equation is that it not valid for transmural pressure values less than zero. Therefore, the external pressure imposed by the elastic band should be less than the mean arterial pressure for identification and estimation.

8.3.3 Two elastic bands with three different external pressures

Consider pulse wave propagation along an arterial segment (e.g. the lower arm) partially enclosed within two external elastic bands. This system configuration creates three distinct arterial segments, a leading segment (segment *A*) enclosed within an elastic band having a PPG sensor embedded in the band, a middle segment (segment *B*) with no elastic band, and a lagging segment (segment *C*) enclosed in an elastic band having a PPG sensor embedded in the band. Each elastic band compresses the tissue underlying it producing a distinct and constant external pressure, P_{ex} on the artery along the length of the band. The two PPG sensors are used to estimate the pulse transit time (*ptt*) of the pressure wave as it travels through the artery under the leading elastic band a distance Δz_A, through the unloaded artery segment a distance Δz_B, and through the artery under the lagging elastic band a distance of Δz_C as show in Figure *8-5*. Again, our analysis assumes that the PPG sensors have negligible width and that the external pressure in the unloaded artery (segment *B*) is equal to zero ($P_{e,B}=0$).

Similar to the identification protocol used in section *8.3.2* a two stage procedure is required to identify the zero pressure pulse wave velocity of the artery being monitored by our sensors. In the first stage pulse transit time measurements (ptt_1) are collected while the leading elastic band applies a constant external arterial pressure ($P_{ex,A}$) equal to an unknown value P_1.

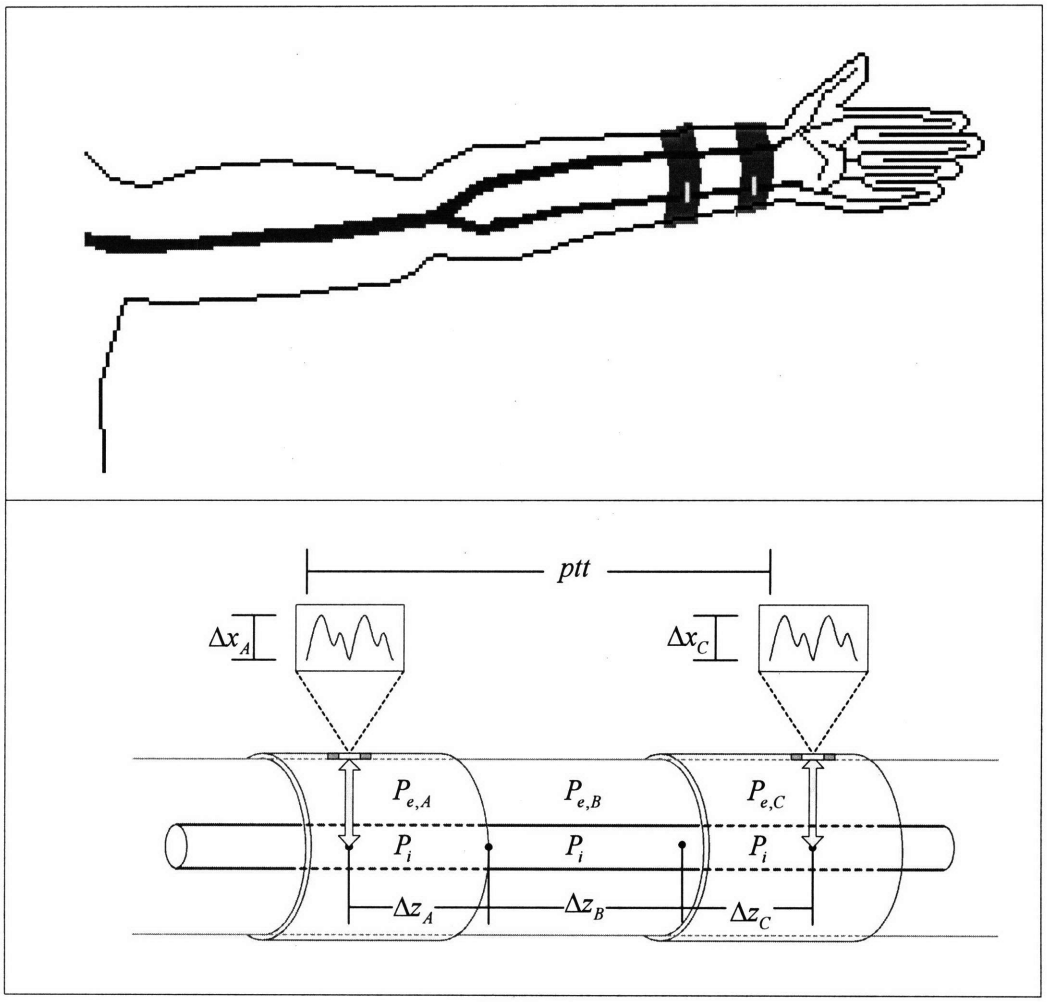

Figure 8-5. Pulse wave propagation through an artery under three external pressures

Again, as described in section *8.2* the pressure difference ΔP_1, can be identified using hydrostatic variation to find the height (h_1) corresponding to the max PPG amplitude ($\Delta x_{A,\ max}$). In the second stage the tension in the elastic band is adjusted and pulse transit time measurements (ptt_2) are collected while the leading elastic band applies a constant external arterial pressure ($P_{ex,A}$) equal to an unknown value P_2. The pressure difference ΔP_2, can be identified during this stage using the technique described in section *8.2*. Throughout both of the two stages the lagging elastic band applies a constant external arterial pressure ($P_{ex,C}$) equal to an unknown value P_3. It is assumed that pressure value P_3, lies within the hydrostatic range of the individual such that the pressure difference ΔP_3, can be identified using the technique described in section 8.*2*.

The relationship between the measured pulse transit time and the transmural pressures acting on the arterial segment for each stage of the procedure are given by (*8.16a*) and (8.16*b*).

$$ptt_1 = \frac{\Delta z_A}{pwv_0}\exp(-k\Delta P_1) + \frac{\Delta z_B}{pwv_0}\exp(-kP_i) + \frac{\Delta z_C}{pwv_0}\exp(-k\Delta P_3) \qquad (8.16a)$$

$$ptt_2 = \frac{\Delta z_A}{pwv_0}\exp(-k\Delta P_2) + \frac{\Delta z_B}{pwv_0}\exp(-kP_i) + \frac{\Delta z_C}{pwv_0}\exp(-k\Delta P_3) \qquad (8.16b)$$

Under the assumption that the intravascular arterial pressure remains approximately constant throughout both stage 1 and stage 2, the difference between the pulse transit times measured during each stage can be used to identify pwv_0, this difference is given in (*8.17*). Note that the expression in (*8.17*) is identical to that in (*8.8*) for our single band system.

$$ptt_1 - ptt_2 = \frac{\Delta z_A}{pwv_0}\left(\exp(-k\Delta P_1) - \exp(-k\Delta P_2)\right) \qquad (8.17)$$

The expression in (8.*17*) can easily be rearranged to solve for the zero pressure pulse wave velocity, pwv_0 as given in (*8.18*).

$$pwv_0 = \frac{\Delta z_A}{ptt_1 - ptt_2}\left(\exp(-k\Delta P_1) - \exp(-k\Delta P_2)\right) \qquad (8.18)$$

As with the single band case, an important aspect of this relationship and of the identified pwv_0 is that the zero transmural pressure point used to identify these terms corresponds to the mean arterial pressure, in other words in our model we have defined $P_i = P_m$.

An initial estimate of mean arterial pressure can be made using this sensor configuration because the external pressure in arterial segment B is zero. Under the assumption that the mean arterial pressure is constant throughout stage 2 of the procedure we can estimate the pulse transit time (ptt_A) of the wave across arterial segment A as in (*8.19*).

$$ptt_A = \frac{\Delta z_A}{pwv_0}\exp(-k\Delta P_2) \qquad (8.19)$$

Similarly we can estimate the pulse transit time (ptt_C) of the wave as it travels across arterial segment C as in (*8.20*).

$$ptt_C = \frac{\Delta z_C}{pwv_0}\exp(-k\Delta P_3) \qquad (8.20)$$

The transit time of the pressure pulse across arterial segment B can be estimated as the difference between the measure pulse transit time and the transit times across segment A and segment B as given in equation (*8.21*).

$$ptt_B = ptt_2 - ptt_A - ptt_C \tag{8.21}$$

The model used to define the pulse transit time in segment B is given in (*8.22*).

$$ptt_B = \frac{\Delta z_B}{pwv_0}\exp(-kP_m) \tag{8.22}$$

The mean arterial pressure can be estimated directly from (*8.22*) as given in (*8.23*).

$$P_m = \frac{1}{k}\left(\ln\left(\frac{1}{ptt_B}\right) - \ln\left(\frac{pwv_0}{\Delta z_B}\right)\right) \tag{8.23}$$

Given this initial estimate of mean arterial pressure the value of the external pressure acting on arterial segment A ($P_{ex,A}$) and on arterial segment C ($P_{ex,C}$) can be estimated from the identified pressure difference as in (8.*24a*) and (8.*24b*).

$$P_{ex,A} = \hat{P}_m - \Delta P_2 \tag{8.24a}$$

$$P_{ex,C} = \hat{P}_m - \Delta P_3 \tag{8.24b}$$

Future estimates of the mean arterial pressure value can be made using the equation given in (*8.25*) under the assumption that the external pressure applied by both of the elastic bands during stage 2 remain constant during the estimation period.

$$\hat{P}_m = \frac{1}{k}\left(\ln\left(\frac{1}{ptt}\right) - \ln\left(\frac{pwv_0}{\Delta z_A \exp\left(kP_{ex,A}\right) + \Delta z_B + \Delta z_B \exp\left(kP_{ex,B}\right)}\right)\right) \tag{8.25}$$

The second term on the left side of equation (8.25) contained within the natural logarithm is equal to the zero pressure pulse transit time.

8.4 IDENTIFICATION OF y_0 USING THE WRISTWATCH PPG SENSOR AND RING PPG SENSOR

The two band measurement system presented in section *8.3.3* with its three different external pressures is identical to the physiologic environment created by the sensors in our device. Our device has a wristwatch PPG sensor housing attached to the wrist with an elastic band that applies an external pressure to the ulnar artery (segment *A*) and a ring PPG sensor

housing attached to the little finger with an elastic band that applies an external pressure to the common digital artery (segment *C*). These two sensors (arterial segments) are separated by a section of artery where the external pressure is negligibly small (segment *B*). Therefore, the technique described in section *8.3.3* to identify the zero pressure pulse wave velocity and estimate the mean arterial pressure is applicable to our device. However, the analysis presented in the previous section neglected to include the effects of hydrostatic pressure (P_h) on pulse wave propagation and these effects will be considered in this section in the development of a full calibration protocol.

If hydrostatic pressure is included in the analysis presented in *8.3.3* than the simple difference in measured pulse transit time between the two stages of the protocol given by equation (*8.17*) is transformed into the more complicated difference equation given by (*8.26*).

$$\frac{ptt_1}{\exp(-kP_{h,1})} - \frac{ptt_2}{\exp(-kP_{h,2})} = \frac{\Delta z_A}{pwv_0}\left(\exp(-k\Delta P_1) - \exp(-k\Delta P_2)\right) \tag{8.26}$$

This expression allows us to compare pulse transit time measurements from the two stages regardless of the height of the measurement point during PTT acquisition. The terms of (*8.26*) can be rearranged to solve for the zero pressure pulse wave velocity as in (*8.27*).

$$pwv_0 = \Delta z_A\left(\exp(-k\Delta P_1) - \exp(-k\Delta P_2)\right)\left(\frac{ptt_1}{\exp(-kP_{h,1})} - \frac{ptt_2}{\exp(-kP_{h,2})}\right)^{-1} \tag{8.27}$$

The effects of hydrostatic pressure can also be incorporated into our mean arterial pressure estimation algorithm. The pulse transit time (ptt_A) of the pressure wave across the arterial segment under the ulnar artery PPG sensor is given in (*8.28*).

$$ptt_A = \frac{\Delta z_A}{pwv_0}\exp\left(-k\left(\Delta P_2 + P_{h,2}\right)\right) \tag{8.28}$$

Similarly we can estimate the pulse transit time (ptt_C) of the wave as it travels across the arterial segment underlying the ring sensor as in (*8.29*).

$$ptt_C = \frac{\Delta z_C}{pwv_0}\exp\left(-k\left(\Delta P_3 + P_{h,2}\right)\right) \tag{8.29}$$

The transit time of the pressure pulse across the middle arterial segment between the two sensors can be estimated as the difference between the measured pulse transit time and the transit times across segment A and segment C as given in equation (*8.30*).

$$ptt_B = ptt_2 - ptt_A - ptt_C \tag{8.30}$$

The model used to define the pulse transit time in segment B is given in (*8.31*).

$$ptt_B = \frac{\Delta z_B}{pwv_0}\exp\left(-k\left(P_m + P_{h,2}\right)\right) \tag{8.31}$$

The mean arterial pressure can be estimated directly from (*8.31*) as given in (*8.32*).

$$P_m = \frac{1}{k}\left(\ln\left(\frac{1}{ptt_B}\right) - \ln\left(\frac{pwv_0}{\Delta z_B}\right)\right) - P_{h,2} \tag{8.32}$$

Given this initial estimate of mean arterial pressure the value of the external pressure acting on arterial segment *A* ($P_{ex,A}$) and on arterial segment *C* ($P_{ex,C}$) can be estimated from the identified pressure difference as in (*8.24a*) and (*8.24b*).

Future estimates of the mean arterial pressure value can be made using the equation given in (*8.33*) under the assumption that the external pressure applied by both of the elastic bands on the finger artery and on the ulnar artery during stage 2 remain constant during the estimation period.

$$\hat{P}_m = \frac{1}{k}\left(\ln\left(\frac{1}{ptt}\right) - \ln\left(\frac{pwv_0}{\Delta z_A \exp\left(kP_{ex,A}\right) + \Delta z_B + \Delta z_C \exp\left(kP_{ex,C}\right)}\right)\right) - P_{h,2} \tag{8.33}$$

This equation can be simplified using our transformed pulse transit time variable (y) and the term y_0 can be calculated as the second logarithmic term in (*8.33*) using the identified variables.

8.5 IMPLEMENTATION OF THE FULL CALIBRATION METHOD

8.5.1 Bi-stable wrist strap design

External arterial pressure change can be easily implemented by the patient using a bi-stable elastic strap to attach the wrist sensor to the test patient's wrist as shown in Figure *8-6*. The wrist sensor is initially attached to the patients's wrist such that the sensor housing applies an initial pressure to the ulnar artery (position 1, $P_{ex} = P_1$). An adjustable bi-stable mechanical mechanism on the elastic strap may be adjusted by the subject to decrease the circumference of the strap and increase the external arterial pressure (position 2, $P_{ex} = P_2$).

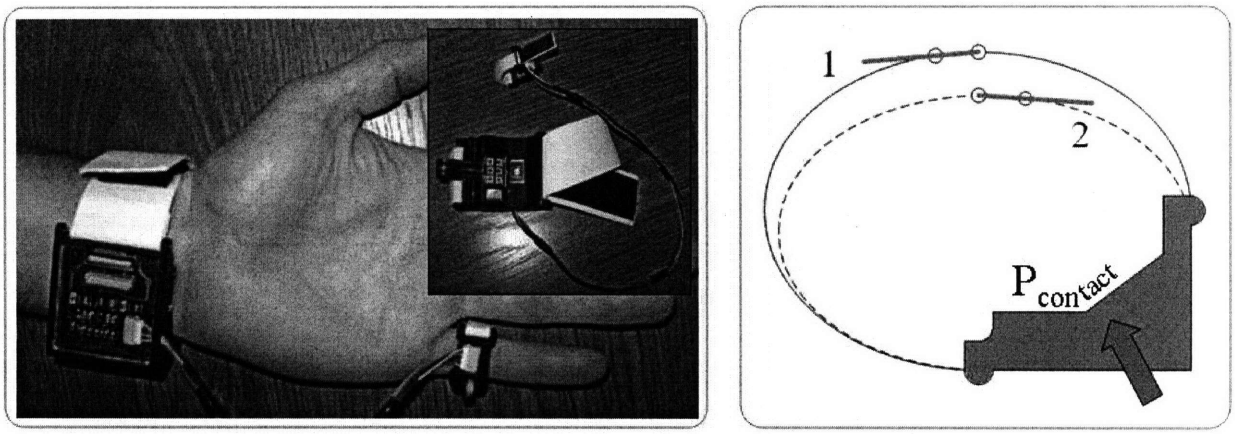

Figure 8-6 Bi-stable sensor strap used to alter the pressure exerted on the ulnar artery by the wrist sensor housing.

8.5.2 Calibration Routine

The hydrostatic pressure variation along with the external pressure change can be combined into a simple calibration routine as shown in Figure *8-7*. During stage one the patient raises and lowers the arm with the wrist sensor exerting an external arterial pressure P_1. After completing a cycle of the height change the bi-stable wrist strap is used to increase the external pressure exerted by the sensor housing on the artery to pressure P_2. The adaptive height calibration algorithm is used to estimate model parameter k during one of the two stages. The appropriate stage should be selected based on the strength of the correlation between $h(t)$ and $y(t)$. The transmural pressure (ΔP_i) acting across the arterial wall underlying the wrist sensor is identified from the height dependent wrist PPG magnitude values for external pressure P_1 during stage 1 and for external pressure P_2 during stage 2. The mean pressure difference between the two external pressure stages can be estimated from the PTT measurements following removal of the hydrostatic pressure effects using the identified model parameter k along with the time varying height measurements.

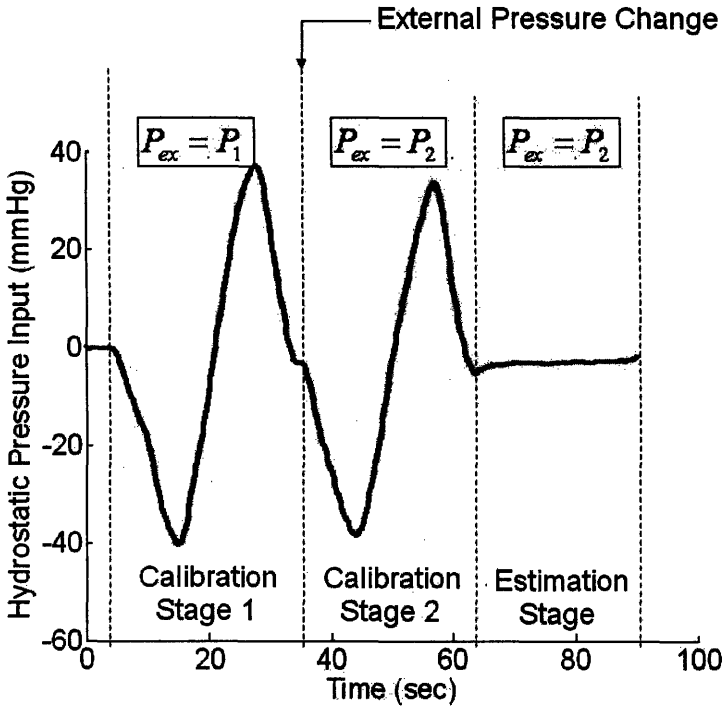

Figure 8-7. Full calibration routine combines relative height variation and external pressure variation

8.6 SENSITIVITY AND ERROR ANALYSIS

A sensitivity analysis of the estimated parameters and an evaluation of the effects of measurement error in our algorithm will begin with a brief investigation into the order of magnitude of the measured values used in our identification algorithm.

8.6.1 Order of Magnitude Analysis

The parameters used in the order of magnitude analysis are derived from our prototype sensor or were identified through human subject testing using our device. Table *8:1* lists typical values for several key physiologic and sensor design parameters.

$k =$	0.02 $mmHg^{-1}$	$\Delta z_A =$	2 cm
$pwv_0 =$	150 (cm/s)	$\Delta z_B =$	11 cm
$P_d =$	80 mmHg	$\Delta z_C =$	1 cm
$P_s =$	120 mmHg	$P_1 =$	80 mmHg
$P_m =$	93.3 mmHg	$P_2 =$	50 mmHg
		$P_3 =$	70 mmHg

Table 8:1. Typical device and physiologic parameter values

Substitution of parameters in Table *8:1* into equations (*8.16a*) and (*8.16b*) allows calculation of the pulse transit times measured in stage 1 and stage 2 of our identification procedure. These values are given along with the equations in (*8.34a*) and (*8.34b*) where we have assumed that our pulse transit time measurements, which are derived from the base of the PPG waveform, are determined by the diastolic pressure, ($P_{tm,\,i} = P_d - P_i$).

$$ptt_1 = 0.0336\,\text{sec.} = \frac{\Delta z_A}{pwv_0}\exp\left(-kP_{tm,1}\right) + \frac{\Delta z_B}{pwv_0}\exp\left(-kP_d\right) + \frac{\Delta z_C}{pwv_0}\exp\left(-kP_{tm,3}\right) \qquad (8.34a)$$

$$ptt_2 = 0.0276\,\text{sec.} = \frac{\Delta z_A}{pwv_0}\exp\left(-kP_{tm,2}\right) + \frac{\Delta z_B}{pwv_0}\exp\left(-kP_d\right) + \frac{\Delta z_C}{pwv_0}\exp\left(-kP_{tm,3}\right) \qquad (8.34b)$$

The difference in pulse transit times measured between the two stages is given in (*8.35*) along with the equation. The percentage change in transit time between the low external pressure stage (stage 2) and the high external pressure stage (stage 1) is 21.8%.

$$ptt_1 - ptt_2 = 0.006\,\text{sec.} \qquad (8.35)$$

8.6.2 Evaluating the Effects of using Mean Arterial Pressure for Parameter Identification

In the proposed calibration algorithm a discrepancy exists between the pressure values that correspond to the measured pulse transit time values, *i.e.* diastolic pressure and our estimation of the transmural pressures acting across the arterial wall at the sensor measurement sites which correspond to mean arterial pressure.

Regardless of whether we are tracking change in diastolic blood pressure or change in mean arterial blood pressure using pulse wave velocity or pulse transit time the slope relating the change in pressure to our pulse transit time variable (y) is identical as given in (*8.36*).

$$\ln\left(\frac{1}{ptt(t)}\right) - \ln\left(\frac{1}{ptt(t-\tau)}\right) = y(t) - y(t-\tau) = k\left(P(t) - P(t-\tau)\right) \qquad (8.36)$$

However, the value of the zero pressure y-intercept (y_0) of our pulse transit time variable (y) depends on whether the definition of transmural pressure refers to diastolic pressure or mean arterial blood pressure. The following analysis demonstrates that although measured pulse transit times correspond to the state of the arterial system at diastolic blood pressures, our algorithm with its definition of transmural pressure relative to the mean arterial pressure still provides a physiologically relevant calibration curve.

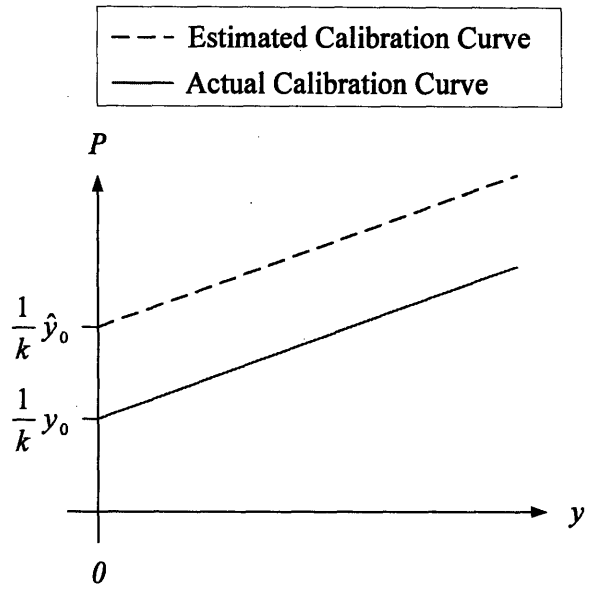

Figure 8-8. Calibration curves for diastolic pressure (Actual) and mean arterial pressure (Identified)

However with it's shifted zero pressure y-intercept value the pressure estimates made with our identified curve will correspond to mean arterial blood pressure rather than diastolic pressure. An example of this is shown in Figure *8-8*.

If the equality given in equation (*8.36*) is true then the identified calibration curve will provide estimates of mean arterial pressure given PTT measurements made from the base of the leading and lagging PPG waveforms that correspond to diastolic blood pressure.

$$\frac{1}{k}\hat{y}_0 - \frac{1}{k}y_0 = P_m - P_d \tag{8.36}$$

In order to establish this proof we will consider the case presented in section 8.*3.3* for two elastic bands with three different external pressures. In this case the initial pressure estimates are made from the un-banded segment of the artery (segment *B*). The definitions of the term y_0 for the estimated curve and actual curve can be substituted into equation (*8.36*) for arterial segment *B* as given in equation (*8.37*). Where the term $p\hat{w}v_0$ represents the zero pressure pulse wave velocity estimated using our algorithm and mean arterial pressure to define transmural pressure.

$$\frac{1}{k}\ln\left(\frac{\Delta z_B}{p\hat{w}v_0}\right) - \frac{1}{k}\ln\left(\frac{\Delta z_B}{pwv_0}\right) = P_m - P_d \tag{8.37}$$

The equation in (*8.37*) can be transformed into the expression given in (*8.38*) through a series of mathematical operations.

$$\hat{pwv}_0 = pwv_0 \exp(-k(P_m - P_d)) \tag{8.38}$$

The equation used to estimate zero pressure pulse wave velocity given in (*8.18*) can be substituted into the right hand side of equation (*8.38*) yielding the expression in (*8.39*).

$$\frac{\Delta z_A}{ptt_1 - ptt_2}(\exp(-k\Delta P_1) - \exp(-k\Delta P_2)) = pwv_0 \exp(-k(P_m - P_d)) \tag{8.39}$$

Assuming that the two measured pulse transit times correspond to diastolic pressure their difference is given in equation (*8.40*).

$$ptt_1 - ptt_2 = \frac{\Delta z_A}{pwv_0}[\exp(-k(P_d - P_1)) - \exp(-k(P_d - P_2))] \tag{8.40}$$

Substituting this expression into equation (*8.39*) along with the definition of ΔP_1 and ΔP_2 given in (*8.3*) and (*8.4*) yields the equation given by (*8.41*).

$$\frac{\exp(-kP_m)(\exp(kP_1) - \exp(kP_2))}{\exp(-kP_d)(\exp(kP_1) - \exp(kP_2))} = \exp(-k(P_m - P_d)) \tag{8.41}$$

Following term cancellation in (*8.41*) we arrive at the final relationship given in (*8.42*) which proves that the equality in (8.36) is true and that our pressure estimates will correspond to mean arterial pressure.

$$P_m - P_d = P_m - P_d \tag{8.42}$$

Using these equations we can also define a relationship between the estimated zero pressure pulse wave velocity and the actual zero pressure pulse wave velocity as given in (*8.43*).

$$\hat{pwv}_0 = pwv_0 \exp(-k(P_m - P_d)) \tag{8.43}$$

From this equation it is apparent that the mean arterial pressure estimates made using our identified calibration curve are valid as long as the difference between mean pressure and diastolic pressure is constant and approximately equal to the difference value observed during the calibration period.

8.6.3 Sensitivity Analysis

The identified zero pressure pulse wave velocity and estimated mean arterial pressure are sensitive to a number of sensor design parameters as well as several physiologic variables. These sensitivities are presented in this section.

The sensor design parameters that effect our identification and estimation algorithm include the transit distances, Δz_A, Δz_B, and Δz_C, and the external arterial pressures, P_1, P_2 and P_3

applied by the wrist and ring sensor housings during the two stage protocol. The important physiologic variables that influence our estimation include diastolic pressure (P_d) and mean arterial pressure (P_m).

The equation used to identify $\hat{pwv}_0$ is given in (*8.18*). A sensitivity analysis of this equation using the parameter values presented in table *8:1* is presented in table *8:2*. Due to the function's dependence on the difference between measured pulse transit time values ($\Delta ptt_{12} = ptt_1 - ptt_2$) and difference in applied external pressure values ($\Delta P_{12} = P_1 - P_2$) we will use these variables in the analysis rather than look at the sensitivity to their individual values. The value of the zero pressure pulse wave velocity used in the analysis is 150 cm/second. Based on this analysis, for these parameter values and the magnitude of the error in our measurements, the estimated zero pressure pulse wave velocity is most sensitive to the measured difference in pulse transit time.

The equation used to initially estimate $\hat{P}_m$ is given in (*8.23*). A sensitivity analysis of this estimation equation using the parameter values given in table *8:1* is presented in table *8:3*. A typical value of mean arterial pressure is approximately 93.3 mmHg. Based on this analysis, for these parameter values and the typical magnitude of the error in our measurements, the estimated mean arterial pressure is most sensitive to the estimated pulse transit time across un-banded arterial segment (segment *B*).

Parameter	*Sensitivity*
$\frac{\partial(\hat{pwv}_0)}{\partial(\Delta ptt_{12})}$	-19.1 $\frac{(cm/\sec)}{m\sec}$
$\frac{\partial(\hat{pwv}_0)}{\partial(\Delta P_{12})}$	7.89 $\frac{(cm/\sec)}{mmHg}$
$\frac{\partial(\hat{pwv}_0)}{\partial(\Delta z_A)}$	5.74 $\frac{(cm/\sec)}{mm}$
$\frac{\partial(\hat{pwv}_0)}{\partial(P_m)}$	-2.30 $\frac{(cm/\sec)}{mmHg}$

Table 8:2. Sensitivity analysis of the identified zero pressure pulse wave velocity, $\hat{pwv}_0$

Parameter	*Sensitivity*
$\frac{\partial(\hat{P}_m)}{\partial(ptt_B)}$	-4.41 $\frac{mmHg}{m\sec}$
$\frac{\partial(\hat{P}_m)}{\partial(pwv_0)}$	-0.33 $\frac{mmHg}{cm/\sec}$
$\frac{\partial(\hat{P}_m)}{\partial(\Delta z_B)}$	0.45 $\frac{mmHg}{mm}$

Table 8:3. Sensitivity analysis of the initial mean arterial blood pressure estimate, $\hat{P}_m$

8.6.4 Error Analysis

The following error analysis examines the effects of pulse transit time measurement error on the error in the mean arterial pressure estimates made using equation (*8.25*) as a function of the calibration period, pulse transit time error according to our sensitivity analysis has the largest impact on estimation accuracy. Although, it is important to note that there are additional sources of measurement error in our algorithm, which include transmural pressure estimation errors at the sensor housing site and error in the measured transit distances these errors will not be considered in this analysis as they are unaffected by the length of the calibration period.

The model used to describe the measured pulse transit time ($\hat{ptt}$) is given in (*8.44*) with *ptt* the actual pulse transit time and σ_e the transit time measurement error.

$$\hat{ptt} = ptt + \sigma_e \qquad (8.44)$$

Based on the analysis presented in Chapter 3, the pulse transit time measurement error (σ_e) is a zero mean variable with a standard deviation equal to 1.6 milliseconds. Using the parameter values presented in table *8:1* to identify the calibration parameters along with a different, set of blood pressure and pulse transit time values used to estimate blood pressure given in table *8:4* a standard deviation of the beat-to-beat blood pressure estimation error as a function of the calibration period was generated using Matlab™ to simulate the identification and estimation protocol through 10,000 simulations. Note any value not specified in Table *8:4* is assumed to be the same as those specified in Table *8:1*.

$P_d =$	85 mmHg
$P_s =$	124.9 mmHg
$P_m =$	98.3 mmHg
$P_{ex,A} = P_2 =$	50 mmHg
$P_{ex,C} = P_3 =$	70 mmHg

Table 8:4. Physiologic variables that comprise the pressure estimation data set

Note that the calibration routine implemented in the simulation is the one described in section 8.5.2 and that the calibration period was considered the total time required to complete both stages of the calibration routine. The frequency of the height variation during each stage was determined by the calibration period length, because the calibration algorithm requires the patient to vary height through the entire range to estimate the transmural pressure acting across the arterial wall. The blood pressure estimation error as a function of the calibration period is given in Figure 8-9. The line indicates the error that corresponded to a total calibration period of 60 seconds, the error was 7.68 mmHg. Calibration periods longer than this duration may impose a significant burden on the patient and should be avoided.

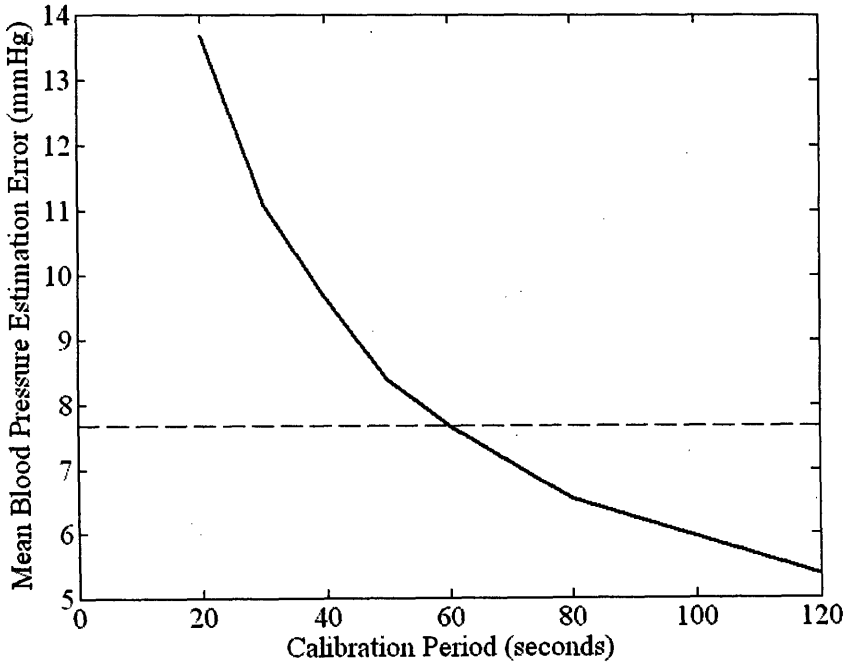

Figure 8-9. Mean arterial pressure error due to variance in the identified model parameters as a function of the calibration period.

CHAPTER 9
FULL CALIBRATION HUMAN SUBJECT TESTING

The goal of this chapter is to describe the experimental protocol used to test the full PTT to mean BP calibration algorithm, explain the procedure used to process the data, and present the results of these experiments to provide a demonstration of the concepts presented in Chapter 8.

9.1 HAND POSTURE AS A MEANS OF EXTERNAL PRESSURE CHANGE

While the final prototype PTT device will have a bi-stable wrist strap capable of exerting two different external pressures on the ulnar artery, the concepts presented in chapter 8 can be implemented using a change in hand posture by the test subject. The mechanism through which external pressurization of the ulnar artery is achieved is shown in Figure *9-1*. The two simple hand postures shown in the figure can be used to exert two different external pressures on the ulnar artery, altering external pressure from a value $P_{ex,A}(t) = P_1$ at time t_1 to a lower pressure $P_{ex,A}(t) = P_2$ at a later time t_2. The change in external pressure exerted on the ulnar artery by the posture change will cause a correlated change in the measured pulse transit time.

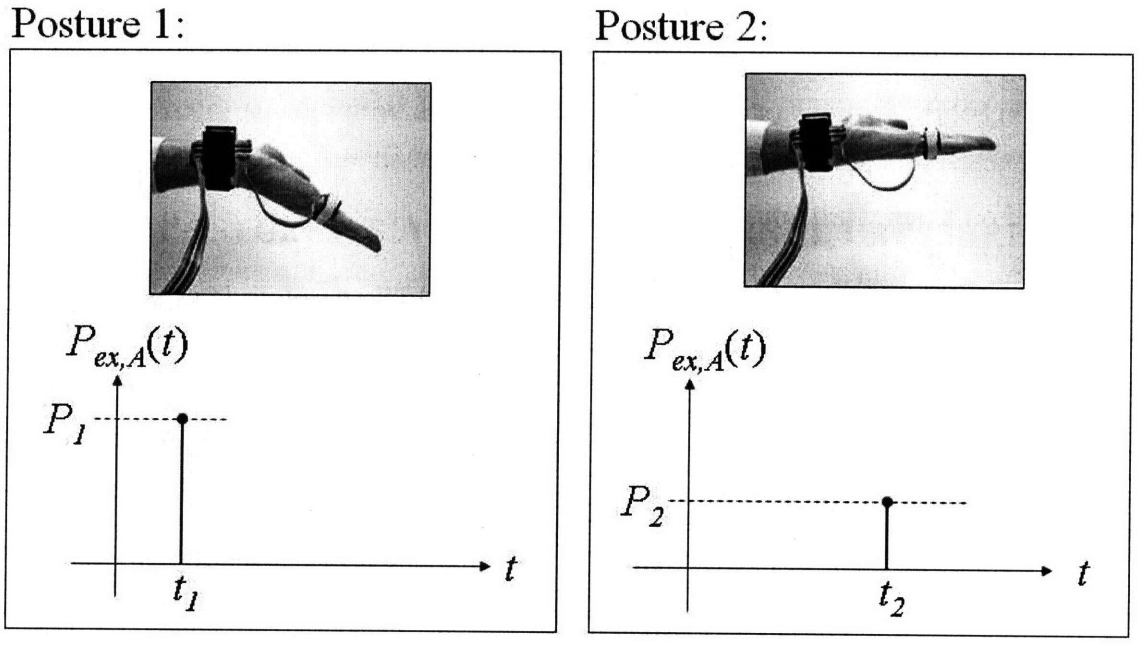

Figure 9-1. A change in external wrist pressure can be implemented using an alteration in hand posture

The ability to alter pulse transit time through a change in hand posture was demonstrated in experimental results presented in chapter 7. These experiments were repeated and the change in external pressure at the sensor contact surface was verified through the use of an external pressure sensor mounted at the contact surface of the wrist PPG sensor. These later experiments clearly demonstrated that the variation in pulse transit time caused by hand posture change was correlated with external pressure change at the wrist sensor surface.

9.2 EXPERIMENTAL PROTOCOL

Human subject data was collected in accordance with an experimental protocol approved by the Massachusetts Institute of Technology's Committee on the Use of Humans as Experimental Subjects (COUHES Approval No. 0403000233) and following Federal regulations for the protection of human subjects established by 45 CFR 46.

Throughout the duration of the experiment data was simultaneously collected from four different sensors; a PPG sensor located at the ulnar artery of the **right** wrist, a PPG sensor located along the digital artery at the base of the little finger of the **right** hand, a manometer type height sensor which consisted of a length of fluid filled tubing connected to an external pressure sensor having its opposite end affixed to the wrist sensor housing, and the Finapres™ blood pressure monitor which was attached to the index finger of **left** hand. Additionally, an Omron HEM 705CP blood pressure cuff was attached to the patients **left** arm. Note the PPG sensors and BP monitors were place on opposite hands, and the left hand was maintained in a stationary position, rested on a table throughout the experiment.

Data from the four sensors was collected using a National Instruments data acquisition board (NI-3452) that had a maximum sample rate of 2 *MHz* and using a program running in the LabView™ 7.1 software environment. The data sample rate of each of the four sensors was *10kHz* (*10kHz x 4 channels = 40kHz*), which was well within the maximum sample rate of our DAQ board. The Omron HEM-705CP oscillometric BP monitor recorded the subject's blood pressure for later review and comparison. Note the time of the cuff measurement was easily identified from the Finapres data which demonstrated significant signal attenuation when the cuff was activated upstream at the brachial artery.

The experimental protocol was performed as follows; throughout the experiment the test subjects remained seated in a chair, the subjects were initially asked to hold their right arm at

heart level with their hand held in posture 1 shown in Figure *9-1*. This height was used to establish the zero level of the height sensor. This hand posture was maintained throughout stage 1 of the experiment. After starting data acquisition the subjected was verbally coached to raise and lower their right hand between its maximum and minimum height at a frequency of approximately 0.04 Hz (T~20 seconds). Following completion of 1-1.5 cycles the subject was instructed to pause at heart level and alter the posture of their hand to posture 2 shown in Figure *9-1*. This posture was maintained throughout stage 2 of the calibration procedure and during the estimation period of the experiment. After completion of 1-1.5 cycles of height variation the subject was instructed to rest their right arm on a table at heart level where it was held throughout the estimation period. The duration of each calibration period was approximately 30 seconds and the duration of the estimation period was approximately 60 seconds.

After approximately 10-15 seconds had elapsed in the estimation period the Omron cuff was activated. Thus the estimation period was divided into an initial phase during which BP estimates could be compared with the Finapres BP monitor and a secondary phase during which BP estimates could be compared to the Omron BP cuff.

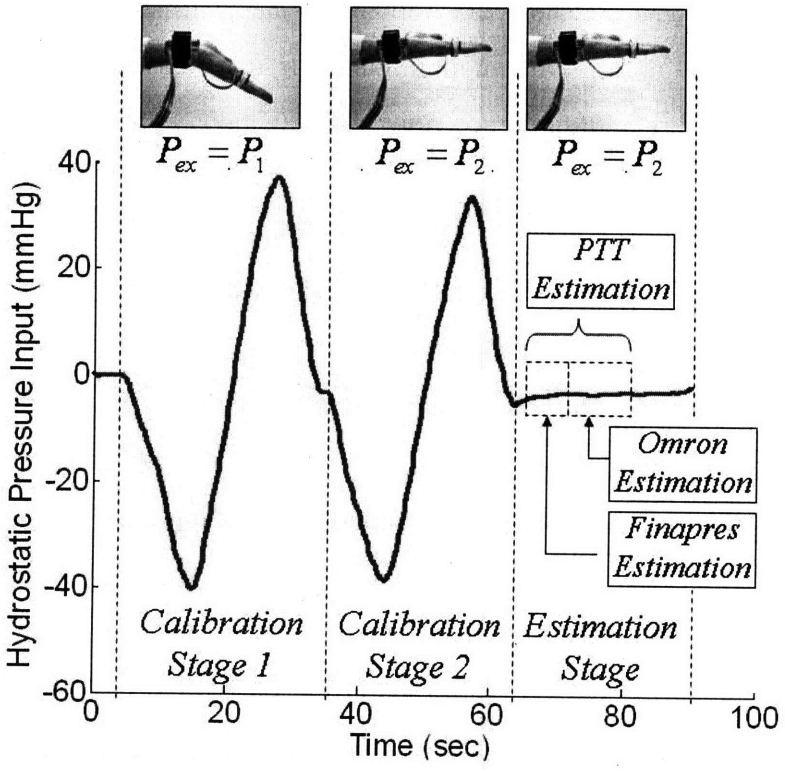

Figure 9-2. Hydrostatic pressure variation and the two external pressures implemented during the three stage human subject tests.

The height variation used in the experiment could be approximately described as a sinusoid with a frequency of 0.04 Hz. This frequency range is lower than the frequency ranges associated with respiratory pressure variation ($f \sim 0.25$ *Hz*) and vasomotor waves ($f \sim 0.1$ *Hz*). An example of the pressure change measured at the wrist by the height sensor during the course of one of the experiments is shown in Figure *9-2*. This figure also illustrates the three different stages of the calibration routine and the wrist postures (external pressures) associated with each stage of the experiment. The figure also depicts the division of the estimation period into an initial Finapres estimation phase and a second Omron Cuff estimation phase.

9.3 TRANSMURAL PRESSURE ESTIMATION

The transmural pressure acting across the sensor wall was identified from the measured height data and PPG waveforms. The magnitude of the PPG signal was estimated as the voltage difference between the maximum and minimum voltage values of the inverted PPG waveform for every cardiac cycle as shown in Figure 9-3.

During each stage of the calibration routine the maximum PPG amplitude value could be identified from the PPG sensor data for both the wrist and the finger PPG sensor. An example of this along with the corresponding hydrostatic pressure measurements is shown in Figure *9-4*.

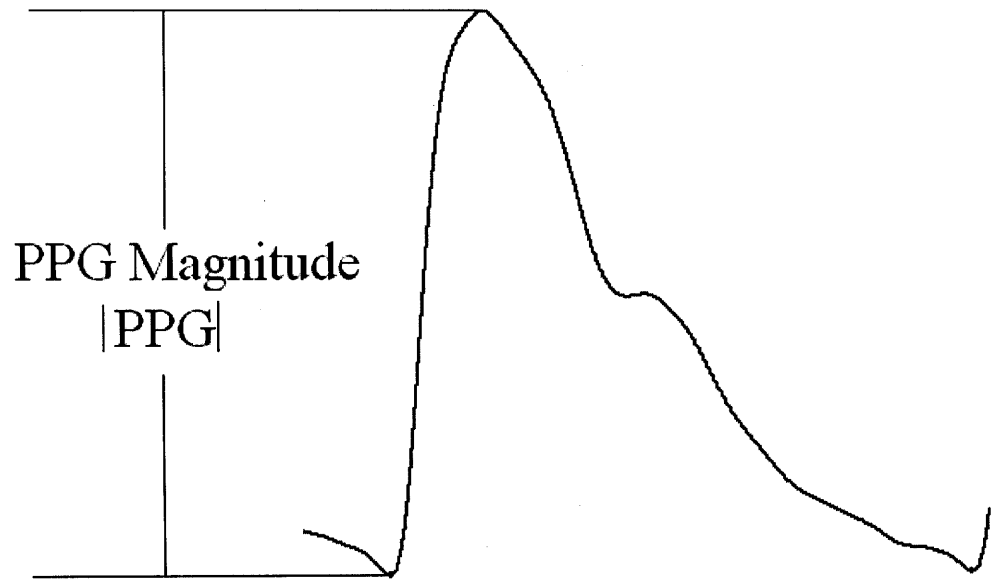

Figure 9.3. PPG magnitude estimated as the difference between the maximum and minimum values of the PPG waveform during each cardiac cycle.

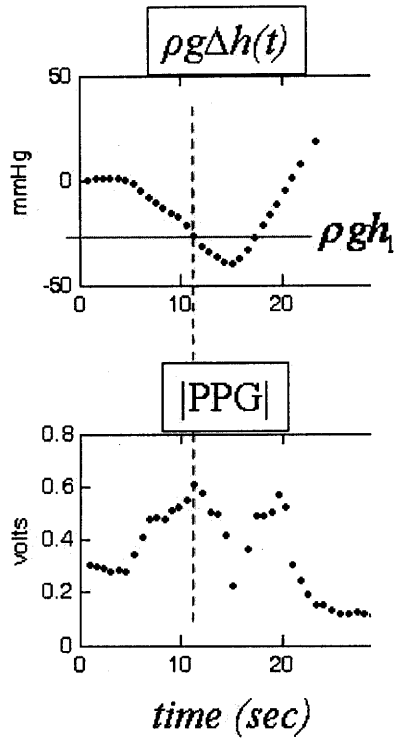

Figure 9-4. Transmural pressure estimation using the maximum PPG magnitude and measured height

Due to the limited sample rate and discrete height measurements a simple quadratic model was used to determine the exact height value corresponding to the maximum PPG amplitude, this model is given in equation (*9.1*). This is a model proposed by Bergel (1960) to describe the compliance of the arterial wall [22].

$$|PPG| = ah^2(t) + bh(t) + c \tag{9.1}$$

The coefficients of this model were identified using a least squares identification technique along with the height and PPG magnitude data from a minimum of three data points surrounding and including the peak magnitude value.

Following identification of the model coefficients the height value corresponding to the peak PPG magnitude was identified by taking the derivative of equation (*9.1*) as given in equation (*9.2*).

$$\frac{d}{dh}(|PPG|) = 2ah(t) + b = 0 \tag{9.2}$$

9.4 EXPERIMENTAL RESULTS

The full calibration protocol was performed in our laboratory at MIT on 11 different subjects. Each of the subjects read and signed a COUHES approved consent form prior to participating in the experiment.

All data processing and analysis was preformed off-line using the MATLAB™ software environment following completion of the eleven experiments. Prior to processing any of the data all four of the recorded sensor signals were low-pass filtered using a fourth order butterworth filter with a cutoff frequency of 20 *Hz*. This cutoff frequency was chosen because the blood pressure waveform can be accurately represented using the first 10 harmonics [21]. The resting heart rate of all the patients in the study was less than 2 *Hz* thus the blood pressure and volumetric PPG waveforms should be accurately captured in a frequency spectrum below 20 *Hz*.

The pulse transit time ($ptt(t)$) between the two sensors was estimated as the timing difference between the arrival time of the finger PPG waveform and the arrival time of the wrist PPG waveform. The arrival time of each of the waveforms was estimated using the minimum point of the waveform as detailed in Chapter 4. Pulse transit time estimates that were less than 0 milliseconds and greater than 80 milliseconds were eliminated from the data set.

The magnitude of the wrist and finger PPG waveforms were estimated for every cardiac cycle and PTT estimates derived from cardiac cycles that had a finger or wrist PPG magnitude of less than 20 millivolts were removed from the data set. Unfortunately, for two of the test subjects, this data screening procedure reduced the number of valid pulse transit time values to an unacceptable level and we were unable to continue with the identification procedure for these individuals.

The height ($h(t)$) that corresponded to each estimated pulse transit time value was determined from the measured output of our height sensor and was selected from the measured data set at a time corresponding to the finger PPG arrival time. To ensure the accuracy of the height sensor it was calibrated against a known height prior to every experimental test session. The height data was converted to internal blood pressure assuming that the density of human blood is 1060 kg/m^3.

The full calibration algorithm was applied to data derived from 9 different test subjects. The model parameter k, was identified using the adaptive height calibration algorithm. Due to the difference in external pressure between the stages the algorithm had to be applied to data taken

during only one of the stages. The stage selected for use in the algorithm was based on which calibration stage demonstrated the largest correlation between the measured *PTT* data and measured height data.

Transmural pressure estimation was performed using the procedure outlined in section 9.3. This procedure was performed on the wrist sensor PPG data in both calibration stages and the finger PPG sensor during stage 2 of the calibration routine. Unfortunately, one of the test subjects exhibited no external pressure difference at the ulnar artery sensor between the two stages and had to be removed from the remainder of the identification procedure.

The pulse transit time difference between calibration stage 1 and calibration stage 2 was determined using pulse transit time values measured when the relative height was approximately equal to the level of the heart. Data measured at this height was used to identify a mean pulse transit time difference between the two stages. Only PTT data from this height could be used because of data correlation issues that will be discussed in depth in chapter 10. Due to the small sample size, only valid PTT data, $ptt_1 > ptt_2$ was selected to estimate the difference.

The model parameter y_0 was identified from the data measured in calibration stage 1 and stage 2 using the adaptive procedure described in chapter 8. Following identification, pulse transit time values measured during the estimation stage could then be used to estimate mean arterial pressure. The average of the mean arterial pressure values estimated during the Finapres estimation period and Omron cuff estimation period using our adaptive PTT based method are shown in Table *9:1.* Also included in this table are the average mean arterial pressure values estimated by the Finapres during the initial phase of the estimation period and the mean arterial pressure value estimated from the Omron Cuff during the second phase of the estimation period.

Subject	Adaptive PTT Mean BP (mmHg)	Finapres Mean BP (mmHg)	Omron Mean BP (mmHg)
1	99.6	104.2	92.7
2	91.1	90.6	93.7
3	88.0	91.1	91.7
4	85.6	118.5	79.3
5	103.6	108.8	93.3
6	93.0	91.7	93.3
7	117.3	102.0	112.3
8	72.7	85.4	84.0

Table 9:1. A comparison of the mean arterial pressure values estimated from the adaptive PTT calibration algorithm, Finapres BP monitor, and Omron BP Cuff

The accuracy of our adaptive PTT estimation method was determined by comparison of its mean arterial blood pressure estimates with the mean arterial pressure measured with the Omron BP cuff. A Bland-Altman plot comparing the difference in mean BP measured with the our adaptive PTT device and the mean arterial blood pressure estimated with the Omron cuff for the eight test subjects is plotted in Figure *9-4*.

The mean BP difference between the estimates made by the two devices was 1.30 mmHg. This mean BP difference is not significant and can be explained by the probability distribution of the measurement error of the two BP measurement techniques. The standard deviation of the BP difference (7.08 mmHg) given in the Bland-Altman plot is not only the result of measurement error associated with the adaptive PTT algorithm but also the result of measurement error associated with the Omron cuff. Any difference value in the plot is the result of adaptive PTT BP error (e_{PTT}) and Omron cuff BP error (e_{cuff}) as given in (*9.3*).

$$BP\ difference = e_{PTT} - e_{cuff} \tag{9.3}$$

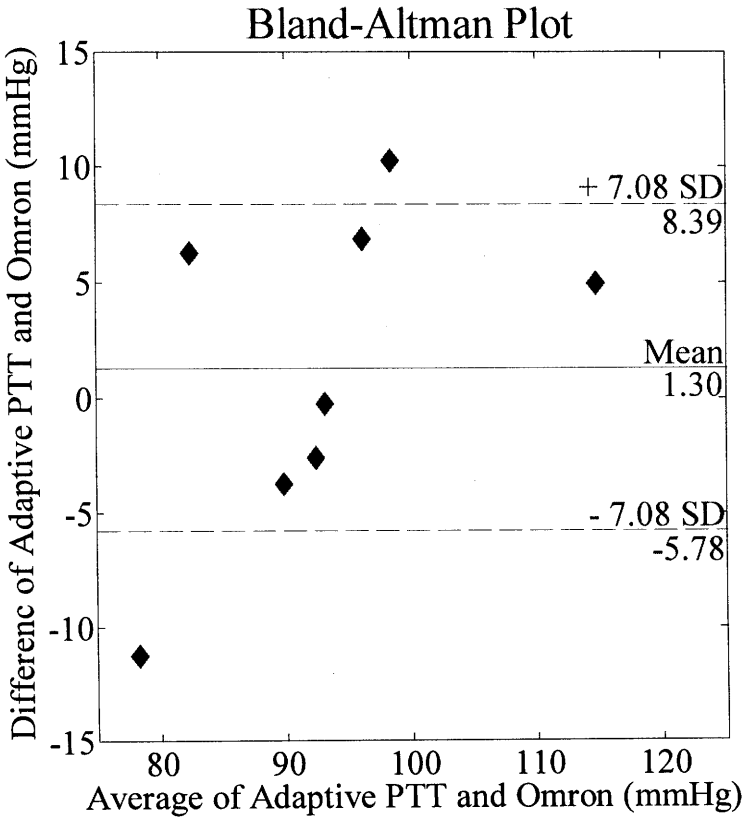

Figure 9-5. Bland-Altman plot comparing the mean arterial blood pressure estimated by the adaptively calibrated PTT algorithm and the Omron BP cuff.

The error statistics of the Omron HEM-705CP are unavailable but it has been recommended as a grade "A" NIBP device according to the British Society of Hypertension [38], this rating indicates that at least 60% of its BP measurements have an error of less than 5 mmHg when compared with a gold standard. Based on this rating, for comparison of our method with the Omron cuff we will assume that the standard deviation of error for the Omron monitor is 5 mmHg and that the error is governed by a normal distribution. Therefore, we have assumed that 68% of the Omron cuff's BP measurements have a BP error of less than 5mmHg. Under the assumption that the BP estimation error in the adaptive PTT algorithm is also governed by a normal distribution, and therefore so is the difference in estimated BP between the two methods, we can identify the standard deviation of BP error for the adaptive PTT calibration algorithm alone based on the formula given in (*9.3*). Based on these assumptions the standard deviation of BP error in measurements made using the adaptive PTT algorithm is approximately 5 mmHg which classifies this novel technique as a grade "A" NIBP device with less than 5mmHg error in at least 60% of its measurements.

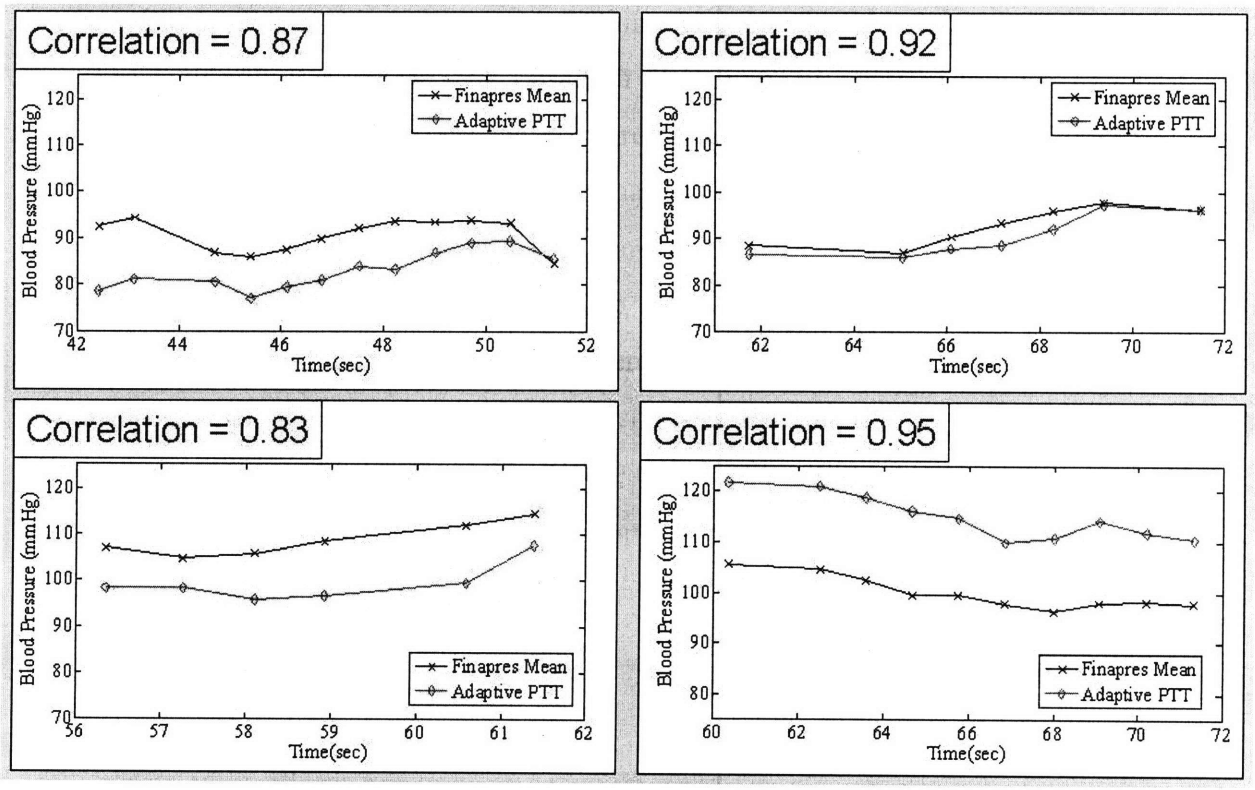

Figure 9-6. A comparison of beat-to-beat mean arterial blood pressure estimated using adaptively calibrated PTT and mean Finapres BP(patient 2, 5, 6 and 7)

In addition to its capability to accurately estimate BP, this new algorithm also provides beat-to-beat estimation capability. The beat-to-beat capability of our adaptive PTT calibration technique can be compared to the Finapres data measured during the initial phase of the estimation stage. A demonstration of this capability is shown in Figure 9-6 for patient 2,5,6, and 7. Based on these results the mean arterial blood pressure estimated with our adaptive calibration algorithm demonstrated that it is capable of providing beat-to-beat BP measurements that exhibit the same dynamic trends as the Finapres mean pressure estimates.

CHAPTER 10
DISCUSSION OF THE FULL CALIBRATION TEST RESULTS

The goal of this chapter of the thesis is to discuss issues that were identified during the human subject testing presented in Chapter 10 and recommend ways to address these issues when implementing the calibration algorithm in the future.

10.1 IMPROVING THE CALIBRATION ROUTINE

The primary issue observed in the experimental data was the difference in correlation between the measured PTT data and the height variation data during the two stages. In a majority of the test subjects the correlation between height and pulse transit time was superior in one of the two stages. Although this issue did not interfere with the adaptive height calibration algorithm which was free to identify the model parameter k, from the stage that contained the most correlated height and PTT data it did prove problematic when attempting to identify the difference in pulse transit time between the two stages caused by external pressure change.

The calibration routine utilized in the human subject tests in Chapter 10 seamlessly combined height variation with the identification of the difference in pulse transit time caused by the external pressure change. Following identification of the model parameter k, using adaptive height calibration the effects of relative height were to be removed from the PTT data measured during each stage ($i = 1,2$) using the expression given in equation (*10.1*).

$$ptt_i(t, h=0) = \frac{ptt_i(t, h(t))}{\exp(-k \cdot \rho g h(t))} \qquad (10.1)$$

The difference in pulse transit time between the two stages was then to be estimated from the PTT measurements $ptt_i(t, h=0)$, following removal of the effects of relative height variation. If one stage of the PTT data was poorly correlated with height then the procedure performed in equation (*10.1*) did not remove the height variation from the data but actually added this correlation to the data making estimation of the pressure difference extremely problematic.

This problem was resolved in the human subject tests in Chapter 10 by only using PTT data to estimate the pressure difference that was measured when the hand was approximately at heart level. While this technique proved successful in processing the data from these experiments, the amount of acceptable data in this height range was limited and future calibration routines would benefit from a larger pool of data from which the pulse transit time difference could be estimated.

There is simple solution to this problem, the calibration routine could be deigned to separate the data set used to estimate the effects of external pressure change from the PTT data set used in the height calibration algorithms. A plot of the hydrostatic pressure variation in a new algorithm is shown in Figure *10-1*. Unfortunately, this type of divided identification algorithm is likely to increase the time required by a calibration routine in order to minimize the effects of PTT error.

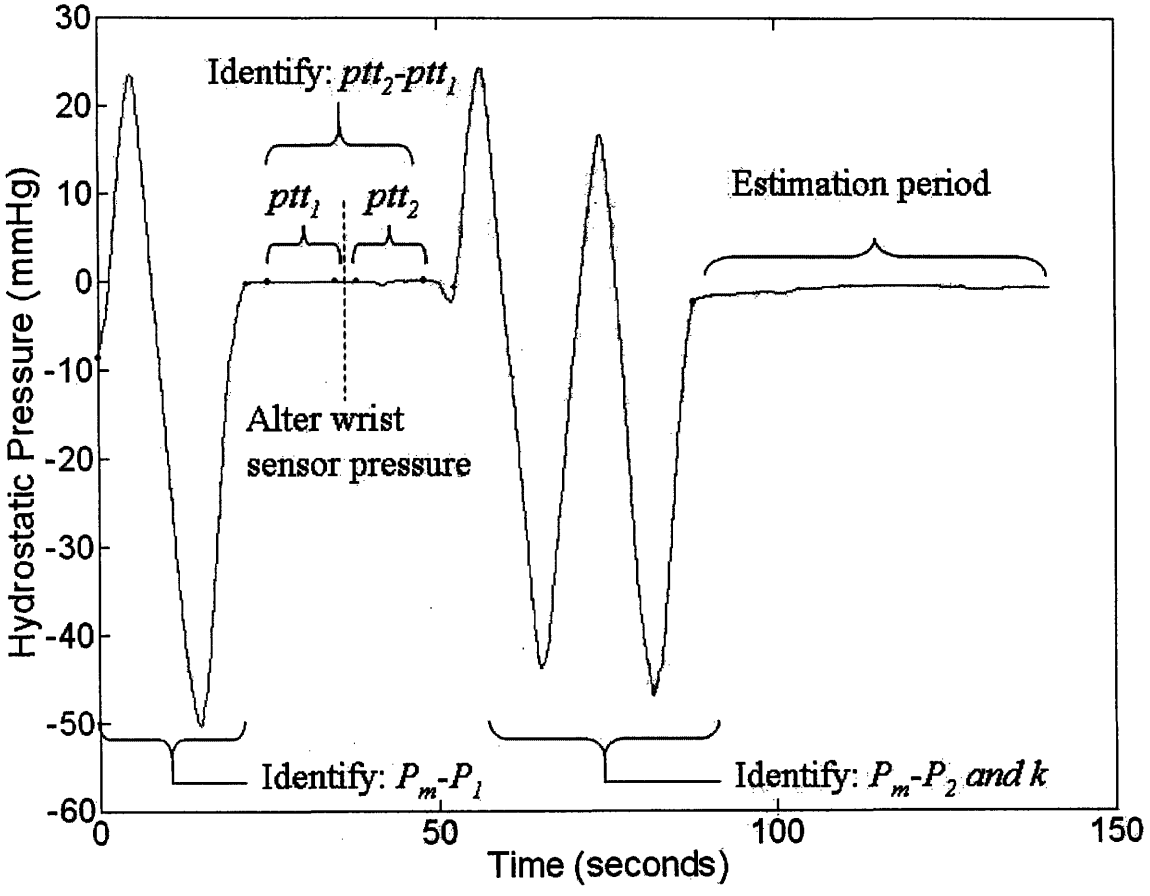

Figure 10-1. Future calibration routines should separate height variation and external pressure change.

10.2 EXTERNAL PRESSURE DEPENDENT CORRELATION BETWEEN PTT & HEIGHT

Although, we have shown that the full calibration algorithm can be successfully implemented using the algorithms and device presented in this thesis, understanding the mechanisms which caused the poor data correlation during one of the stages may allow further improvement of the calibration routine and possibly offer an opportunity to reduce the inherent error present when estimating pulse transit from our in-line PPG sensors. The difference in correlation between PTT and height variation in the two experimental stages may have been caused by two different mechanisms, correlated arterial blood pressure variation and the dynamics of the arterial pressure-volume relationship observed by our PPG sensors.

Correlated arterial blood pressure variation is the result of patient anticipation and relaxation before and after various tasks in the calibration routine are performed. This type of error may be corrected for by neglecting data from our identification algorithm that is collected just prior to and just after the start of a task during the calibration routine. The length of these correlated periods will need to be identified through future experimental testing. Correlated pressure change may also be minimized by increasing a patient's familiarity with the calibration routine.

10.2.1 Arterial Wall Dynamics and PPG Onset: The Thin Wrist Sensor Pressure Test

The A.C. portion of the PPG signal is a measure of the volume change in the artery underlying the measurement site. As described in detail in Chapter 4 the non-linear compliance of the arterial wall causes amplification and attenuation of various segments of the pressure waveform as it varies throughout the cardiac cycle. The external pressure exerted on the artery by the PPG sensor shifts the range of transmural pressure values across which the arterial pressure waveform oscillates, in effect controlling which portions of the blood pressure waveform are amplified or attenuated. In chapter 4 it was suggested that the scaling effect of the arterial compliance could be mitigated by selecting the waveform minimum value as the onset marker of the PPG waveform. Later in chapter 7 the variation in phase delay produced by the non-linear arterial stiffness was eliminated as a potential source of error when estimating arrival time with the PPG waveform. However, the PPG waveform does exhibit a significant amount of

hysteresis throughout the cardiac cycle as shown in Figure 2-3 and the dynamic effects observed in the loading and unloading of the arterial wall may influence the volumetric PPG signal and potentially alter the timing and magnitude of various features on the PPG waveform such as the minimum value. The waveforms shown in Figure *10-2* represent the measured Finapres BP signal and the corresponding wrist PPG signal measured while a mild external pressure ($P_{ex} < P_{mean}$) was exerted by the wrist sensor housing.

Examination of this PPG waveform in comparison to the BP waveform reveals some very interesting behavior. The waveform minimum highlighted as feature "A" in the blood pressure waveform is no longer a minimum point in the PPG waveform. The PPG waveform peak highlighted as feature "B" appears to arrive much later than does the peak of the BP waveform. Both of these features represent locations on the BP and PPG waveform where the pressure acting across the arterial wall has transitioned between a loading and unloading pressure. Based on this pattern of behavior we should expect that the magnitude and timing of the PPG waveform minimum highlighted as feature "C" may also be altered by this natural loading and unloading process. This type of behavior cannot be explained by a simple non-linear algebraic scaling of the PPG produced by the non-linear arterial stiffness but rather must this phenomenon can only be explained by the dynamic behavior of the arterial wall.

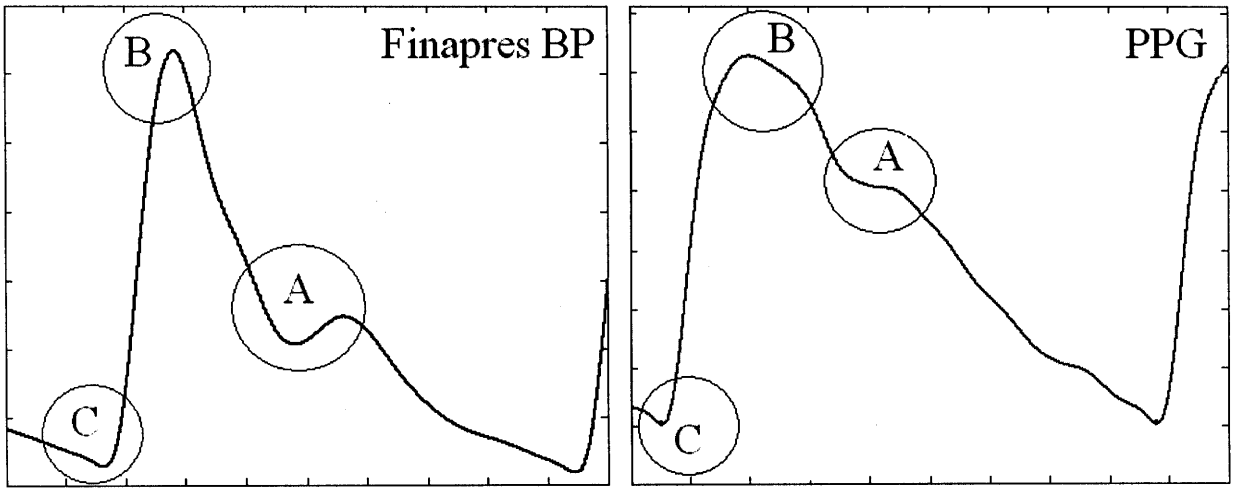

Figure 10-2. The effect of external sensor pressure on the magnitude and estimated arrival time of various blood pressure waveform features in the wrist PPG waveform

A set of experiments were preformed to determine the magnitude of the pulse transit time change produced by these dynamic effects due to alteration in external sensor pressure. In order to eliminate the effects of pulse wave velocity variation in the arterial segment underlying the sensor housing prior to signal acquisition a new wrist sensor housing was designed that had a very small contact width. The contact width of the new wrist sensor housing was 0.5 cm compared to 3.2 cm for the typical wrist sensor housing. The new wrist sensor housing is shown in Figure *10-3*.

The experimental protocol was as follows; an EKG signal and an ulnar artery PPG signal at the left wrist were measured simultaneously. The thin wrist PPG sensor was attached to the subject with an elastic band providing an initial external pressure to the measurement site, $P_w(t=0)$. The experiment was separated into three different stages; each stage was approximately 30 seconds in duration. At the onset of each successive stage the external pressure applied by the wrist sensor housing was increased and then held constant throughout the remainder of the stage. The pulse transit time in each stage was estimated from the difference of the arrival time of the wrist PPG waveform minimum and the peak time of the QRS complex of the EKG waveform. Sample results collected for a healthy male subject from one of the experiments is shown in Figure *10-4*.

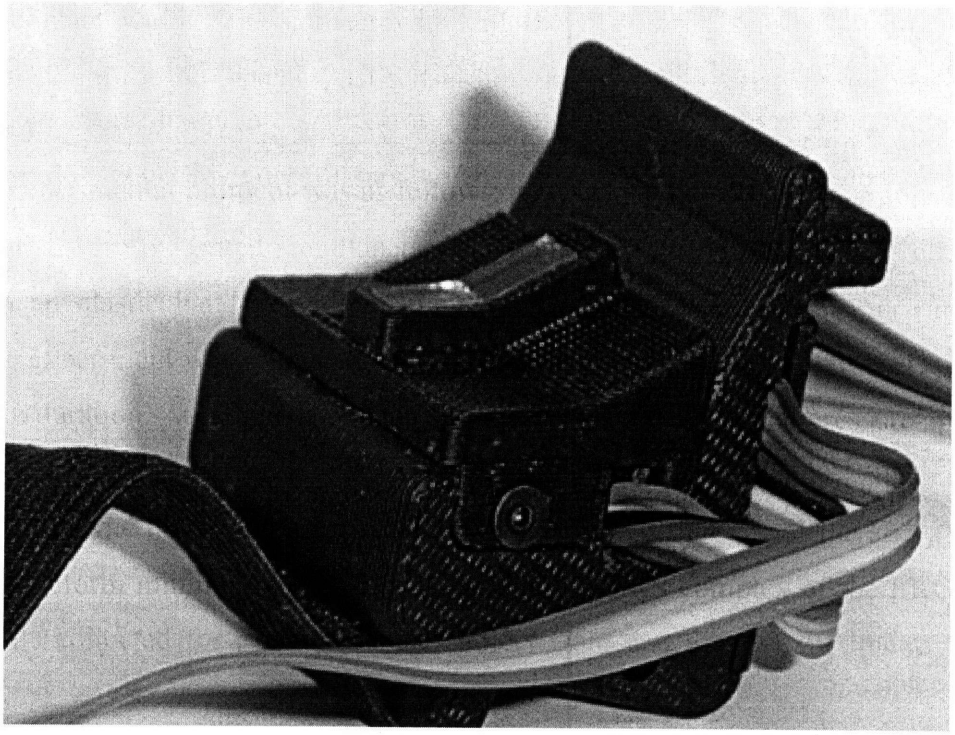

Figure 10-3. Wrist sensor housing with a thin contact width

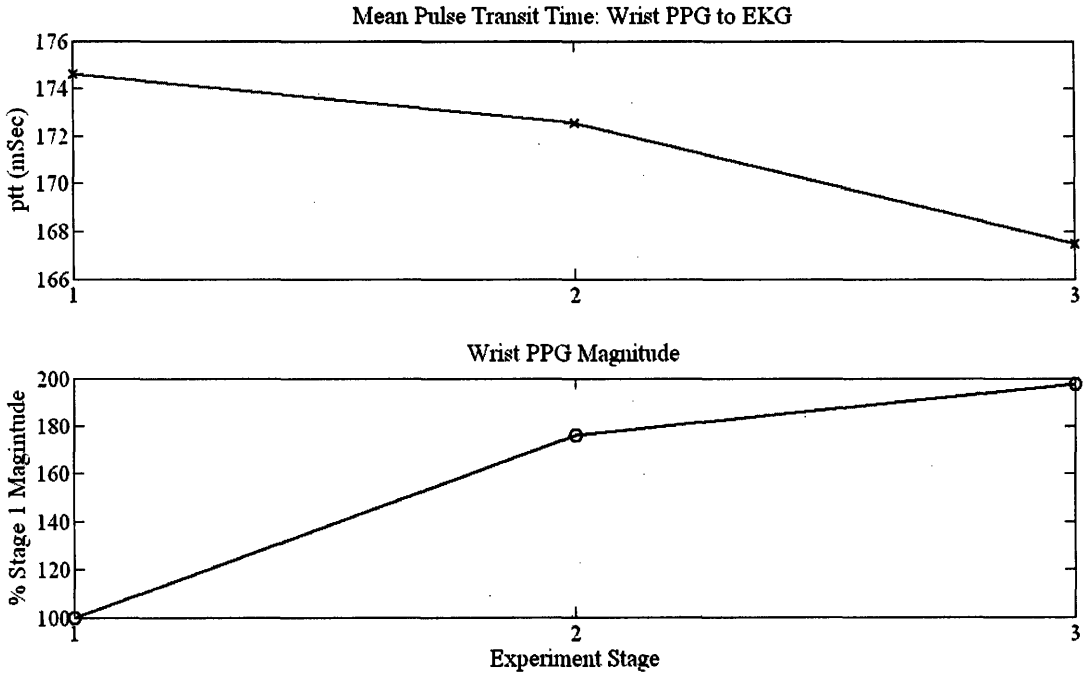

Figure 10-4. Pulse transit time estimated from the wrist PPG waveform and EKG during multi-stage progressive increases in external wrist sensor pressure.

The data in shown in Figure *10-4* shows that a negative correlation exists between external pressure variation and pulse transit time change in that result from alteration to the waveform morphology at the minimum point. This behavior is opposite to the effect on arrival time predicted by pulse wave velocity variation due to increased external sensor pressure. Thus, as external sensor pressure was increased the dynamic variation in the PPG waveform caused the pulse transit time to decrease between our EKG and wrist PPG. These changes made it appear as though the pulse wave velocity between the left ventricle and ulnar artery at the wrist had increased.

The negative correlation between external pressure and pulse transit time was consistently observed in all the experiments performed on this subject. The pulse transit time results from three different experiments performed on the same male subject given a progressive, three stage pressurization of the thin wrist sensor housing are presented in Table *10:1*. The average change in pulse transit time observed in the three tests between the third and first stages of the experiments was -6.8 milliseconds and the standard deviation of the three tests was 0.5 milliseconds.

	Test 1	Test 2	Test 3
ptt_1 (*msec*)	172.9	178.6	173.7
ptt_3 (*msec*)	166.7	167.5	166.7
$\Delta ptt_{31} = ptt_3 - ptt_1$ (*msec*)	-6.2	-7.1	-7.0

Table 10:1. Pulse transit time between the wrist PPG waveform and EKG waveform following progressive pressurization of the thin wrist PPG sensor housing.

Based on observation of the plots in Figure *10-4* and the trends demonstrated by the pulse transit time data from the other two experiments it appears that the pulse transit time variation caused by dynamic changes in the timing of waveform features are a function of transmural pressure. However, this dependence appears only to be true while the transmural pressure of the base of the pressure waveform is greater than zero. This additional trend can be observed in the pulse transit time data measured during test 1 and which is presented in Figure *10-5*.

The downward trend in the PPG magnitude data between stage 2 and stage 3 suggests that the external pressure has exceeded the mean arterial pressure between these stages and passed through the maximum compliance value of the arterial wall. However, even as the external arterial pressure was progressively increased the difference in *ptt* between stage 2 and 3 was nearly constant ($\Delta ptt_{32} = ptt_3 - ptt_2 = 166.69\text{-}166.68 = 0.01$ milliseconds).

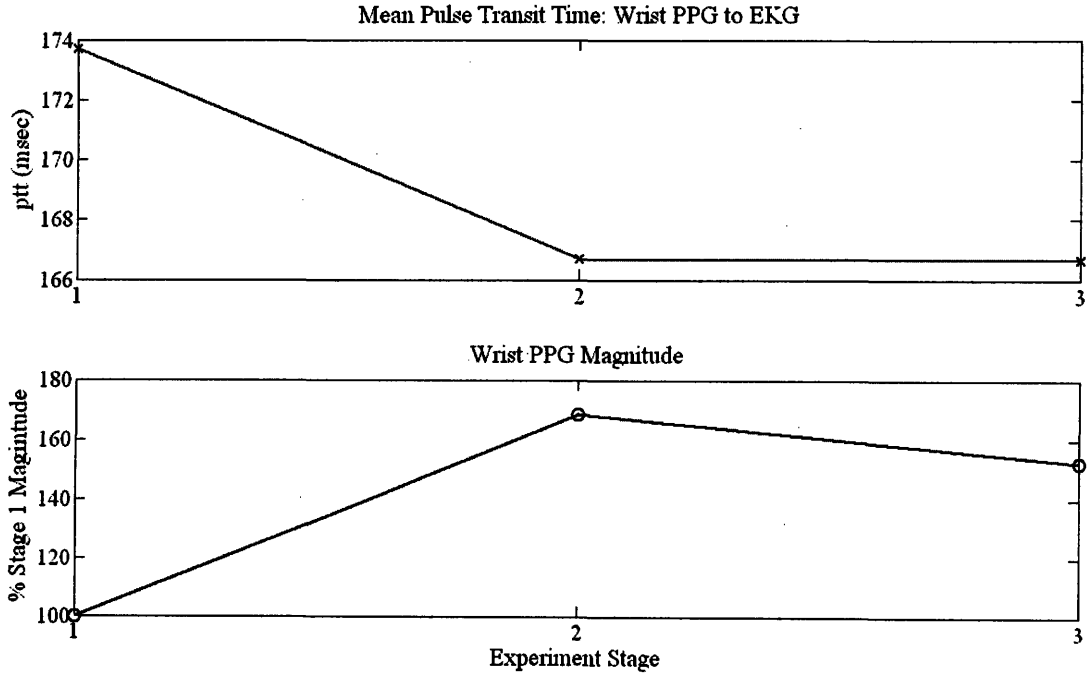

Figure 10-5. The variation in PPG magnitude and pulse transit time are dependent on arterial compliance

Therefore, the data presented in Table *10:1* appears to be about the maximum change in arrival time that the pressure dependent dynamics can produce for this individual.

This behavior may be used to explain the difference in correlation observed between the two experimental stages in our test subjects. The effects of wall dynamics on pulse transit time are non-linear as shown in Figure 10-5. This non-linearity causes the wall dynamics to have a larger influence on PPG arrival time and on the measured pulse transit time values when the height is varied over a specific range of transmural pressures. When there is an abrupt shift in the external pressure as occurred in our experiments the influence of the wall dynamics on PPG arrival time may be significantly reduced as the transmural pressure values are varied with height. Thus the estimated pulse transit times are not significantly affected by the wall dynamics and are more representative of the pulse wave velocity change being produced by the height variation.

This behavior suggests that our calibration routine which examines the affects of height variation on PTT under two different loading pressures offers a natural way to minimize the effects of arterial wall dynamics on PPG arrival time in our adaptive height calibration algorithm. Future experimentation may yield an even better understanding of these dynamic effects and an adaptive arrival time methodology may be produced that may completely eliminate the effects of this behavior.

CHAPTER 11
CONCLUSION

11.1 SUMMARY OF CONTRIBUTIONS

In order for a wearable BP device to be effective it must meet a number of requirements, the device must be unobtrusive, compact, lightweight, low power, and self calibrating. The major obstacle preventing many non-invasive BP devices from achieving these goals has been the requirement for some form of actuated cuff during device calibration and BP measurement. These actuated cuffs are not only obtrusive but increase the power requirements of the device. Alternative existing wearable BP devices that operate without actuation based on pulse wave velocity also operate without a means of self-calibration and are therefore subject to inaccuracy if changes in the initial calibrated cardiovascular state occur.

In this thesis we have developed an enabling set of technologies for wearable blood pressure devices that allows actuator free, self calibration of peripheral pulse transit time using natural human motion. This new technique combines relative height variation and external arterial pressure change with a set of novel adaptive calibration algorithms.

This new set of calibration tools was combined with a novel peripheral pulse wave velocity sensor architecture to create for the first time ever, an actuator free, self calibrating, wearable blood pressure monitor that is capable of providing beat-by-beat mean arterial blood pressure measurements.

The capability of this device and these calibration techniques were demonstrated through human subject testing performed in the laboratory. These tests have shown that the device was capable of providing blood pressure measurements comparable to an Omron BP cuff and capable of estimating beat-to-beat mean arterial blood pressure that exhibited the same dynamic trends as the mean beat-to-beat BP measurements made with the Finapres BP monitor.

The specific contributions of this thesis are:

(1) Pioneered the concept of using relative height variation to calibrate peripheral pulse transit time measurements and experimentally demonstrated the correlation between height and peripheral pulse transit time.

(2) Designed, developed, and tested an in-line optical pulse transit time sensor that can be worn unobtrusively by the patient as a wrist watch and a ring. The use of peripheral PPG sensor architecture eliminated the EKG and allowed PTT calibration through height variation.

(3) Based on experimental observation and theoretical analysis we provided guidelines for the minimum transit distance between in-line PPG sensors based on blood pressure estimation error and sample rate.

(4) Based on a novel linear system formulation we developed an algorithm based on adaptive noise cancellation that utilizes height to calibrate peripheral pulse transit time despite unknown variation in blood pressure throughout the calibration period.

(5) Based on theoretical analysis we provided guidelines for the duration of the calibration for our adaptive height calibration algorithm based on model parameter variance

(6) Demonstrated through human subject testing that the adaptive height calibration algorithm could identify model parameters as accurately as the actual BP measurements made using the Finapres BP monitor.

(7) Contributed to the physiologic knowledge base regarding the influence of external pressure applied to the skin surface and its affect on pulse transit time.

(8) Developed a system model for our in-line sensors that included the loading conditions imposed on the arterial transit path by the PPG sensor housing. Theoretical analysis demonstrated that this model was capable of predicting the negative correlation observed between the model parameters k and y_0 observed in experimental human subject tests.

(9) Pioneered the concept of using external pressure variation applied at the skin surface to calibrate pulse transit time and experimentally demonstrated the correlation between external contact pressure and pulse transit time measurements.

(10) Developed a calibration technique that combined relative height variation and external pressure change to allow mean BP estimation from the measured PTT using only natural human motion.

(11) Demonstrated through human subject testing that this combined adaptive calibration algorithm could estimate mean BP with accuracy comparable to an Omron BP cuff

and that the beat-to-beat estimates exhibited dynamic trends that were similar to the trends exhibited by mean BP measured with the Finapres BP monitor.

(12) Based on experimental observation and theoretical analysis provided novel insights into the dynamic relationship between BP and PPG and their effect on the identified pulse arrival time.

11.2 FUTURE RESEARCH DIRECTIONS

This thesis has provided an enabling set of calibration techniques and innovations in device design that can serve as platform technologies towards radical innovation of a truly wearable BP monitor. However, the process of realizing a prototype device that is suitable for use by patients in the current marketplace is in its infancy and will require a great deal of hard work in the future.

The cyclic design and development process for this device is shown in Figure *11-1*. Through the course of the work presented in this thesis we have gone completely through this development cycle a minimum of three times. Each time through this process we have identified new requirements of the technology, identified new factors that influence its capability, and made significant improvements in the device and its performance. To realize the potential of this device this cyclic process will have to be continued until the rate of improvement in these various elements decreases to a much smaller level, where each design cycle provides only incremental improvements in the technology.

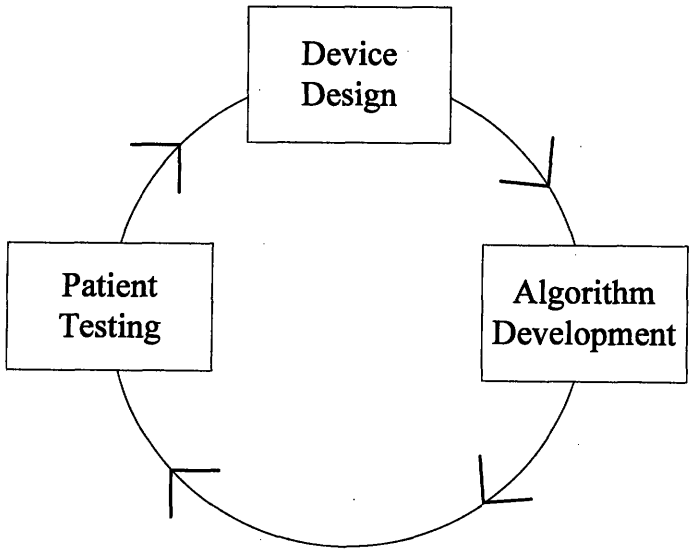

Figure 11-1. Cyclic design and development process for a wearable BP monitor

Some of the major issues that should be improved in a future BP device are, to simplify the calibration routine reducing the complication and burden to the patient and to explore the recursive capabilities of these adaptive algorithms to better utilize the enormous amounts of data that are gathered by the device to reduce error in the identified parameters and BP estimates.

REFERENCES

[1] D.M. Lloyd-Jones, J.C. Evans, and D. Levy, "Hypertension in adults across the age spectrum: current outcomes and control in the community," *Jama*, vol. 294, no.4, pp. 466-472, July 2005.

[2] I. Hajjar, J.M. Kotchen, and T.A. Kotchen, "Hypertension: trends in prevalence, incidence, and control," *Annu. Rev. Public Health,* vol. 27, pp. 465-490, 2006.

[3] Z.V. Edmonds, W.R. Mower, L.M. Lovato, R. Lomeli. "The reliability of vital sign measurements," *Ann Emerg Med,* vol. 39, no. 3, pp.233-237, Mar 2002.

[4] D.W. Jones, L.J. Appel, S.G. Sheps, E.J. Roccella, C. Lenfant, "Measuring blood pressure accurately: new and persistent challenges," *Jama,* vol. 289, no. 8, pp.1027-1030, Feb 2003.

[5] B.P. McGrath, "Ambulatory blood pressure monitoring," *Med J Aust*, vol. 176, no.12, pp. 588-592, June 2002.

[6] H. Reims, E. Fossum, S.E. Kjeldsen, and S. Julius, "Home blood pressure monitoring. Current knowledge and directions for future research," *Blood Press.,* vol. 10, no.5-6, pp. 271-287, 2001.

[7] D. Herpin, T. Pickering, G. Stergiou, P. de Leeuw, and G. Germano, "Consensus Conference on Self-blood pressure measurement. Clinical applications and diagnosis," *Blood Press. Monit.,* vol. 5, no. 2, pp. 131-135, Apr 2000.

[8] J.A. Staessen, "Epidemiology of ambulatory blood pressure monitoring," *Blood Press. Monit.,* vol. 2, no. 2, pp. 61-64, Apr 1997.

[9] T.G. Pickering, D. Shimbo, and D. Haas, "Ambulatory blood-pressure monitoring," *N. Engl. J. Med.,* vol. 354, no. 22, pp. 2368-2374, June 2006.

[10] J.D. Bronzino, *Biomedical Engineering Handbook Volume 2.* 2nd ed., CRC press, Boca Raton, FL, 2000, ch. 70.

[11] W.M. Nichols and M.F. O'Rourke, *McDonald's Blood Flow in Arteries Theoretical, experimental, and clinical principals.* 4th ed., Hodder Arnold Publication, London, 1998, ch. 3.

[12] C.C.Young, J.B. Mark, W.White, A. DeBree, J.S. Vender, A. Fleming, "Clinical evaluation of continuous noninvasive blood pressure monitoring: accuracy and tracking capabilities," *J Clin Monit.*, vol. 11, no.4, pp. 245-252, Jul 1995.

[13] W. Chen, T. Kobayashi, S. Ichikawa, Y. Takeuchi, and T. Togawa, "Continuous estimation of systolic blood pressure using pulse arrival time and intermittent calibration," *Med. Biol. Eng. Comp.*, vol. 38, pp. 569-574, 2000.

[14] M. Nitzan, B. Khanokh, Y. Slovik, "The difference in pulse transit time to the toe and finger measured by photoplethysmography," *Physiol Meas*, vol.23, no.1, pp. 85-93, Feb 2002.

[15] J.R. Jago and A. Murray, "Repeatability of peripheral pulse measurements on ears, fingers and toes using photoelectric plethysmography," *Clin. Physiol. Meas.*, vol. 9, no. 4, pp. 319-329, 1998

[16] L.M. Van Bortel, D. Duprez, M.J. Starmans-Kool, et al. "Clinical applications of arterial stiffness, Task Force III: recommendations for user procedures," *Am J Hypertens*, vol.15, no.5, pp .445-452, May 2002.

[17] C. Poon, and Y. Zhang, "Cuff-less and Non-invasive measurements of arterial blood pressure by pulse transit time," Proc. Of the 27th IEEE Engineering in Medicine and Biology, EMBC 2005, Shanghai, China, Vol. 1, pp. 913-916, August 2005.

[18] A.C. Guyton and J.E. Hall, *Textbook of Medical Physiology.* 9th ed., Philadelphia, PA: WB Saunders, 1996, ch. 18.

[19] P. Shaltis, A. Reisner, and H. Asada, "A Hydrostatic Pressure Approach to Cuffless Blood Pressure Monitoring," in *Proc. 26th Annu. IEEE Int. Conf. Engineering in Medicine and Biology*, San Francisco, Sept. 2004.

[20] D. McCombie, A. Reisner, and H. Asada, "Adaptive blood pressure estimation from wearable PPG sensors using peripheral artery pulse wave velocity measurements and multi-channel blind identification of local arterial dynamics." In *Proc. 28th IEEE Int. Conf. Engineering in Medicine and Biology,* New York, pp. 3521-3524, Aug. 2006.

[21] J.R. Doyle and M.J. Botte, *Surgical Anatomy of the Hand & Upper Extremity*, Lippincott Williams & Wilkins, Philadelphia, 2003, pp. 250-270.

[22] Y.C. Fung, *Biomechanics Circulation.* 2nd ed. Springer-Verlag, New York, 1997, ch. 3.

[23] D.J. Hughes, C.F. Babbs, L.A. Geddes, and J.D. Bourland, "Measurements of Young's Modulus of Elasticity of the Canine Aorta with Ultrasound," *Ultrasonic Imaging*, vol. 1, pp. 356-367, 1979.

[24] L.A. Geddes, M.H. Voelz, C.F. Babbs, J.D. Bourland, and W.A. Tacker, "Pulse Transit Time as an Indicator of Arterial Blood Pressure," *Psychophysiology*, vol. 18, no. 1, pp. 71-74, 1981.

[25] J.G. Bramwell, A.C. Downey, and A.V. Hill, "The effect of blood pressure on the extensibility of the human artery," Heart, vol. 10, pp. 289-300, 1923.

[26] G.J. Langewouters, A. Zwart, R. Bussess, and K.H. Wesseling, "Pressure-diameter relationships of segments of human finger arteries," *Clin. Phys. Physiol. Meas.*, vol. 7, no. 1, pp. 43-55, 1986.

[27] P. Gizdulich, and K.H. Wesseling, "Forearm arterial pressure-volume relationships in man," *Clin. Phys. Physiol. Meas.*, vol. 9, pp. 123-132, 1988.

[28] G.J. Langewouters, K.H. Wesseling, and W.J.A. Goedhard, "The Static Elastic Properties of 45 Human Thoracic and 20 Abdominal Aortas In Vitro and the Parameters of a New Model," *J. Biomechanics*, vol. 17, no. 6, pp. 425-435, 1984.

[29] X. Girerd, G. London, P. Boutouyrie, J.J. Mourad, M. Safar, and S. Laurent, "Remodeling of the Radial Artery in Response to a Chronic Increase in Shear Stress" Hypertension, vol. 27, pp. 799-803, 1996.

[31] R.A. Norman, *Principles of Bioinstrumentation.* John Wiley & Sons, New York, 1998, ch. 11.

[32] P. Shaltis, A. Reisner, H. Asada, "Wearable, Cuff-less PPG-Based Blood Pressure Monitor with Novel Height Sensor," in *Proc. of the 28th IEEE International Engineering in Medicine and Biology Conference, EMBC 2006*, New York, NY, pp.908-911, Aug 2006.

[33] X.F. Teng and Y.T. Zhang, "The effect of applied sensor contact force on pulse transit time," *Physiol. Meas.,* vol 27, pp. 675-684, May 2006.

[34] B. Widrow, et al. "Adaptive Noise Canceling: Principles and Applications," *Proc. of the IEEE*, vol. 63, no.12, pp. 1692-1716, Dec. 1975.

[35] L. Ljung, *System Identification*, Prentice Hall, Upper Saddle River, NJ, 1999.

[36] X.F. Teng, and Y.T. Zhang, "Theoretical Study on the Effect of Sensor Contact Force on Pulse Transit Time," IEEE Trans. Biomed. Eng., vol. 58, no. 8, pp.1890-1898, August 2007.

[37] R.A. Payne, C.N. Symeonides, D.J. Webb, S.R. Maxwell, "Pulse transit time measured from the ECG: an unreliable marker of beat-to-beat blood pressure," *J Appl Physiol*, vol. 100, no. 1, pp.136-141, Jan 2006.

[38] E. O'Brien, B. Weber, G. Parati, J. Staessen, and M.G. Meyers, "Blood pressure measuring devices: recommendations of the European Society of Hypertension," *British Medical Journal*, vol. 322, pp. 531-536, 2001.

[39] Y.C. Fung, *Biomechanics Mechanical Properties of Living Tissues.* 2nd ed. Springer-Verlag, New York, 1993, ch. 8.